UNIVERSIDADE FEDERAL DO PARÁ
INSTITUTO DE GEOCIÊNCIAS
PROGRAMA DE PÓS-GRADUAÇÃO EM GEOLOGIA GEOQUÍMICA

DISSERTAÇÃO DE MESTRADO Nº 569

GEOLOGIA E PETROLOGIA DOS ENXAMES DE DIQUES MÁFICOS DA REGIÃO DE SANTA MARIA DAS BARREIRAS-CONCEIÇÃO DO ARAGUAIA: EVIDÊNCIAS DE EVENTOS DISTINTOS DE MAGMATISMO INTRACONTINENTAL NO CENTRO-NORTE DO BRASIL

Dissertação apresentada por:

DANILO JOSÉ DO NASCIMENTO CRUZ
Orientador: Prof. Dr. Paulo Sérgio de Sousa Gorayeb (UFPA)

BELÉM
2019

Dados Internacionais de Catalogação na Publicação (CIP) de acordo com ISBD Sistema de Bibliotecas da Universidade Federal do Pará
Gerada automaticamente pelo módulo Ficat, mediante os dados fornecidos pelo(a) autor(a)

C955g

Cruz, Danilo José do Nascimento

Geologia e petrologia dos enxames de diques máficos da região de Santa Maria das Barreiras-Conceição do Araguaia: evidências de eventos distintos de magmatismo intracontinental no Centro- Norte do Brasil / Danilo José do Nascimento Cruz. — 2019.

xiv, 74 f. : il. color.

Orientador(a): Prof. Dr. Paulo Sérgio de Sousa Gorayeb

Dissertação (Mestrado) - Programa de Pós-Graduação em Geologia e Geoquímica, Instituto de Geociências, Universidade Federal do Pará, Belém, 2019.

1. Petrologia (PA). 2. Geoquímica. 3. Mineralogia química. 4. Diques máficos. 5. Cinturão Araguaia. I. Título.

CDD 552.0098115

Universidade Federal do Pará
Instituto de Geociências
Programa de Pós-Graduação em Geologia e Geoquímica

GEOLOGIA E PETROLOGIA DOS ENXAMES DE DIQUES MÁFICOS DA REGIÃO DE SANTA MARIA DAS BARREIRAS-CONCEIÇÃO DO ARAGUAIA: EVIDÊNCIAS DE EVENTOS DISTINTOS DE MAGMATISMO INTRACONTINENTAL NO CENTRO-NORTE DO BRASIL

DISSERTAÇÃO APRESENTADA POR

DANILO JOSÉ DO NASCIMENTO CRUZ

Como requisito parcial à obtenção do Grau de Mestre em Ciências na Área de GEOLOGIA E GEOQUÍMICA, linha de pesquisa PETROLOGIA E EVOLUÇÃO CRUSTAL

Data de Aprovação: 28 / 10 / 2019

Banca Examinadora:

Prof. Dr. Paulo Sergio de S. Gorayeb
Orientador – UFPA

Prof. Dr. Sergio de Castro Valente
Membro – UFRJ

Prof. Dr. Fabio Braz Machado
Membro – UNIFESP

À Cosma e Vanderley,
por serem as pessoas mais especiais que conheço
e os melhores pais que se pode ter.

AGRADECIMENTOS

Agradeço à minha família, em especial aos meus pais Cosma e Vanderley e ao meu irmão Lucas. Não há, em toda Terra, uma rocha tão dura que possa se comparar com a solidez do embasamento que eles me proporcionam em todos os campos da minha vida.

Ao Prof. Dr. Paulo Sérgio de Sousa Gorayeb, pelas oportunidades e ensinamentos e pelas conversas de motivação que foram de extrema importância para mim.

Ao Conselho Nacional de Desenvolvimento Científico e Tecnológico (CNPq) pelo projeto Universal Nº 427225/2016-7 que deu apoio à realização deste trabalho, bem como pela concessão da bolsa de mestrado Nº 130794/2017-1.

À Universidade Federal do Pará (UFPA) e à Faculdade de Geologia (FAGEO) por fornecerem a infraestrutura necessária à realização deste trabalho.

À Magali Alves da Silva e Raimundo Lopes Noleto (Seu Vovô) pelo apoio logístico na cidade de Araguacema.

À técnica Gisele Marques pelo auxílio nas análises mineralógicas e na utilização do MEV e da microssonda do Laboratório de Microanálises do Instituto de Geociências da UFPA. À técnica Jacqueline Menez por todo o apoio oferecido no Laboratório de Microssonda Eletrônica do Instituto de Geociências da Universidade de Brasília (UNB).

À Laiane Cruz por todo o carinho e afeto que me proporcionou quando os problemas pareciam irresolúveis e maiores do que eram.

Aos meus amigos Alexandre Cardoso, Luan Martins e Williamy Felix pelo companheirismo e pelas diversas discussões enriquecedoras sobre Geologia. À minha parceira de empreitadas acadêmicas, Daniella Vieira. À minha amiga Brenda Marques, pelo entusiasmo acadêmico que serve de inspiração.

Agradeço, por fim, a todos que, direta ou indiretamente, contribuíram para a realização deste trabalho.

"The world is my country, all mankind are my brethren, and to do good is my religion."
– Thomas Paine in: The Age of Reason, III, 1794

RESUMO

Enxames de diques máficos subparalelos de direção N-S e NNW-SSE ocorrem intrudindo as rochas metassedimentares do Grupo Tocantins, Cinturão Araguaia, centro-norte do Brasil. Eles são pouco estudados, não havendo nenhuma informação acerca da natureza de sua fonte mantélica e dos processos petrológicos envolvidos em sua gênese, além de uma incerteza quanto à sua idade. Para discutir essas questões, foram estudados diques máficos representativos da região de Santa Maria das Barreiras-Conceição do Araguaia, na fronteira entre os estados do Pará e Tocantins. Foi possível separar os diques em dois grupos: um consistindo de diabásios afetados pelo metamorfismo regional neoproterozoico do Cinturão Araguaia com grau variado de transformações e deformação mineral; e outro contendo diabásios e leucodiabásios sem metamorfismo e deformação. Os diques estudados foram composicionalmente classificados como basaltos sub-alcalino de afinidade toleítica. No entanto, os metadiabásios apresentam uma assinatura arco-*like* caracterizada por uma anomalia negativa de Nb-Ta, enquanto que os leucodiabásios e diabásios não apresentam anomalia negativa de Nb-Ta e exibem padrões enriquecidos de LREE, que se assemelha às assinaturas de rochas basálticas geradas por plumas mantélicas. Ambos os grupos de diques foram interpretados como sendo originados em ambiente tectônico intracontinental com a ajuda de diagramas de discriminação Ti–V, Zr–Zr/Y e Zr–Ti. Há indícios de importante contribuição de componentes mantélicos enriquecidos (EN) na fonte dos metadiabásios e significante contribuição de componentes do manto primitivo (PM) na fonte dos leucodiabásios e diabásios. Sugeriu-se que os metadiabásios representam os condutos expostos de basaltos intracontinentais com assinatura arc-*like* que precedem o metamorfismo Neoprotezoico da área e que os leucodiabásios e diabásios representam os condutos expostos de basaltos intracontinentais cujo magmatismo é posterior ao evento metamórfico. As rochas do evento mais antigo compartilham similaridades com rochas máficas Neoproterozoicas do leste do Cinturão Araguaia, enquanto que as rochas do evento mais recente são bastante similares com basaltos e diques de diabásios da CAMP que se encontram próximos à área de estudo.

Palavras-chave: Petrologia ígnea. Diques de diabásio. Magmatismo intracontinental. Grandes Províncias Ígneas. Cinturão Araguaia.

ABSTRACT

N-S and NNW-SEE-trending subparallel mafic dike swarms are intruded into metasedimentary rocks of the Tocantins Group, Araguaia Belt, central-north Brazil. They are under-examined and there is little to no information about their origin and mantellic sources and uncertainty about their ages. Representative mafic dikes from the Santa Maria das Barreiras-Conceição do Araguaia region, at the boundary between the states of Pará and Tocantins, were studied in order to address these problems. It was possible to separate the dikes into two groups: one consisting of diabases affected by the Neoproterozoic regional metamorphism of the Araguaia Belt with varied degrees of transformations and mineral deformation; and the other consisting of unmetamorphosed and undeformed diabases and leucodiabases. The studied dikes are compositionally classified as subalkaline basalts with tholeiitic affinity. However, metadiabases present an arc-like geochemical signature characterized by a pronounced Nb-Ta negative anomaly, whereas leucodiabases and diabases lack a negative Nb-Ta anomaly and show a LREE-enriched pattern, which resembles the signatures of plume-generated basaltic rocks. Both group of dikes were interpreted to be originated in an intracontinental setting with the aid of Ti–V, Zr–Zr/Y and Zr–Ti discrimination diagrams. There is evidence of important contribution of enriched (EN) mantle components in the source of metadiabases and significant contribution of primitive mantle (PM) to the source of both leucodiabases and diabases. We suggested that the metadiabases represent the exposed plumbing system of arc-like intracontinental basalts which precede the regional Neoproterozoic metamorphism of the area and the leucodiabases and diabases represent the exposed conduits of intracontinental basalts whose magmatism succeed the metamorphic event. The rocks from the older event share several similarities with Neoproterozoic mafic rocks from the eastern domain of the Araguaia Belt and nearby Tonian rocks of the 1100 Ma Rincón del Tigre-Huanchaca LIP event, while the rocks from the newer event are remarkably similar to nearby CAMP basalts and diabase dikes.

Keywords: Igneous petrology. Diabase dikes. Intracontinental magmatism. Large Igneous Provinces. Araguaia Belt.

LISTA DE ILUSTRAÇÕES

LISTA DE TABELAS

SUMÁRIO

CAPÍTULO 1 INTRODUÇÃO

1.1 APRESENTAÇÃO E LOCALIZAÇÃO

A presente pesquisa está relacionada ao desenvolvimento de uma dissertação de mestrado no âmbito do Programa de Pós-Graduação em Geologia e Geoquímica do Instituto de Geociências da Universidade Federal do Pará (PPGG/IG/UFPA) e está vinculado ao Grupo de Pesquisa "Petrologia e Evolução Crustal" (GPEC) do CNPq/UFPA. O objeto de estudo compreende um enxame de diques máficos que ocorre na região entre as cidades de Conceição do Araguaia, Santa Maria das Barreiras (PA), Couto Magalhães, Araguacema e Pequizeiro (TO), na região norte do País, mais precisamente na fronteira dos estados do Pará e do Tocantins cuja área de estudo pode ser visualizada na Figura 1. Parte da sua porção oeste está inclusa na Folha Redenção (SC.22-X-A), e o restante encontra-se na Folha Conceição do Araguaia (SC.22-X-B).

A área está inserida no norte da Província Tocantins, na porção centro-norte do Cinturão Araguaia, que representa um extenso orógeno evoluído no Neoproterozoico formado a partir da convergência e subsequente colisão entre os crátons Amazônico, São Francisco-Congo e o Bloco Parnaíba (Alvarenga *et al*. 2000, Gorayeb *et al*. 2008, Hodel *et al*. 2019). O Cinturão Araguaia limita-se a oeste pelo Cráton Amazônico; ao norte, nordeste e leste é encoberto pela Bacia do Parnaíba; ao sudoeste é encoberto pela Bacia do Bananal; e a sul e sudeste faz limite com o Maciço de Goiás (Gorayeb *et al*. 2008).

Diques máficos tem ocorrência nas mais diversas partes do território brasileiro. Os mais conhecidos são do Mesozoico que, juntos com *sills* e derrames, são registros da ruptura do Supercontinente Pangea e consequente abertura do oceano atlântico. Eles se estabilizaram entre o Neojurássico e o Eotriássico (202-190 Ma) e fazem parte da Província Magmática do Atlântico Central (CAMP), uma Grande Província Ígnea (LIP) reportada por Marzoli *et al*. (1999).

As ocorrências relativamente mais próximas da área de estudo são diques máficos, soleiras e rochas vulcânicas relacionadas à CAMP. Por exemplo, os derrames de basaltos e soleiras de diabásio da Formação Mosquito, na porção oeste da Bacia do Parnaíba (Fodor *et al*. 1990, Merle *et al*. 2011); o diabásio Penatecaua, na borda nordeste da Bacia do Amazonas (Nascimento *et al*. 2011); os diques de diabásio que cortam as rochas do Cráton São Luís e do Cinturão Gurupi, no norte-nordeste do Brasil (Klein *et al*. 2013); o diabásio Cassiporé, na porção sudeste do Escudo das Guianas (Rosa-Costa, 2014) e os diques de diabásio e gabro

da porção norte e leste do Escudo das Guianas (Deckart *et al*. 2005). Recentemente, diques mesozoicos da região de Carajás, no sudeste do Cráton Amazônico foram associados à CAMP (Giovanardi *et al*. 2019, Teixeira *et al*. 2019).

Episódios de magmatismo máfico mais antigos também ocorrem próximos à área de estudo. Por exemplo, Gorayeb *et al*. (2010) obteve idades de U-Pb em zircão de 750 a 870 Ma para metagabros da Suíte Intrusiva Xambica, no domínio leste do Cinturão do Araguaia. Na região de Carajás, foram identificados diques máficos de 535 Ma e 1882 Ma (Giovanardi *et al*, 2019, Teixeira *et al*. 2019). E um pouco mais distante da área de estudo, no Terreno Rio Apa, sudoeste do Cráton Amazônico, ocorrem diques máficos de 1100 Ma da LIP Ricón del Tigre-Huanchaca, relacionada à quebra do supercontinente Rodínia (Lima *et al*. 2017, Teixeira *et al*. 2014).

O estado da arte do estudo de enxames de diques máficos revela que eles são um importante registro de expressivos eventos de magmatismo predominantemente máfico e de curta duração que antecedem a quebra de continentes, conhecidos como LIPs (Ernst *et al*. 2005). Além disso, por serem rochas provenientes diretamente do manto, os diques máficos são considerados “janelas” para se entender os processos mantélicos. Desse modo, os corpos de diabásio envolvidos neste estudo são elementos chaves para se compreender a evolução crustal e geodinâmica do segmento crustal que engloba a porção sudeste do Cráton Amazônico, o Cinturão Araguaia e a Bacia do Parnaíba.

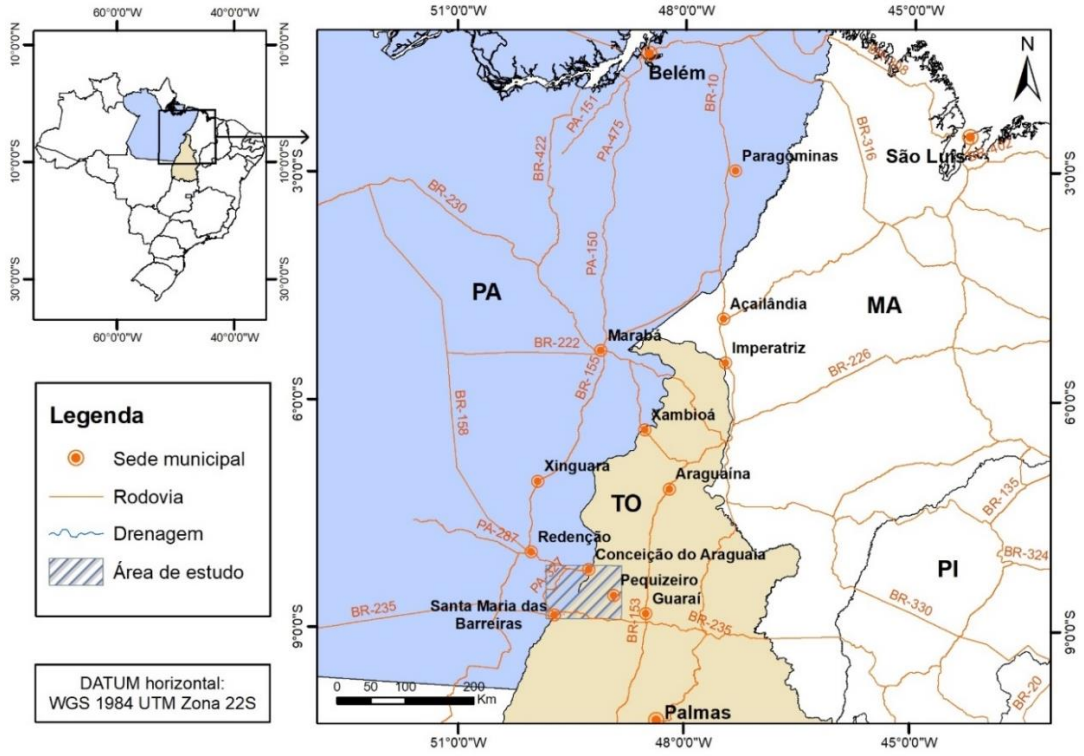

Figura 1 – Mapa de localização da área de estudo.

1.2 JUSTIFICATIVA

Apesar de haver alguns dados em relação aos diques máficos que ocorrem entre Santa Maria das Barreiras e Conceição do Araguaia, eles ainda permanecem pouco conhecidos na literatura científica e pouco estudados. Pesquisas acerca de sua natureza, origem e fonte são inexistentes, assim como dados de química mineral e litoquímica. A maioria das informações disponíveis, como descrições petrográficas e idades K-Ar, são pontuais e provenientes de relatórios de projetos de mapeamentos regionais (1:1.000.000, 1:250.000) executados por agências governamentais ou de estudos geocronológicos regionais. Há, portanto, ausência de estudos sistemáticos em relação a estes diques.

Ademais, mesmo os dados existentes na literatura são inconclusivos. Por exemplo, embora os diques tenham sido historicamente descritos como compostos de diabásios e gabros sem deformação e metamorfismo (Hasui *et al*. 1980, Gorayeb 1981, Olivatti *et al*. 2001, Vale & Neves, 1999), recentemente, indícios de transformações foram reportados por Gorayeb *et al* (2017).

Também é difícil de apontar o significado geológico do amplo intervalo de idades K-Ar: 185-208 Ma, 480-560 Ma, 780 Ma e 1086 Ma (Cunha *et al*. 1981, Gorayeb 1981, Hasui *et al*. 1980, Olivatti *et al*. 2001). Para explicar essa discrepância, Hasui et al. (1984) sugeriram

dois eventos magmáticos de difícil separação no campo: um do Neoproterozoico e outro do Mesozoico. Olivatti *et al*. (2001) apoiaram a hipótese de dois eventos e consideraram a idade K-Ar de 1086 ± 16 Ma como a idade mínima do evento mais antigo e as outras idades neoproterozoicas como idades que representariam episódios de resfriamento após a colagem do evento Brasiliano/Pan-Africano.

Além do mais, os mapas geológicos que abrangem a área de estudo (1:250.000), tais como as folhas Redenção (Neves & Vale 1999) e Conceição do Araguaia (Figueiredo & Souza 2001), encontram-se desatualizados e não fazem jus à verdadeira distribuição e extensão dos diques máficos estudados.

Com base no exposto, listam-se os principais problemas que foram identificados nesta investigação:

- Mapas de ocorrência e distribuição dos diques desatualizados;
- Carência de um estudo sistemático com amostragem representativa dos diversos diques;
- Petrografia incipiente ou inexistente;
- Ausência de dados litoquímicos e de química mineral;
- Dados geocronológicos inconclusivos quanto à idade desse evento de diques;
- Indeterminação quanto ao número e natureza dos corpos de dique e de eventos magmáticos.

1.3 OBJETIVOS

A partir das observações acima, o objetivo principal deste trabalho é caracterizar os diferentes corpos de diques da região, discutir a natureza do magmatismo e os processos de formação dessas rochas, contextualizá-las na evolução crustal e geodinâmica do Cinturão Araguaia, discutir a hipótese de diferentes eventos magmáticos e compará-los com eventos de magmatismo próximos à área de estudo. Para tal, os seguintes objetivos específicos foram estabelecidos:

- Delimitar a ocorrência e a forma dos diques e entender suas relações de contato com as unidades geológicas adjacentes;
- Identificar as fases minerais primárias e secundárias, as variações texturais e microestruturais, os componentes químicos que controlaram o equilíbrio mineral e discutir o seu significado;

- Definir a natureza do magmatismo, tipologia, assinaturas geoquímicas e os processos que controlaram a evolução desses corpos;
- Estabelecer comparações com outros eventos magmáticos similares da literatura científica;
- Definir e discutir os processos e a evolução magmática e metamórfica dessas rochas.

1.4 MATERIAIS E MÉTODOS

A fim de se alcançar os objetivos propostos, as técnicas e métodos de investigação abaixo foram empregadas.

1.4.1 Pesquisa bibliográfica

Essa etapa consistiu primeiramente do levantamento bibliográfico acerca do conhecimento geológico geral do Cinturão Araguaia disponível na literatura científica. Após, enfatizou-se o conhecimento científico teórico sobre diques máficos, magmatismo básico e LIPs da região e de contexto similar. Além disso, foram analisados artigos científicos e livros sobre temas relacionados à petrologia e evolução crustal de rochas máficas, para aprofundamento teórico sobre a temática.

1.4.2 Levantamento e organização de acervo material

Como já existiam trabalhos anteriores sobre essas rochas foi realizado um levantamento do material existente no acervo do grupo GPEC, uma vez que se encontram disponíveis amostras de mão e lâminas delgadas correspondentes a diques máficos da dissertação de Gorayeb (1981), assim como mapas geológicos que abrangem a região de Santa Maria das Barreiras-Conceição do Araguaia e Pequizeiro. O material foi posteriormente organizado e sistematizado para ser utilizado neste trabalho.

1.4.3 Integração e elaboração de bases cartográficas

Bases cartográficas geológicas das áreas de ocorrência dos diques foram compiladas a fim de integrar as informações registradas ao longo dos anos. Adicionalmente, novos dados foram adquiridos a partir da análise de imagens aerogeofísicas obtidas no banco de dados do Serviço Geológico do Brasil (CPRM; www.geosgb.cprm.gov.br). A análise focou especialmente nos mapas da 1ª Derivada Vertical do Campo Magnético, onde há uma nítida

correlação entre as respostas de maior magnitude e os corpos de diques máficos. Com a integração desses dados e elaboração de uma base SIG, foram delimitados com precisão os diversos corpos de diques e elaborado um mapa-base para apoio aos trabalhos de campo. O mapa aerogeofísico pode ser visto no Anexo A.

1.4.4 Levantamento geológico e amostragem

A maioria das amostras estudadas foi coletada no trabalho de campo coordenado pelo Prof. Dr. Paulo Sérgio de Sousa Gorayeb durante o período de 2 a 11 de novembro de 2016. Outros dois levantamentos de campo complementares foram realizados nos períodos de 23 a 30 de novembro de 2017 e de 2 a 6 de novembro de 2018. Utilizando-se o mapa-base foram visitados os principais corpos de dique no leito do Rio Araguaia. A navegação se deu através de barcos "Voadeira" e com o apoio da Cooperativa de Pesca de Araguacema e de Conceição do Araguaia. As amostras foram coletadas de modo a evitar qualquer indício de intemperismo, em fragmentos de tamanho representativo para cada finalidade: a) Petrografia – amostra de mão; b) Geoquímica – saco de 1 kg (fragmentos de 3 a 5 cm); c) Separação mineral – Saco de 10 kg (fragmentos de 5 a 10 cm) . O resultado final dessa etapa foi a elaboração do mapa geológico atualizado da área, com destaque ao enxame de diques da região de Santa Maria das Barreiras-Conceição do Araguaia. A tabela de amostras e o mapa de amostragem podem ser vistos, respectivamente, nos Anexo B e C.

1.4.5 Análise petrográfica

Os estudos petrográficos foram realizados no Laboratório de Petrografia do IG/PPGG (LAPETRO) e estiveram voltados para a identificação do conteúdo mineralógico e classificação das rochas de acordo com as percentagens modais, composição mineralógica e análise textural/microestrutural. A análise modal foi realizada utilizando-se o contador automático de pontos da marca Swift do LAPETRO e cada análise de lâmina delgada envolveu a contagem de 1500 pontos. Imagens fotomicrográficas foram obtidas em microscópio petrográfico com câmera digital acoplada da LEICA utilizando o software LAS-EZ do LAPETRO. Utilizaram-se as seguintes bases bibliográficas para apoio ao estudo petrográfico: Best (2003); Deer *et al*. (2013); Fettes *et al*. (2007); Gill (2010); Le Maitre *et al*. (2002); Nesse (2013); Passchier & Trouw (2005); Spear (1995); Vernon (2004); e Winter (2010).

1.4.6 Análises mineralógicas

Análises de espectroscopia de raios X de dispersão por comprimento de onda (WDS) foram realizadas em 12 amostras no Laboratório de Microssonda do Instituto de Geociências da Universidade de Brasília (IG/UnB) e em quatro amostras no Laboratório de Microanálises do IG/UFPA. Ambos os laboratórios são equipados com microssonda modelo JEOL JXA-8230. O equipamento na UnB operou com voltagem de aceleração de coluna de 15 kV, corrente de 10 nA e tempo de análise de 10 segundos; utilizou os cristais analisadores LDE1 (F), LIF (Ti, Cr e Mn), LIFH (Ni, Fe e V), PETJ (Ca, K e Cl) e TAP (Na, Mg, Al e Si); e os seguintes padrões de calibração: microclina (Al, Si e K), pirofanita (Ti e Mn), forsterita (Mg), andradita (Ca), albita (Na), vanadinita (Cl e V), topázio (F), Fe_2O_3 (Fe), Cr_2O_3 (Cr) e NiO (Ni). O equipamento do IG/UFPA operou com voltagem de aceleração de coluna de 15 kV, corrente de 20 nA e tempo de análise variando de 20 a 40 segundos dependendo do elemento; usou os cristais analisadores LDE1 (F), LIF (Ni, Fe, Mn, Ba e Ti), PETJ (Cr, Ca, K e Sr), PETH (V) e TAP (Na, Mg, Al e Si); e os seguintes padrões de calibração: ortoclásio (Si e K), rutilo (Ti), anortita (Al), hematita (Fe), forsterita (Mg), rodonita (Mn), wollastonita (Ca), sodalita (Na), celestina (Sr), barita (Ba), vanadinita (V) e NiO (Ni).

1.4.7 Litogeoquímica

Foram analisadas 23 amostras representativas dos diques para dosagem de elementos maiores, menores e traços nos laboratórios da ALS GLOBAL, de acordo com o procedimento a seguir. Primeiramente, as amostras foram reduzidas de tamanho no triturador de mandíbulas e moinho de cilindro de aço (*shatterbox*) da Oficina de Preparação de Amostras do IG/UFPA. Em seguida, as amostras foram quarteadas e consequentemente pulverizadas em moinho rotativo de ágata. Por fim, separou-se alíquotas para encaminhamento ao laboratório.

As dosagens dos elementos maiores e menores foram obtidas por espectrometria de emissão atômica por plasma acoplado indutivamente (ICP-AES; método ME-ICP06); as concentrações dos elementos traços, incluindo os elementos terras-raras (ETR), foram determinadas por espectrometria de massa por plasma acoplado indutivamente (ICP-MS; método ME-MS81); e os elementos Co, Cu, Ni e Zn foram analisados por ICP-AES (método ME-4ACD81). Outras informações sobre os métodos analíticos e limites de detecção podem ser acessados na webpage: www.alsglobal.com/geochemistry.

CAPÍTULO 2 CONTEXTO GEOLÓGICO REGIONAL

2.1 GENERALIDADES

A área de estudo está inserida no Cinturão Araguaia (Fig. 2), uma unidade geotectônica do Neoproterozóico que corresponde à porção norte da Faixa Paraguai-Araguaia (Alvarenga *et al*. 2000). Ela está localizada na Província Estrutural Tocantins (Almeida *et al*. 1981) e apresenta orientação geral N-S, com comprimento de aproximadamente 1.200 km e largura superior a 100 km (Gorayeb *et al*. 2008). Limita-se a oeste pelo Cráton Amazônico; ao norte, nordeste e leste é encoberto pela Bacia do Parnaíba; ao sudoeste é encoberto pela Bacia do Bananal; e a sul e sudeste faz limite com o Maciço de Goiás (Gorayeb *et al*. 2008).

O Cinturão Araguaia é composto predominantemente por sequências de rochas psamíticas e pelíticas metamorfizadas com contribuições menores de rochas sedimentares químicas, ofiolitos e intrusões máficas e graníticas (Gorayeb *et al*. 2008). O metamorfismo regional é do tipo Barroviano e zonas metamórficas com orientação N-S são mapeadas ao longo do Cinturão. Tanto a deformação quanto o grau metamórfico aumentam de oeste para leste, variando de incipiente até a fácies anfibolito médio (Gorayeb 1981, Silva 1980). As sequências pelíticas mostram a seguinte variação de associação mineral de acordo com o aumento do grau metamórfico: sericita-clorita, muscovita-clorita-epidoto, muscovita-biotita±clorita, muscovita-biotita-granada, biotita-muscovita-granada-estaurolita, biotita-granada-cianita e, finalmente, pacotes quartzo-feldspáticos e pequenos corpos graníticos em áreas restritas com fusão parcial (Alvarenga *et al*. 2000, Gorayeb 1981, Gorayeb *et al*. 2008).

A evolução estrutural do Cinturão Araguaia, de acordo com estudos geocronológicos de Moura & Gaudette (1993) em rochas graníticas sin a tardi-tectônicas associadas às rochas supracrustais dessa unidade, está relacionada à Colagem Brasiliana/Pan-Africana durante a amalgamação do Supercontinente Gondwana Ocidental no Neoproterozoico. A colagem se deu através da convergência e conseguinte colisão entre três blocos continentais: os paleocontinentes Amazônico e São Francisco-Congo e o bloco Parnaíba (Hodel *et al*. 2019).

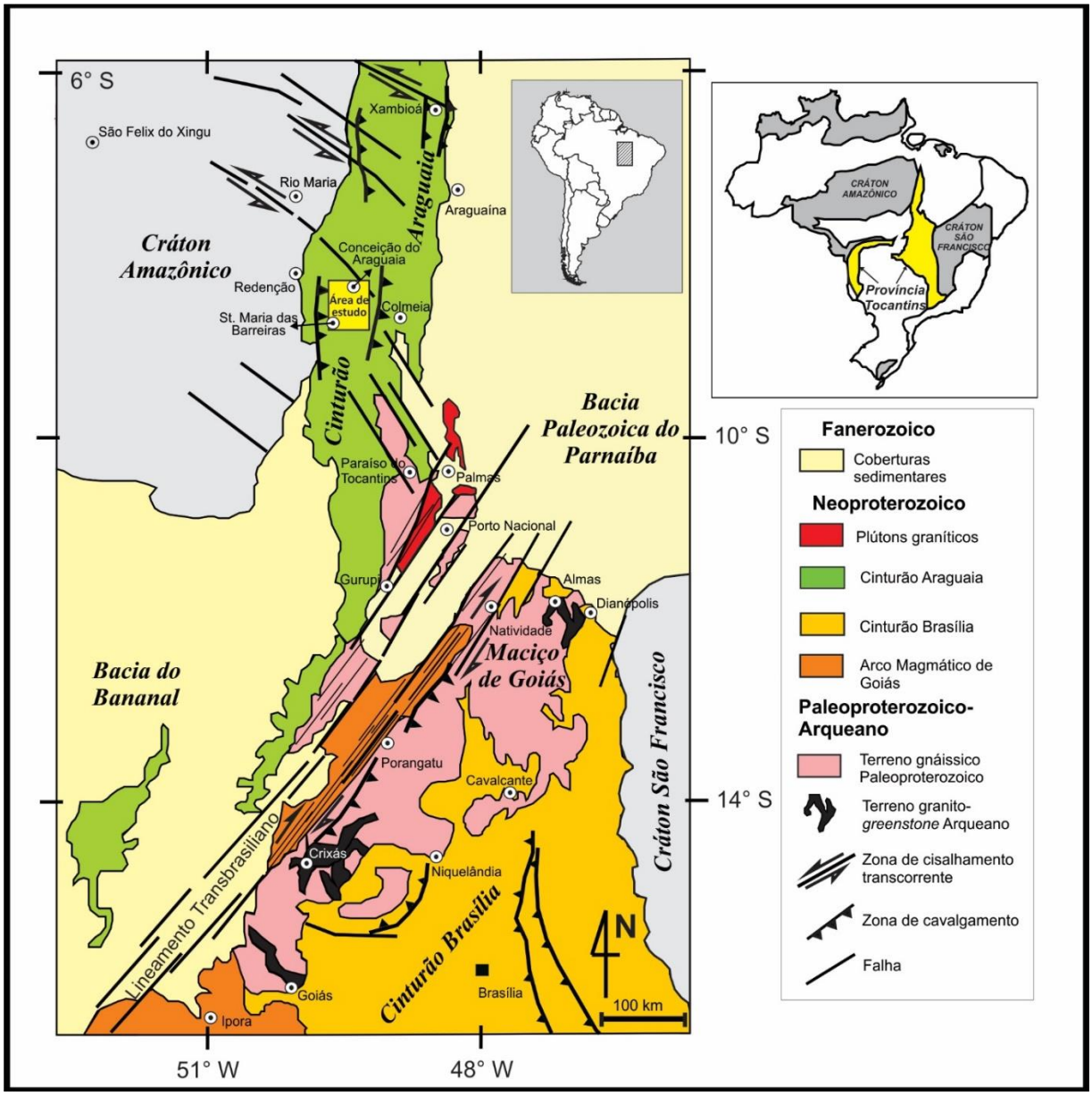

Figura 2 – Mapa regional do norte da Província Tocantins, com enfoque para o Cinturão Araguaia. No quadrado amarelo encontra-se localizada a área de estudo do presente trabalho. Adaptado de Gorayeb *et al* (2019).

2.2 EMBASAMENTO

O embasamento do Cinturão Araguaia é composto por um segmento norte (setentrional) e um segmento sul (meridional) (Arcanjo *et al*, 2013, Arcanjo & Moura 2000). A porção setentrional é representada por ortognaisses de idade arqueana do Complexo Colmeia. Baseado na similaridade geoquímica entre as sequências desse segmento e seus correspondentes cronológicos no Cráton Amazônico adjacente, Moura & Gaudette (1994) consideraram o segmento setentrional como uma extensão do Cráton Amazônico para leste. Na porção meridional, ocorrem sequências metavulcanossedimentares arqueanas do Grupo Rio do Coco, no entanto, esse segmento é melhor representado pelos amplos terrenos arqueanos e paleoproterozoicos do Maciço de Goiás.

Tendo em vista as diferenças de idade entres os dois segmentos, Arcanjo *et al* (2013) sugeriram que o segmento meridional deve representar um terreno mais novo, justaposto às rochas arqueanas do Cráton Amazônico durante o Paleoproterozoico. O segmento meridional também possui uma área de afloramento significativamente maior, fazendo contato tectônico a leste com as sequências de alto grau metamórfico do Maciço de Goiás (Hasui *et al*. 1984). As rochas do embasamento do Cinturão Araguaia afloram no interior de braquianticlinais no seu segmento setentrional, enquanto que na porção meridional elas não se encontram confinadas a esse tipo de estrutura (Hasui *et al*. 1984).

O Complexo Colmeia (Costa, 1980) reúne ortognaisses de idade 2,85 Ga (Moura & Gaudette 1999) e é constituído por gnaisses trondhjemíticos, tonalíticos e granodioríticos (suíte TTG), além de raros anfibolitos.

O Grupo Rio do Coco (Costa *et al*. 1983) é formado por um núcleo restrito de idade arqueana de 2,6 Ga (Pb/Pb em zircão) (Arcanjo, 2002), caracterizado como uma sequência metavulcanossedimentar do tipo *greenstone belt* por Barreira & Dardenne (1981). É constituído por uma sequência de metapelitos, rochas quartzo feldspáticas, metavulcânicas dacíticas contendo sulfetos, metabasitos e metaultramafitos com formações ferríferas intercaladas (Costa *et al*. 1983).

O Complexo Rio dos Mangues (Costa *et al*. 1983) é constituído por rochas metassedimentares e metaígneas félsicas e máficas, que sofreram transformações metamórficas na fácies anfibolito médio a alto resultando em gnaisses tonalíticos, granodioríticos e cálcio-silicáticos migmatizados, granada biotita paragnaisses, ortoquartzitos, granito-gnaisses e anfibolitos subordinados (Costa *et al*. 1983). O complexo apresenta protólitos ígneos com idades mínimas de cristalização em torno de 2,06 Ga e idades modelos que sugerem que os protólitos

foram gerados a partir de duas fontes, uma mantélica (TDM = 2,21 – 2,25 Ga) e outra crustal (TDM = 2,35 Ga) (Arcanjo *et al*. 2013).

O Granito Serrote (Costa *et al*. 1983) refere-se a plútons com idades de 1,86 Ga (Moura & Souza 1996) e com tramas augen-porfiróides e milonítica representadas por microclínio granitos e leucogranitos potássicos (Gorayeb, 1996) e está alojado na porção centro-norte do Complexo Rio dos Mangues. Encaixada nas rochas do complexo, também se encontra a Suíte Monte Santo (Costa *et al*. 1983), que compreende dois corpos de gnaisses alcalinos: Serra da Estrela e Monte Santo, este último recoberto em parte pelo Grupo Estrondo. Análises em granitos sieníticos associados com o plúton da Serra da Estrela obtiveram idades de 1,00 Ga (Moura & Souza 1996).

2.3 LITOESTRATIGRAFIA

As principais unidades estratigráficas do Cinturão Araguaia estão sintetizadas em Abreu (1978), Hasui *et al*. (1984), Alvarenga *et al*. (2000) e Gorayeb *et al*. (2008). As rochas metassedimentares do Cinturão Araguaia foram agrupadas por Abreu (1978) no Supergrupo Baixo Araguaia que, por sua vez, está dividido nos grupos Estrondo e Tocantins. O Grupo Estrondo encontra-se na porção leste do Cinturão e é subdivido nas formações Morro do Campo e Xambioá, enquanto que o Grupo Tocantins se situa na porção central e oeste e é subdividido nas formações Pequizeiro e Couto Magalhães (Abreu, 1978). O Grupo Tocantins sobrepõe concordantemente o Grupo Estrondo. Ocorrendo em meio às sequências metassedimentares, principalmente no Grupo Tocantins, encontram-se também corpos máficos e ultramáficos com transformações metamórficas.

A Formação Morro do Campo representa a unidade basal do Grupo Estrondo e é composta predominantemente por quartzitos puros e micáceos com cristais de cianita e magnetita, além de meta-conglomerados com intercalações de biotita xistos, quartzo mica xistos e xistos grafitosos (Gorayeb *et al*. 2008).

A Formação Xambioá representa a porção superior do Grupo Estrondo, sobrepondo-se concordantemente à Formação Morro do Campo. É composta por mica xistos com quantidades variáveis de biotita, muscovita, cianita, staurolita e granada, calcoxistos, mármores, xistos feldspáticos e anfibolitos. É amplamente distribuída ao longo do Cinturão Araguaia e é a unidade que atingiu as condições de relativamente maior grau metamórfico (Gorayeb *et al*. 2008).

A Formação Pequizeiro é composta por clorita xistos, quartzo-muscovita xistos, clorita-muscovita-quartzo xistos, com intercalações subordinadas de magnetita-muscovita filitos, quartzitos e talco xistos. Em geral, apresentam foliação pervasiva, definida principalmente pela xistosidade, com direção geral N-S, NNW ou NNE e mergulhos variáveis para leste (Dall'Agnol *et al*. 1988, Gorayeb 1981). De acordo com estudos de Silva (1980) e Gorayeb (1981), essa unidade atingiu condições de metamorfismo na fácies xisto verde.

A Formação Couto Magalhães é composta por um conjunto de rochas de baixo grau metamórfico representadas por ardósias, filitos, metarcósios, metassiltitos e lentes de quartzitos (Gorayeb, 1981). Essa formação apresenta estruturas sedimentares primárias preservadas como estratificações planoparalelas e cruzadas. Em geral, o metamorfismo nessas rochas varia do anquimetamorfismo a fácies xisto verde (Gorayeb *et al*. 2008)

Os ofiolitos estão alojados tectonicamente ao longo do Cinturão Araguaia, principalmente nas rochas metassedimentares do Grupo Tocantins, e encontram-se dispostos concordante ou discordantemente à sua estruturação principal. São representados por peridotitos e dunitos serpentinizados, com cromititos e seus produtos metamórficos (esteatito, talco xisto, tremolita-actinolita xisto e cloritito), em adição à chert e jaspilito (Gorayeb, 1989). Dentre os corpos mais expressivos estão os maciços Quatipuru, Serra do Tapa e Morro Grande. Ao longo dos anos, esses corpos foram sendo objeto de diversos estudos científicos. A interpretação mais aceita atualmente é de que esses corpos seriam fragmentos de suítes ofiolíticas (Barros & Gorayeb 2013, Gorayeb 1989, Kotschoubey *et al*. 2005, Miyagawa & Gorayeb 2013, Paixão *et al*. 2008, Paixão & Gorayeb 2014).

Corpos de metagabros com escapolita dispostos em mica xistos foram mapeados na região de Xambioá-Araguanã. Eles foram agrupados por Gorayeb *et al*. (2004) na Suíte Gabroica Xambica. Datação de gabros desta suíte deram idades de evaporação Pb-Pb em zircão de 817 ± 5 Ma (Gorayeb *et al.* 2004) e idades U-Pb em zircão de 878 ± 22, 804 ± 35 e 752 ± 23 Ma (Barros, 2010). Esses corpos são interpretados como toleítos continentais que intrudiram as sequências metassedimentares do Grupo Estrondo antes do metamorfismo e evolução tectônica do cinturão Araguaia. Sucessões de derrames basálticos com afinidade toleítica também ocorrem na sequência vulcano-sedimentar do Grupo Tucuruí, na zona de transição entre o Cinturão Araguaia e o Cráton Amazônico (Dutra 2012, Dutra *et al*. 2014).

Os diques estudados encontram-se encaixados nas rochas metassedimentares da Formação Couto Magalhães e foram descritos primeiramente por Barbosa *et al*. (1966). Eles foram agrupados por Gorayeb *et al*. (2017) na Suíte Máfica Santa Maria das Barreiras-

Conceição do Araguaia. São caracterizados por formarem corpos subparalelos e subverticais quilométricos com disposição geral NNW-SSE, apresentando dezenas a centenas de metros de espessura (Gorayeb, 1981). Dados geocronológicos estão disponíveis para alguns destes diques, a saber: a) idades K-Ar de 780 ± 12, 565 ± 6 e 480 ± 22 Ma foram obtidas por Hasui *et al*. (1980) em plagioclásios de diques de gabros; b) idade K-Ar em rocha total de 197 ± 4 Ma para uma amostra de dique de diabásio foi reportada por Cunha *et al*. (1981); c) e idade K-Ar de 1086 ± 16 Ma e idades K-Ar de intervalo de 200-185 Ma para dois diques de diabásio distintos foram reportadas por Olivatti *et al*. (2001).

Corpos graníticos associados ao domínio de maior grau metamórfico do Grupo Estrondo ocorrem ao longo do Cinturão Araguaia. Esses corpos têm sido considerados como produtos de fusão parcial de sequências supracrustais durante o pico do metamorfismo (Abreu & Gorayeb 1994, Alvarenga *et al*. 2000, Dall'Agnol *et al*. 1988). A idade de evaporação Pb-Pb em zircão de 539 ± 5 Ma obtida no Granodiorito Presidente Kennedy é interpretada como a idade do metamorfismo que afetou o cinturão (Gorayeb *et al*. 2019).

CAPÍTULO 3 PETROLOGY OF THE MAFIC DIKE SWARMS OF THE ARAGUAIA BELT: EVIDENCE FOR DISTINCT EVENTS OF INTRACONTINENTAL MAGMATISM IN CENTRAL-NORTHERN BRAZIL.

Danilo José do Nascimento Cruz[1]; Paulo Sergio de Sousa Gorayeb[1]
1 - Universidade Federal do Pará, Instituto de Geociências, Programa de Pós-Graduação em Geologia e Geoquímica (PPGG/IG/UFPA). Av. Augusto Correa Nº 1, 66075-110, Belém-Pará-Brasil (danilocruz@ufpa.br; gorayebp@ufpa.br)

ABSTRACT: N-S and NNW-SEE-trending subparallel mafic dike swarms are intruded into metasedimentary rocks of the Tocantins Group, Araguaia Belt, central-north Brazil. They are under-examined and there is little to no information about their origin and mantellic sources and uncertainty about their ages. Representative mafic dikes from the Santa Maria das Barreiras-Conceição do Araguaia region, at the boundary between the states of Pará and Tocantins, were studied in order to address these problems. It was possible to separate the dikes into two groups: one consisting of diabases affected by the Neoproterozoic regional metamorphism of the Araguaia Belt with varied degrees of transformations and mineral deformation; and the other consisting of unmetamorphosed and undeformed diabases and leucodiabases. The studied dikes are compositionally classified as subalkaline basalts with tholeiitic affinity. However, metadiabases present an arc-like geochemical signature characterized by a pronounced Nb-Ta negative anomaly, whereas leucodiabases and diabases lack a negative Nb-Ta anomaly and show a LREE-enriched pattern, which resembles the signatures of plume-generated basaltic rocks. Both group of dikes were interpreted to be originated in an intracontinental setting with the aid of Ti–V, Zr–Zr/Y and Zr–Ti discrimination diagrams. There is evidence of important contribution of enriched (EN) mantle components in the source of metadiabases and significant contribution of primitive mantle (PM) in the source of both leucodiabases and diabases. We suggested that the metadiabases represent the exposed plumbing system of arc-like intracontinental basalts which precede the regional Neoproterozoic metamorphism of the area and the leucodiabases and diabases represent the exposed conduits of intracontinental basalts whose magmatism succeed the metamorphic event. The rocks from the older event share several similarities with Neoproterozoic mafic rocks from the eastern domain of the Araguaia Belt and nearby Tonian rocks of the 1100 Ma Rincón del Tigre-Huanchaca LIP event, while the rocks from the newer event are remarkably similar to nearby CAMP basalts and diabase dikes.

Keywords: Igneous petrology. Diabase dikes. Intracontinental magmatism. Large Igneous Provinces. Araguaia Belt

3.1 INTRODUCTION

The state-of-the-art in the study of mafic dike swarms has shown that they are important indicators of Large Igneous Provinces (LIP), which are extensive accumulations of predominantly mafic rocks formed by short-lived igneous events that precede the breakup of continents and whose processes fundamentally differ from those of modern plate boundaries. (Ernst, 2014; Ernst et al., 2005). Due to their nature, mafic dikes also provide a window into the Earth's mantle. Therefore, they are key elements to understand the crustal and geodynamic evolution of an area and mantellic processes.

There are several mafic dike swarms in Brazil. The most well-known dikes are from the Mesozoic era, which are – along with sills and flood basalts – linked to the breakup of the supercontinent Pangea and the subsequent opening of the Central Atlantic Ocean. They are part of the Central Atlantic Magmatic Province (CAMP; Marzoli et al., 1999), a LIP whose eruptions occurred around 200 million years ago, at the Triassic-Jurassic boundary. Recently, mafic magmatism associated with the 1100 Ma Rincón del Tigre-Huanchaca LIP event and the breakup of Rodinia has also been reported in the south of the Amazon Craton, northwest of Brazil (Lima et al., 2017; Teixeira et al., 2014).

Nevertheless, there are mafic bodies which are still little known and under-examined in the central-north region of Brazil. They occur as extensive, NNW-SEE-trending, subparallel dike swarms intruded into the low-grade metasedimentary rocks of the western section of the Tocantins Group, Araguaia belt. These swarms were firstly reported by Barbosa et al. (1966) and were assembled in the Conceição do Araguaia-Santa Maria das Barreiras Intrusive Suite by Gorayeb et al. (2017).

Research on their origin and source of these mafic dikes is virtually non-existent and most of the available data, such as petrographic descriptions and geochronological dates, are punctual and scattered and usually comes from reports of large-scale projects or from regional K-Ar geochronological studies. Thus, there is a lack of systematic studies focusing on them.

Furthermore, even the existing data are often inconclusive. For instance, these dikes have been previously described as composed of undeformed and unmetamorphosed diabases and gabbros (Gorayeb, 1981; Hasui et al., 1980; Olivatti et al., 2001; Vale and Neves, 1999), nevertheless, Gorayeb et al. (2017) identified compelling evidence of metamorphic

transformations in samples of the dikes. In addition, the geological significance of the K-Ar dates is difficult to pin down due to their broad distribution: 185-208 Ma, 480-560 Ma, 780 Ma and 1086 Ma (Cunha et al., 1981; Gorayeb, 1981; Hasui et al., 1980; Olivatti et al., 2001). In order to explain the discrepant ages, Hasui et al. (1984) suggested two magmatic events, hardly distinguishable in the field: one in the Neoproterozoic and the other in the Mesozoic. Finally, the available maps of the Conceição do Araguaia-Santa Maria das Barreiras region (Figueiredo and Souza, 2001; Neves and Vale, 1999) do not do justice to the real extension of the dike swarms.

Due to the problems pointed above, the present paper aims to identify and characterize the mafic dike swarms of the Conceição do Araguaia-Santa Maria das Barreiras region, investigate the petrological processes involved in their genesis, make comparisons with nearby mafic rocks and shed light on the hypothesis of distinct magmatic events. In order to do so, it was employed a systematic approach, consisting of aero-geophysical data analysis, geological field mapping, petrography, mineral chemistry and geochemistry.

3.2 GEOLOGICAL SETTING

3.2.1 Araguaia Belt

The Araguaia Belt (AB; Fig. 1) is a Neoproterozoic geotectonic unit that belongs to the Tocantins Structural Province (Almeida et al., 1981), which is the result of the Brasiliano/Pan-African orogeny that was formed from the convergence and subsequently collision among three major continental blocks during the assembly of the West Gondwana between 800 and 550 Ma: the Amazonian and São Francisco-Congo paleocontinents and the Parnaíba block (Alkmim, 2015; Alvarenga et al., 2000; Fuck et al., 2014; Hodel et al., 2019).

The AB has an N-S orientation and is approximately 1,200 km long and over 100 km wide. It borders Archean tonalite-trondhjemite-granodiorite (TTG) terranes and granite-greenstone belts and Paleoproterozoic granitoids of the Amazonian Craton to the west; and Paleoproterozoic gneiss and granulite terranes of the Goiás Massif to the southeast (Alvarenga et al., 2000). On its eastern domain, the Archean basement is exposed in the eroded cores of dome-like structures, represented by the gneisses of the Colméia Complex (2.85 Ga), which are correlated with the TTG suites of the oriental portion of the Amazonian Craton (Gorayeb et al., 2019; Moura and Gaudette, 1993). To the north and east, the belt is covered by sedimentary rocks of the Parnaíba Basin and by Cenozoic deposits.

The AB is one of three Neoproterozoic belts identified as the main constituents of the Tocantins Province together with the Paraguay Belt, developed along the southeastern edge of

the Amazonian Craton, and the Brasília Belt, which margins the São Francisco Craton to the west (Gorayeb et al., 2000; Pimentel et al., 2000). The Araguaia Belt is composed of metamorphosed psammitic and pelitic sequences with minor contributions of carbonaceous metasedimentary rocks, ophiolites and basaltic, gabbroid and granitic bodies (Gorayeb et al., 2008).

The metasedimentary successions were assembled in the Baixo Araguaia Supergroup, which is divided into the Estrondo Group, exposed in the eastern portion of the belt, and the Tocantins Group, occurring in the western and mid-western section (Abreu, 1978). The Estrondo Group is subdivided into the Morro do Campo and the Xambioá formations and is composed of pure and micaceous quartzites sometimes bearing kyanite, pure and impure marbles, several mica schists containing garnet, staurolite and kyanite; graphite schists, feldspathic schists, calc-silicate schists and amphibolite (Gorayeb et al., 2008). The Tocantins Group overlays the former group and is subdivided into the Pequizeiro Formation, which consists of chlorite-muscovite-quartz schists intercalated with calc-schists, quartzites and magnetite-muscovite phyllites, and the Couto Magalhães Formation, which comprises slates, phyllites, meta-arkoses, metasiltstones and quartzite lenses (Gorayeb et al., 2008).

Mafic-ultramafic rocks such as pillow basalts and serpentinized peridotites and dunites are tectonically embedded in the low-grade metasedimentary rocks of the Tocantins Group (Miyagawa and Gorayeb, 2013). They are often interpreted as ophiolites and among the most expressive bodies are the ones of Quatipuru, Serra do Tapa, Morro do Agostinho e Morro Grande (Barros and Gorayeb, 2013; Gorayeb, 1989; Kotschoubey et al., 2005; Miyagawa and Gorayeb, 2013; Paixão et al., 2008; Paixão and Gorayeb, 2014).

Several metamorphosed mafic bodies (scapolite metagabbros, metadiabases, amphibolites, garnet amphibolites) are embedded within the mica schists of the Estrondo Group, in the Xambioá-Araguanã region. They were assembled by Gorayeb et al. (2004) in the Xambica Gabbroic Suite. Some of its gabbro samples were dated and yielded Pb-Pb zircon evaporation dates of 817 ± 5 Ma (Gorayeb et al., 2004) and U-Pb zircon ages of 878 ± 22, 804 ± 35 and 752 ± 23 Ma (Barros, 2010). They are interpreted as continental tholeiites plutons that intruded into the sedimentary sequences of the Estrondo Group, preceding the metamorphism and tectonic evolution of the Araguaia Belt. Furthermore, successions of basalts flows with tholeiitic affinity occur in the volcano-sedimentary sequence of the Tucuruí Group, in the transition zone between the Araguaia Belt and the Amazonian Craton (Dutra, 2012; Dutra et al., 2014).

A set of dikes, which are the object of this study, has been identified in the border region of Pará and Tocantins state intruding into the rocks of the Couto Magalhães Formation (Gorayeb et al., 2017). According to Gorayeb et al. (2017) the dikes are composed of diabases, gabbros and leucogabbros with or without metamorphic transformations. The age of the dikes is not yet well-defined, however, geochronological data is available for a few of their samples: Hasui et al. (1980) obtained K-Ar dates of 780 ± 12, 565 ± 6 and 480 ± 22 Ma for plagioclases from gabbros; a K-Ar isochron date of 197 ± 4 Ma for a diabase dike was reported by Cunha et al. (1981); and Olivatti et al. (2001) reported K-Ar ages of 1086 ± 16 Ma and three K-Ar dates of 185 ± 3 Ma, 198 ± 5 Ma and 202 ± 4 Ma for plagioclases from two distinct diabase dikes.

The syn- to late-kinematic granitic intrusions are associated with medium-grade metamorphic rocks of the Estrondo Group. Their genesis has been related to anatexis of supracrustal sequences during peak metamorphism (Abreu and Gorayeb, 1994; Alvarenga et al., 2000; Dall'Agnol et al., 1988). The Pb zircon evaporation date of 539 ± 5 Ma from the President Kennedy Granodiorite is interpreted as the metamorphism age of the belt (Gorayeb et al., 2019).

The regional metamorphism is Barrovian-type and both deformation and metamorphic grade increase from west toward east, ranging from incipient to medium-grade amphibolite facies, respectively (Gorayeb, 1981; Silva, 1980). Metamorphic zones separated by isograds of sericite, chlorite-epidote-magnetite, biotite, staurolite, garnet and kyanite are recognizable and mappable. Finally, restricted zones of anatexis are recorded by the formation of neosomes consisting of quartz and k-feldpsar in feldspathic biotite schists (Abreu and Gorayeb, 1994; Alvarenga et al., 2000; Gorayeb et al., 2008).

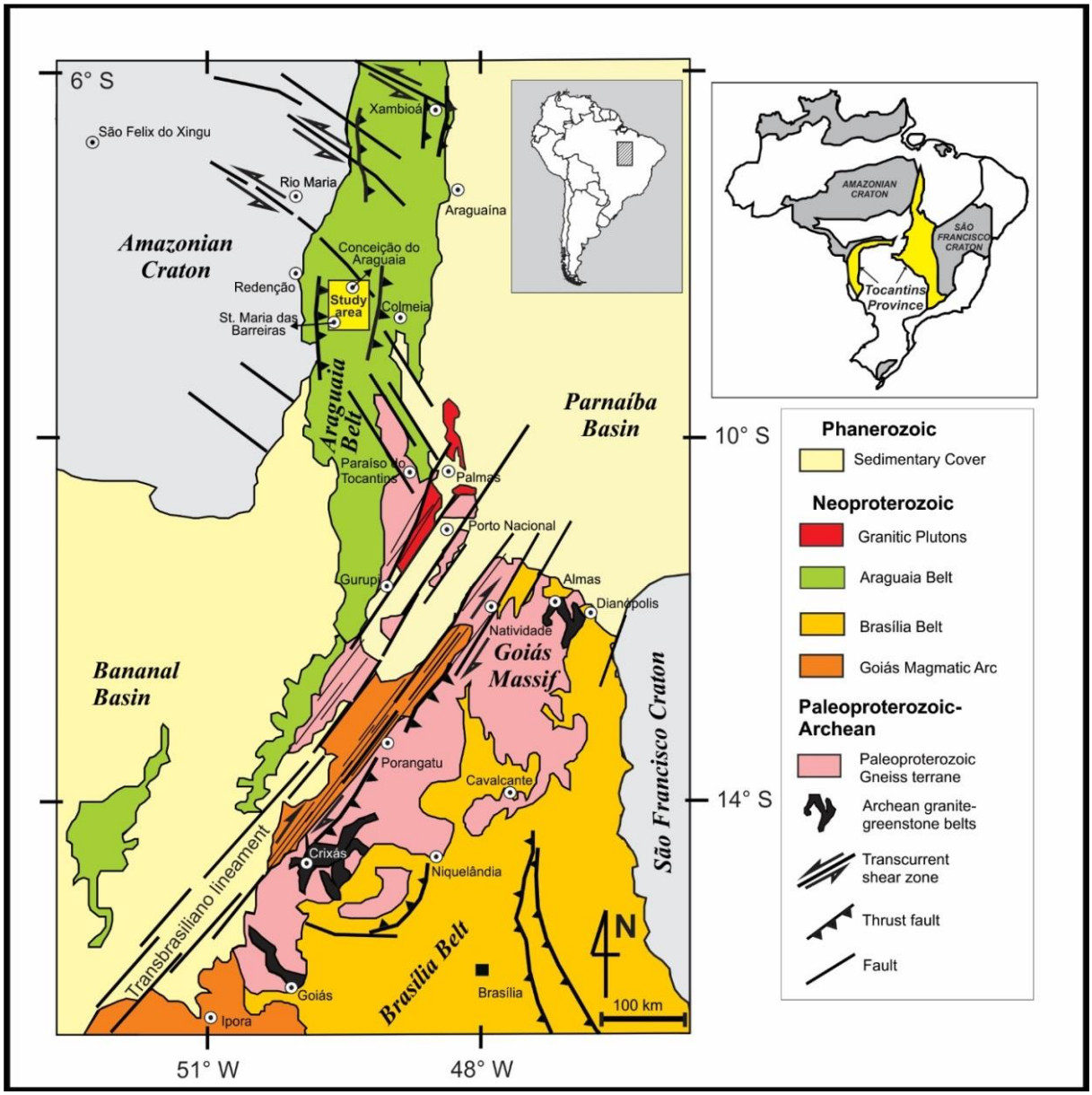

Figure 1 – Regional geologic map of the northern section of the Tocantins Province, highlighting the Araguaia Belt. The study area is represented as a yellow box. Adapted from Gorayeb et al. (2019)

3.2.2 Large Igneous Provinces in the adjacent geological units

Occurrences of mafic magmatism near the study area are mainly represented by mafic dikes, sills and volcanic rocks associated with the CAMP LIP event. For instance, the basalt flows and diabase sills of the Mosquito Formation (Fodor et al., 1990; Merle et al., 2011), in the western section of the Parnaíba Basin; the "Penatecaua" diabase, in the northeastern edge of the Amazonas Basin (Nascimento et al., 2011); the diabase dikes from the São Luís Craton and from the Neoproterozoic Gurupi Belt, north-northeastern Brazil (Klein et al., 2013); the "Cassiporé" diabase from the southeastern edge of the Guiana Shield (Rosa-Costa, 2014) and

dolerite and gabbro dikes from the northern and eastern edge of the Guiana shield (Deckart et al., 2005). According to Klein et al. (2013), the volcanic rocks of the Mosquito Formation and the dikes from the São Luís Craton and the Gurupi Belt are correlated by their geographical proximity and geochemical affinity (Klein et al., 2013). Recently, Mesozoic mafic dikes of the Carajás region, southeast of the Amazonian Craton, have also been associated with the CAMP (Giovanardi et al., 2019; Teixeira et al., 2019).

Episodes of older magmatism relatively close to the study area also occur. The Rio Perdido suite (Lima et al., 2017) is located in the Rio Apa Terrane, southwest portion of the Amazonian Craton, and is linked to the 1100 Ma Ricón del Tigre-Huanchaca LIP event. This suite consists of diabase dikes without signs of deformation and metamorphism.

3.3 MATERIALS AND METHODS

The mapping of the mafic dikes relied heavily on field work and aero-geophysical surveys provided by the Geological Survey of Brazil (CPRM) on their online database (www.geosgb.cprm.gov.br) as those rocks are rarely seen on satellite or radar images and do not form positive reliefs. A pre-field work map was elaborated based on the first vertical derivative of the magnetic field data of the study area, which shows a strong correlation between the dikes and the responses with the highest magnitudes. Then, with the aid of the pre-field work map and previously available maps, it was possible to revisit as well as identify new dikes during the geological field mapping.

27 samples of mafic dikes were collected during the field work. Special care was taken to avoid weathered and altered portions and to collect rocks with an adequate and representative size. 30 μm thick polished thin sections of the collected rock samples and also of 5 samples previously collected by Gorayeb (1981) were made for petrographic studies. In addition, the polished thin sections were also carbon-coated to be suitable for wavelengths dispersive spectroscopy (WDS) analyses.

The WDS analyses were performed in 12 samples at the Microprobe Laboratory of the Geoscience Institute of the University of Brasília (UnB) and in 4 samples at the Microanalysis Laboratory of the Geoscience Institute of the Federal University of Pará (UFPA). Both laboratories are equipped with a JEOL JXA-8230 microprobe with five wavelengths dispersive spectroscopy (WDS) spectrometers and one energy dispersive spectroscopy (EDS) spectrometer. The equipment at UnB operated with column accelerating voltage of 15 kV, current of 10 nA and analysis time of 10 seconds; used the analyzer crystals LDE1 (F), LIF (Ti,

Cr and Mn), LIFH (Ni, Fe and V), PETJ (Ca, K and Cl) and TAP (Na, Mg, Al and Si); and the calibration standards microcline (Al, Si and K), pyrophanite (Ti and Mn), forsterite (Mg), andradite (Ca), albite (Na), vanadinite (Cl and V), topaz (F), Fe_2O_3 (Fe), Cr_2O_3 (Cr) and NiO (Ni). The equipment at UFPA operated with column accelerating voltage of 15 kV, current of 20 nA and analysis time varying from 20 to 40 seconds depending on the element; used the crystals LDE1 (F), LIF (Ni, Fe, Mn, Ba and Ti), PETJ (Cr, Ca, K and Sr), PETH (V) and TAP (Na, Mg, Al and Si); and the calibration standards orthoclase (Si and K), rutile (Ti), anorthite (Al), hematite (Fe), forsterite (Mg), rhodonite (Mn), wollastonite (Ca), sodalite (Na), celestine (Sr), barite (Ba), vanadinite (V) and NiO (Ni).

Twenty-three representative samples were analyzed for major, minor and trace elements at ALS GLOBAL laboratories according to the following procedure. Trimmed and clean slabs of eighteen rock samples were crushed by utilizing a combination of jaw crusher and disk mill, then splits of the crushed samples were grinded into a fine-grained powder in a shatterbox and an agate mill. Major and minor oxides concentrations were obtained by lithium borate fusion digestion and ICP-AES (method ME-ICP06); trace elements, including rare-earth elements, were determined using lithium borate fusion digestion and ICP-MS (method ME-MS81); Co, Cu, Ni and Zn were analyzed by four-acid digestion and ICP-AES (method ME-4ACD81). Further descriptions of ALS GLOBAL's preparation packages and analytical methods can be found at their webpage (www.alsglobal.com/geochemistry).

3.4 GEOLOGY AND PETROGRAPHY

The study area is located at the boundary between the states of Pará and Tocantins, central-north Brazil, and is inserted in the central-western portion of the Araguaia Belt. The main outcropping unit of the area is the Couto Magalhães Formation, which consists of a succession of weakly metamorphosed sedimentary rocks (metasiltstone, metasandstone, metamudstones, metarkoses, metaconglomerate, slate and phyllite). These rocks have preserved sedimentary structures, such as, cross-stratification and plane-parallel bedding as well as mesoscopic antiforms and synforms and recumbent folds with incipient foliation (slate cleavage and fine schistosity).

Intruded in these metasedimentary rocks, extensive mafic dike swarms are found. Based on field data, mineralogical content, texture and microstructural features, it was possible to discriminate between a group of mafic dikes with partial transformations of primary phases and a group of non-metamorphosed and undeformed mafic dikes. The metamorphosed dikes are

mostly found in the bed of the Araguaia river, where they become visible during dry season (Fig. 3a). They extend along several kilometers with N-S and NNW-SSE trends and thicknesses varying from 30 to around 100 m. They are composed of metadiabases, which sometimes might be in association with serpentinized olivine cumulates containing magnetite and apatite. Their outcrops are moderately cut by three sets of fractures with trends NNE-SSW, NE-SW and NW-SE and by quartz and calcite veins (Fig. 3b; 3c). The non-metamorphosed dikes – though also found in the bed of the Araguaia river - are more usually encountered in land, where they occur as spheroidal dark boulders of diabases and leucodiabases roughly aligned with the general NNW-SSE trend (Fig. 3d; 3e). Both types of dikes occur close to outcrops of metasedimentary rocks of the Couto Magalhães Formation, such as, meta-arenites, slates and phyllites (Fig. 3f).

N-S-trending elongated ophiolites are tectonically emplaced in the rocks of the Couto Magalhães Formation. The most significant bodies are the Serra do Quatipuru (western area), Morro do Agostinho (near Araguacema) and the ones located in the center of the area, such as Morro Grande, Salto, Pau Ferrado and Serrinha (Gorayeb, 1989). They are composed of serpentinized peridotites and dunites, chromitites, pillow basalts and ferruginous cherts which are affected by incipient metamorphism.

The Pequizeiro Formation occurs in the eastern portion of the area and is represented by a set of schists with varying proportions of quartz, chlorite, muscovite and biotite in addition to phyllites, calc-schists and quartzites. These rocks exhibit N-S oriented schistosity and banding and antiform and synform folds. However, the most remarkable structures are the N-S oriented subvertical or subhorizontal crenulation cleavages.

Additionally, alluvial deposits of the Araguaia River and its tributaries and laterite deposits are registered in the area. Nickel laterite ore deposits are encountered on the summit of hills and on slopes. They are a product of intense weathering of the serpentinites (Paixão and Gorayeb, 2014) and are currently being explored by nickel and platinum-group metal (PGM) mining companies.

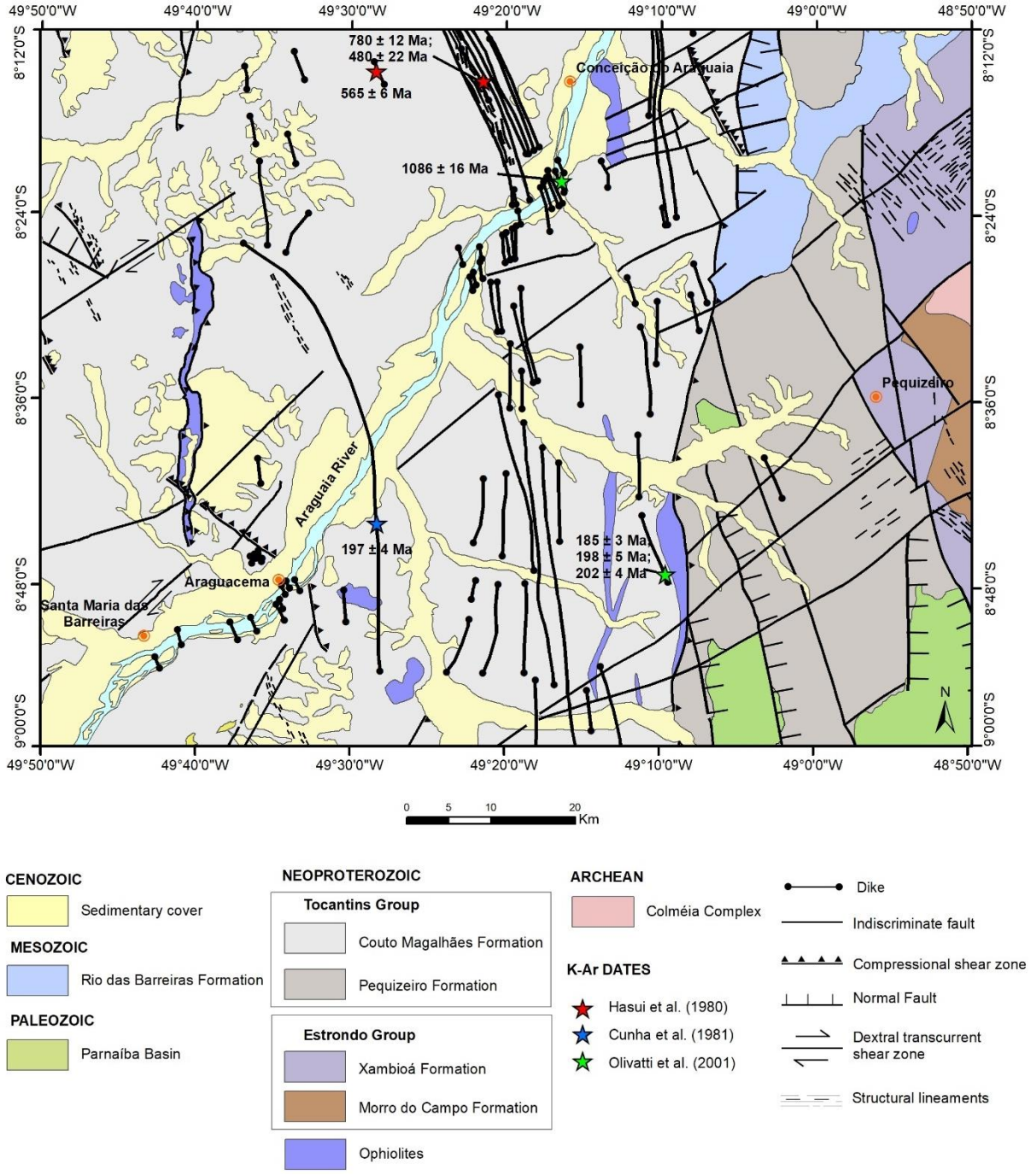

Figure 2 - Geological map of the study area with the available geochronological data for the mafic dikes. Modified from Figueiredo and Souza (2001) and Neves and Vale (1999).

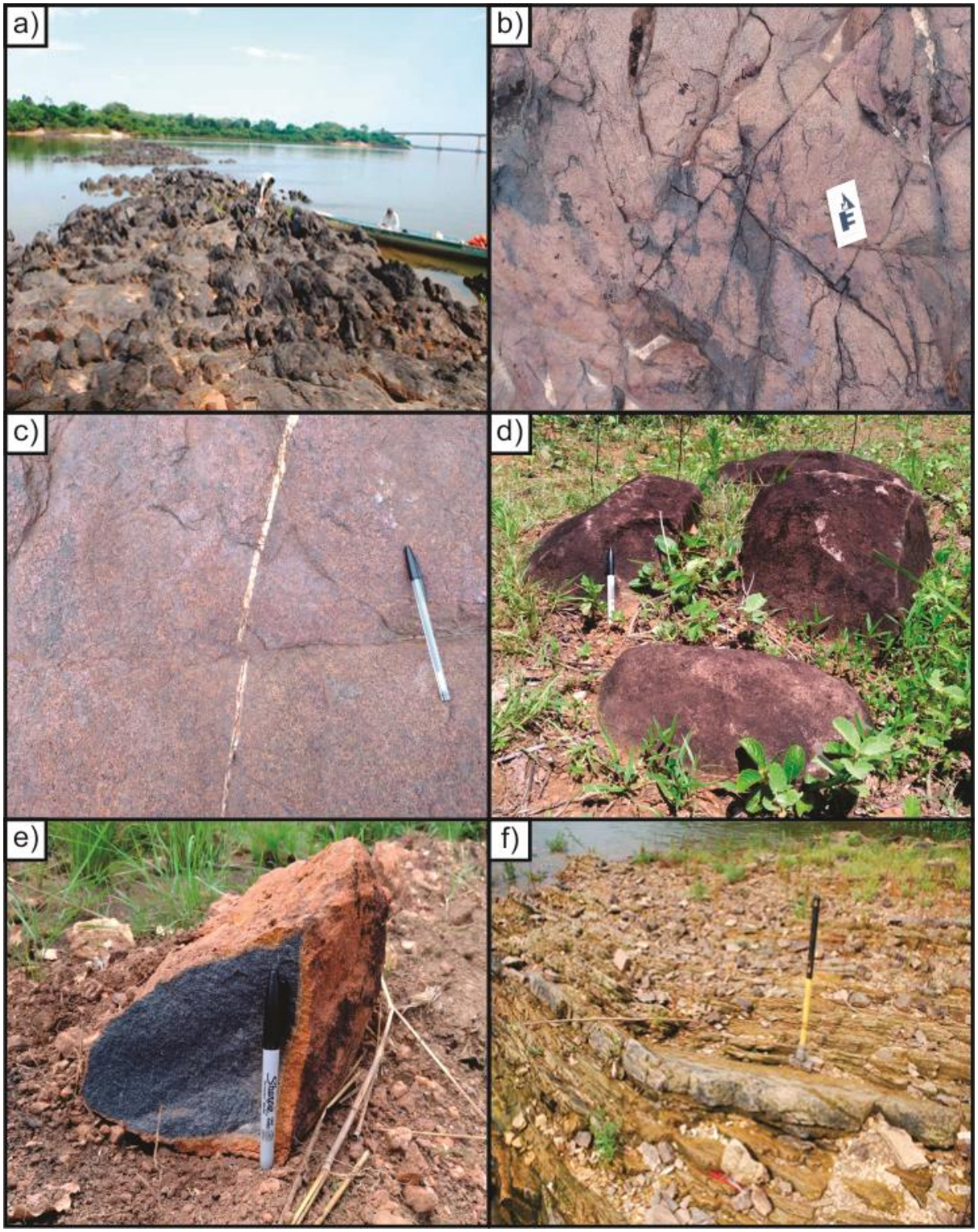

Figure 3 – General field aspects of the mafic dikes: a) Dikes of metadiabase crossing the Araguaia River; b) Fractured outcrop of metadiabase; c) a fracture cross-cutting a quartz vein in a metadiabase; d) boulders of diabases in land; e) a close-up of a gray-colored diabase; f) Meta-arenites of the Couto Magalhães Formation by the bank the of Araguaia River.

3.4.1 Metadiabases

The metadiabases are dark gray, mesocratic to melanocratic (M'=42-72), holocrystalline and medium-grained, with grain sizes ranging from 1 to 3 mm in diameter depending on the thickness of the dike and on whether the rock is in its center or border. Plagioclase and clinopyroxene are the dominant primary phases in all metadiabase samples, and ilmenite and sulfides are ubiquitous. In the most evolved rocks, hornblende, biotite and quartz are present as minor phases. Apatite and opaque minerals are common accessory minerals phases. To a greater or lesser extent depending on the sample, breakdown of primary phases takes place, generating a metamorphic paragenesis.

Plagioclase (28 – 55 %; 0.8 – 4 mm) forms randomly oriented, subhedral crystals with tabular habit or lath-shaped. It is partly or almost entirely replaced by aggregates of sericite, tiny epidote and occasionally calcite, leaving its remainders more albitic (Fig. 4a). It might show albite twinning, though it is usually obliterated by the transformations.

Subhedral, prismatic clinopyroxene (32 – 62 %; 0.5 – 3 mm) occupies the angular space between the plagioclase laths, typical of the intergranular texture (Fig. 4a). It can be either well-preserved with only uralitized borders or it can be partly replaced by a metamorphic patch of randomly acicular actinolite and fine-grained chlorite (Fig. 4b). Simple twinning in the well-preserved crystals are not uncommon.

Hornblende (0 – 16 %; 0.8 – 1.2 mm) is moderately pleochroic with X = yellowish-brown, Y = reddish-brown and Z = dark brown. It can occur as euhedral, prismatic individual crystals (Fig. 4c) or as irregular grains mantling clinopyroxene (Fig. 4d). Some hornblendes have been subjected to mild chloritization. Simple twinning is observed in a handful of crystals and inclusions of opaque minerals, apatite and biotite are present.

Quartz (0 – 4 %) can occur : a) as anhedral crystals (~ 0.2 mm) occupying the interstitial space between plagioclase laths, usually with undulose extinction; b) in myrmekitic intergrowth with plagioclase; c) in micrographic intergrowth with alkali-feldspar (Fig. 4d); d) and as anhedral crystals (0.3 – 0.6 mm) associated with calcite in veins.

Biotite (0 – 3 %; ~ 0.2 mm) forms subhedral, lamellar grains. It is strongly pleochroic with X = pale yellow and Y-Z = dark reddish-brown. Some crystals are partly or entirely replaced by chlorite. Deformed biotite with kink-band features is not uncommon.

Apatite crystals (0 – 1 %; ~ 0.05 mm) are euhedral and acicular. They are normally included in plagioclase and quartz. Opaque minerals (0.4 – 11 %) are represented mostly by

millimetric, subhedral aggregates of chalcopyrite and pyrite and by trellis-type ilmenite lamellae in remnants of titanomagnetites, which are now replaced by titanite.

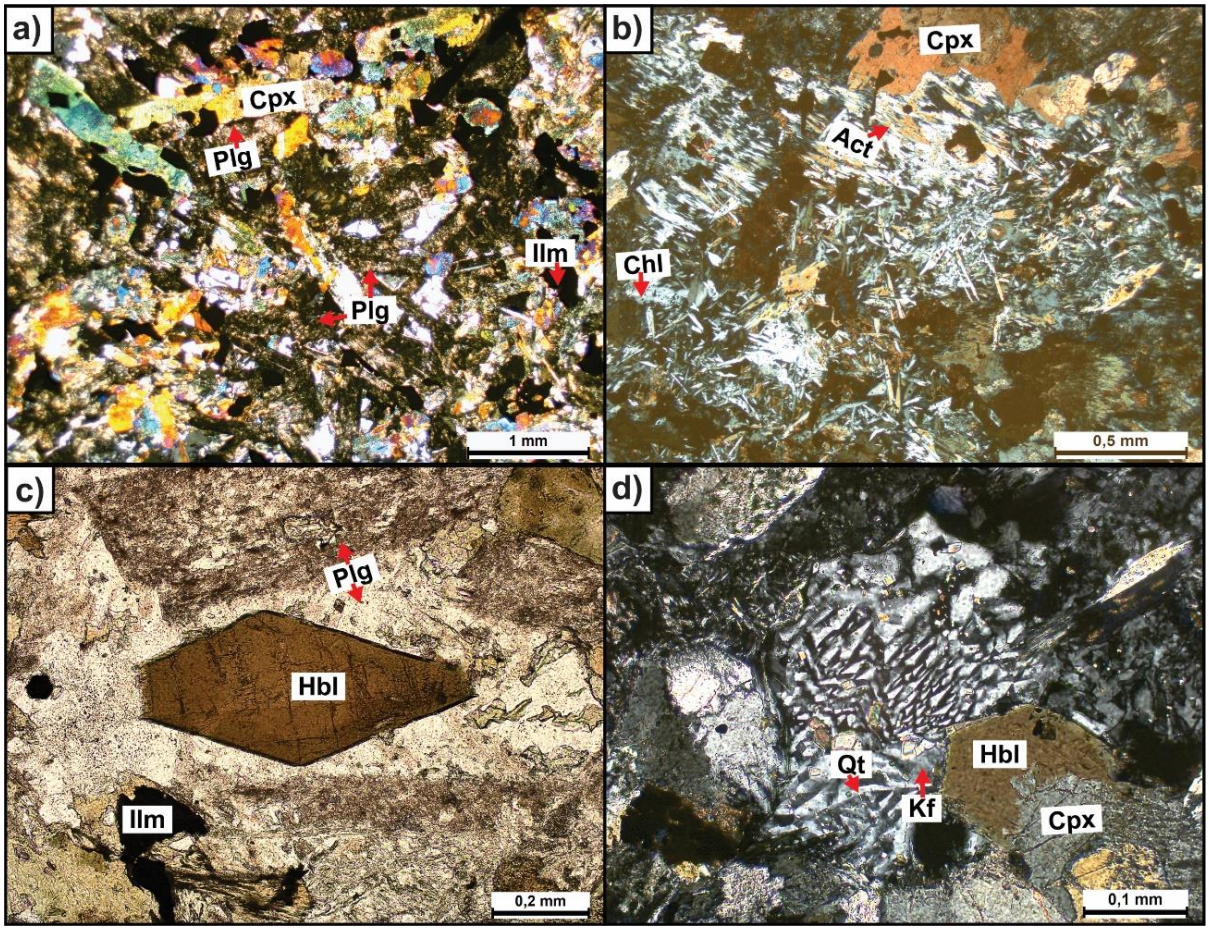

Figure 4 – General petrographic characteristics of metadiabases: a) Clinopyroxene and saussuritized plagioclase in an intergranular arrangement (DA-28); b) Clinopyroxene replaced by actinolite and chlorite (DA-17); c) Euhedral, dark-brown hornblende associated with plagioclase (DA-21); and d) Micrographic intergrowth of quartz and alkali-feldspar filling interstitial space. Note dark-brown hornblende mantling clinopyroxene (DA-06). Photomicrographs a), b) and c) are under cross-polarized light.

3.4.2 Diabases and leucodiabases

The diabases are gray, mesocratic (M'=43-50), holocrystalline and medium-grained, with grain size ranging from 1 to 2 mm. Labradorite and clinopyroxene are the dominant phases and apatite, quartz, pyrite and ilmenite are accessories. The main texture is intergranular, which is evidenced by the occurrence of clinopyroxene within the angular space between the laths of plagioclase (Fig. 5a). Labradorite (An_{57-60}; 0.8 – 1,2 mm) comprises between 49 and 56% of the volume of these rocks. It forms subhedral or euhedral laths with polysynthetic twinning. Sometimes the plagioclase grains may be sericitized. Clinopyroxene (35 – 43 %; 1 – 2 mm) occur as subhedral, prismatic, colorless crystals without pleochroism. Augites with simple twinning are common. Euhedral, acicular apatite inclusions (~0.1 mm) are ubiquitous .

The leucodiabases are light gray, leucocratic (M'=32-35), holocrystalline and medium-grained, with grain size varying from 3 to 4 mm. They are composed essentially of labradorite and clinopyroxene, but olivine may occur as a minor component. Apatite, quartz, alkali-feldspar, chalcopyrite and ilmenite are accessory phases. Like the diabases, the main texture is intergranular (Fig. 5b), however, subophitic texture is observed in portions where the plagioclase laths occur inside large pyroxene crystals (Fig. 5c). Micrographic intergrowth between quartz and alkali-feldspar is also present. Labradorite (An_{51-53}; 2.5 – 3 mm) comprises between 60 and 62% of the mode and forms subhedral laths or tabular-shaped crystals. Its grains may exhibit compositional oscillatory zoning (Fig. 5d), polysynthetic twinning and may show weak to moderate sericitization. Clinopyroxene (22 – 28 %; 2 – 4 mm) forms subhedral, prismatic, colorless crystals without pleochroism. Some of its grains exhibit simple twinning and/or deuteric alteration to uralite. Olivine (2 – 6 %; ~3 mm) occurs as anhedral and granular grains. Iddingsite may be found as pseudomorphs after olivine or along microfractures of olivine. Inclusions of euhedral, acicular apatite (~0.1 mm) are ubiquitous.

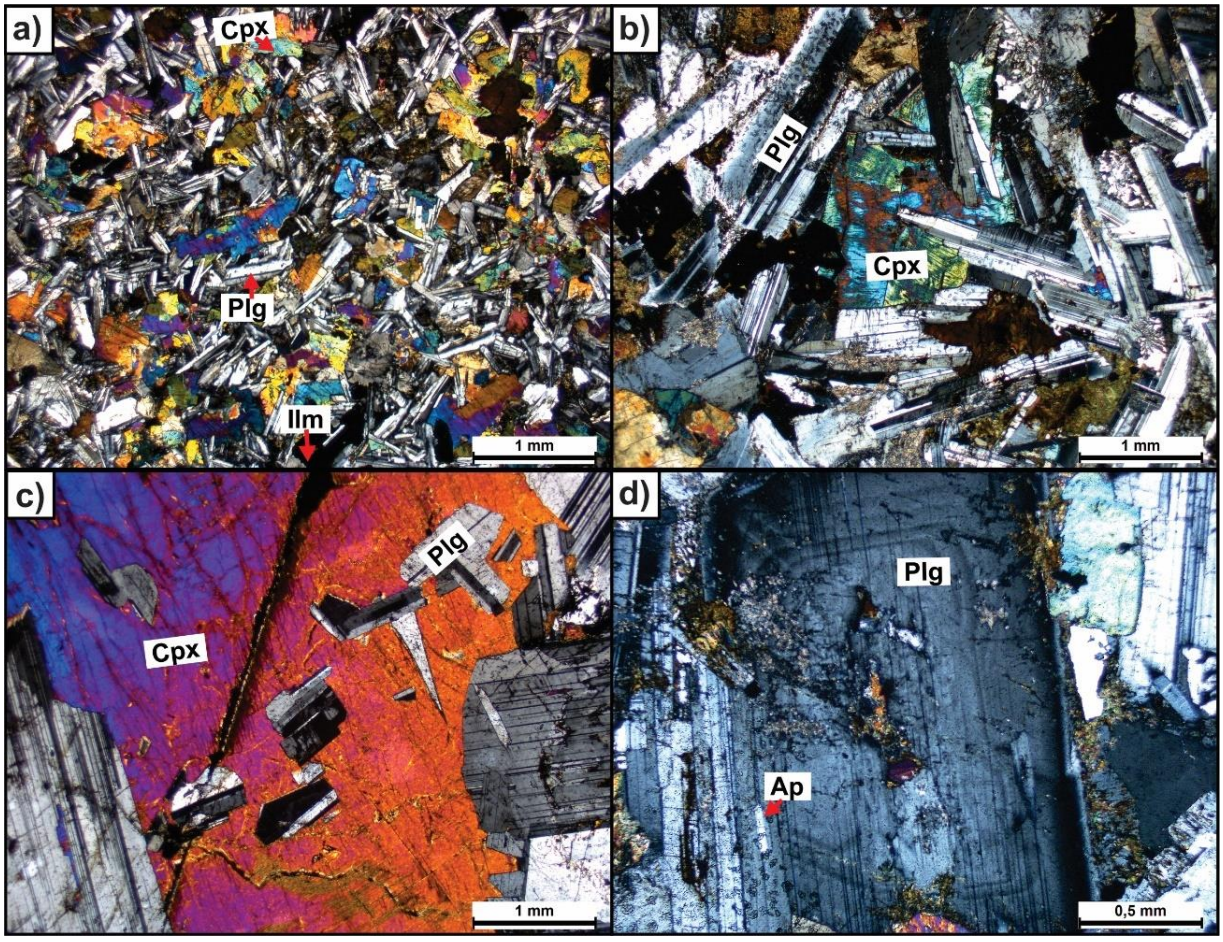

Figure 5 – General petrographic characteristics of diabases: a) Clinopyroxene and plagioclase in an intergranular texture in diabase (17-DA-02); b) Clinopyroxene occupying the interstices of the plagioclase laths in a

leucodiabase (DA-25); c) Inclusions of plagioclase enclosed in large crystal of clinopyroxene in a leucodiabase (DA-25); and d) Compositional zoning in an euedral plagioclase with inclusions of apatite (78-DA-04). All figures under cross-polarized light.

In Table 1, a summary of the mineralogical content of leucodiabases, diabases and metadiabases is shown. For the metadiabases, the estimated mode of the parent rock was calculated from 16 samples where minerals are well-preserved or where the metamorphic minerals can be reliably traced back to the original magmatic minerals. It was assumed that metamorphic transformations occurred at constant volume. 1,500 points were counted for the estimations. The rocks were classified as gabbros and quartz gabbros in the QAP ternary diagram (Streckeisen, 1976; Fig. 7a). Then, they were plotted in the Plg-Px-Ol and Plg-Px-Hbl classification diagrams for gabbroic rocks (Le Maitre et al., 2002; Fig. 7b) and were further classified in the Plg-Opx-Cpx diagram (Le Maitre et al., 2002; Fig. 7c), where they fell within the gabbro field. Due to medium grain size of the rocks, the term diabase was preferred. The color index was used as a prefix to differentiate diabases from leucodiabases and the prefix meta was used to differentiate the metamorphosed rocks from the non-metamorphosed.

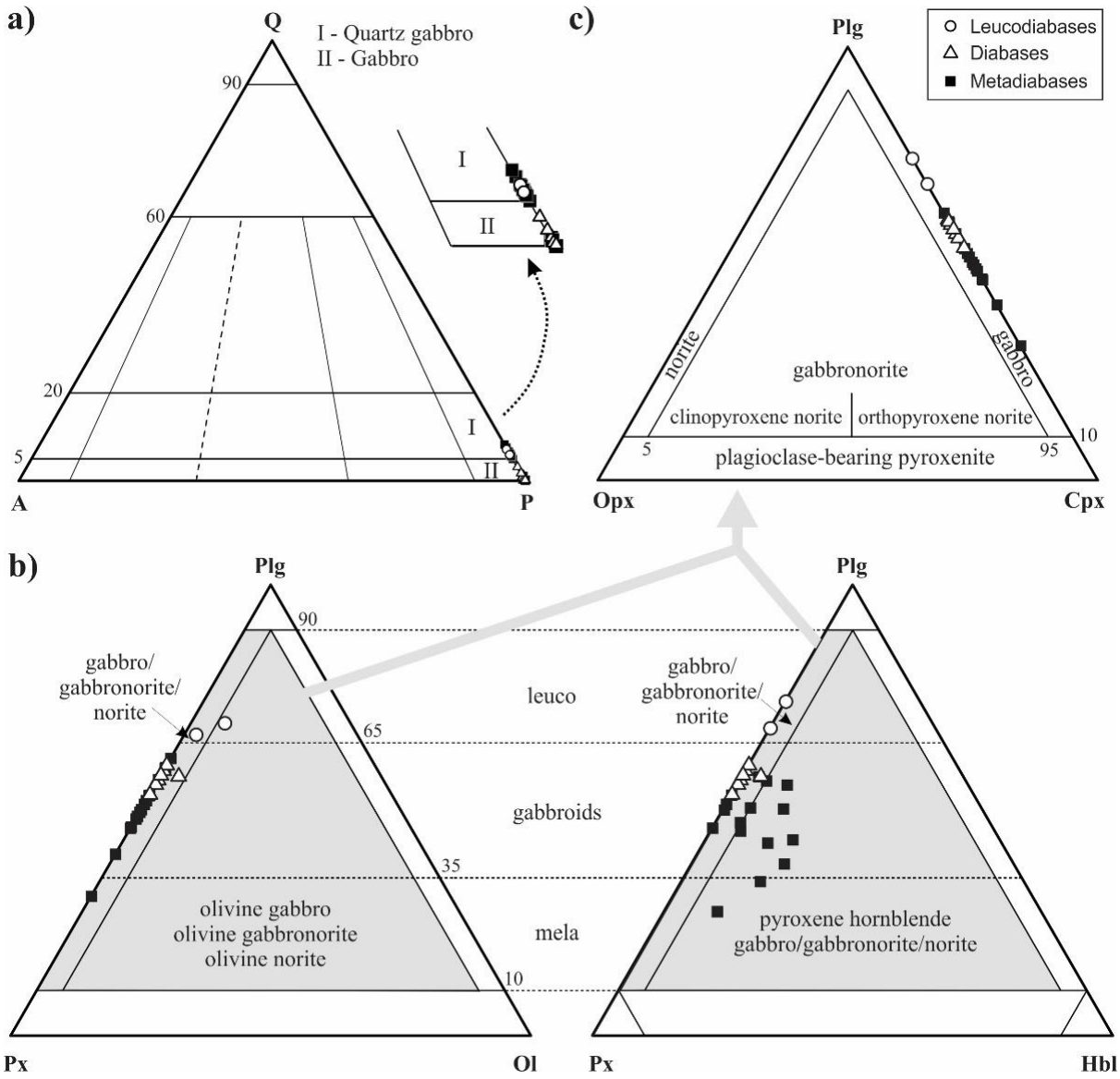

Figure 6 – Classification digrams for the studied rocks based on mineral proportions. a) Q-A-P classification diagram for plutonic rocks (after Streckeisen, 1976); b) Pl-Px-Ol and Pl-Px-Hb classification diagrams for gabbroic rocks (after Le Maitre et al., 2002); c) Plg-Opx-Cpx classification diagram to further divide the rocks which fell within the shaded area in Figure 6b (after Le Maitre et al., 2002).

Table 1 – Mode and estimated mode for the metadiabase, diabase and leucodiabase samples (in volume per cent).

Rock	Leucodiabases		Diabases							Metadiabases															
Sample / Mineral	DA-25	78-DA-04	17-DA-01	17-DA-02	78-DA-01	78-DA-02	78-DA-03	78-DA-05	78-DA-08	DA-01	DA-05	DA-07	DA-09	DA-12	DA-13	DA-15	DA-16	DA-17	DA-18	DA-19	DA-20	DA-21	DA-23	DA-24	DA-27
Plg	61.9	60.4	51.5	55.6	56.3	50.9	52.4	51.9	49.3	40.7	40.2	47.7	35.2	33.5	27.5	48.3	47.2	48.6	38.4	48.6	50.0	51.9	54.6	42.1	45.3
Cpx	21.5	28.0	39.3	39.0	37.5	37.2	35.5	41.2	42.8	42.8	36.8	36.2	40.7	49.6	61.7	47.9	41.4	42.4	44.9	46.0	33.9	32.4	37.4	45.3	46.0
Hbl	-	-	-	-	-	-	-	-	-	11.7	15.5	10.9	16.4	14.8	10.0	0.2	4.7	-	-	-	4.5	8.9	3.0	5.3	4.5
Bt	-	-	-	-	-	-	-	-	-	0.3	-	-	1.2	-	0.1	0.4	-	-	2.9	0.2	1.7	0.3	-	0.1	0.5
Qt	4.8	3.8	0.1	-	0.5	1.6	0.1	-	0.8	3.3	3.3	3.1	-	0.3	0.2	2.5	3.4	4.4	2.7	3.0	3.3	3.0	3.5	2.5	3.0
Ap	0.9	0.9	0.1	-	-	0.3	0.2	-	-	-	0.6	0.2	0.7	-	0.1	-	-	-	0.2	0.5	0.8	-	0.1	0.3	-
Kfs	0.1	-	-	-	-	-	0.1	-	-	-	-	-	-	-	-	-	-	-	-	-	-	-	-	-	-
Op	5.0	4.9	9.0	5.4	5.8	9.9	8.5	6.7	7.1	1.2	3.6	1.9	5.8	1.8	0.4	0.7	3.3	4.6	10.9	1.7	5.8	3.5	1.4	4.4	0.7
Ol	5.8	2.0	-	-	-	-	3.2	-	-	-	-	-	-	-	-	-	-	-	-	-	-	-	-	-	-

3.5 GEOCHEMISTRY

3.5.1 Alteration and element mobility

Whole-rock geochemical data for 23 gabbroic samples are presented in Table 2. The loss on ignition (LOI) content of both leucodiabases (1.16 - 2.57 wt.%) and diabases (0.42 - 1.18 wt.%) is relatively low, whereas the content in metadiabases is high (3.77 - 4.99 wt.%), probably due to hydration associated with incipient metamorphic transformations. To evaluate the possible effects of post-magmatic alteration, the rocks were plotted in an igneous spectrum diagram (Fig. 7) derived from Hughes (1972). All leucodiabases and diabases fell within the igneous spectrum field and are, thus, unlikely to have undergone post-magmatic alteration. Four samples of metadiabase fell outside the igneous field, suggesting the influence of the metamorphic transformations on the chemistry of at least a few of their samples.

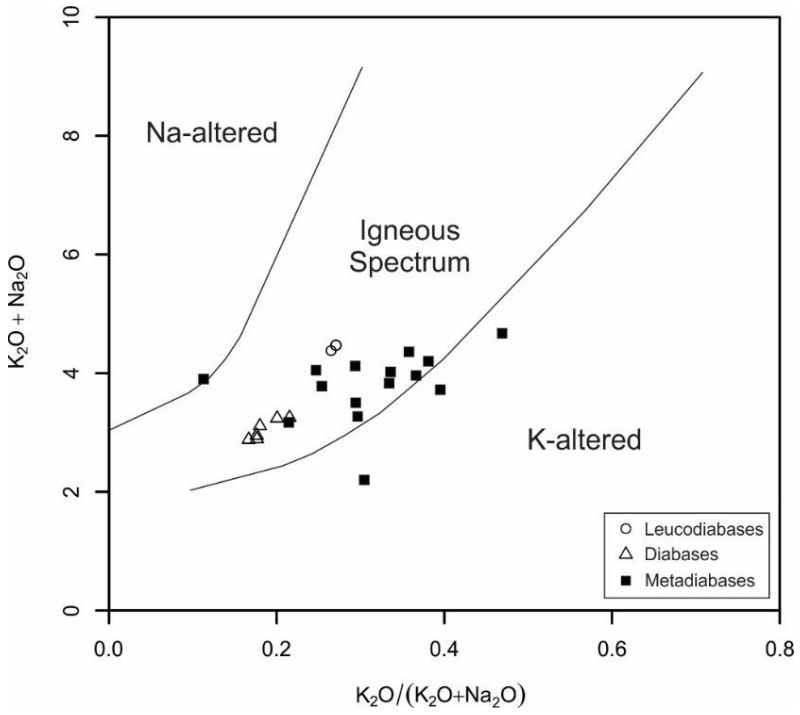

Figure 7 – $K_2O + Na_2O$ vs. $K_2O/(K_2O+Na_2O)$ diagram for evaluation of post-magmatic alteration (after Hughes, 1972), with data from the studied rocks.

Bearing that in mind, the mobility of the elements in the metadiabases was further assessed by employing a method proposed by Cann (1970), which consists of constructing bivariate diagrams with a generally accepted immobile element on the horizontal axis and an element to be evaluated on the vertical axis. According to the method, if the samples are cogenetic and the two elements are immobile, there should be a strong correlation between

them. Yttrium was used on the horizontal axis since it demonstrates immobility during hydrothermal alteration and metamorphism (MacLean and Barrett, 1993).

In the Figure 8, bivariate diagram of Y versus selected elements are shown with their respective correlation coefficient. Very strong spearman rank-order correlation coefficients (ρ >0.7 or <-0.7) between Y and rare earth elements (REE); high field strength elements (HFSE) such as Nb, Ta, Hf, Th, U and Zr; and some major elements (Mg, Ca, Ti and P) indicate they are immobile. In contrast, most transition metal elements (V, Co, Cu, Cr and Ni); large-ion lithophile elements (LILE) such as Rb, Sr and Ba; and the major elements Na, Si, Al and Fe are weakly correlated with Y and are likely to have been mobilized. Therefore, in order to make petrogenetic interpretations about the metadiabases and draw comparisons between them and the leucodiabases and diabases, this study will use only the elements which were evaluated as immobile.

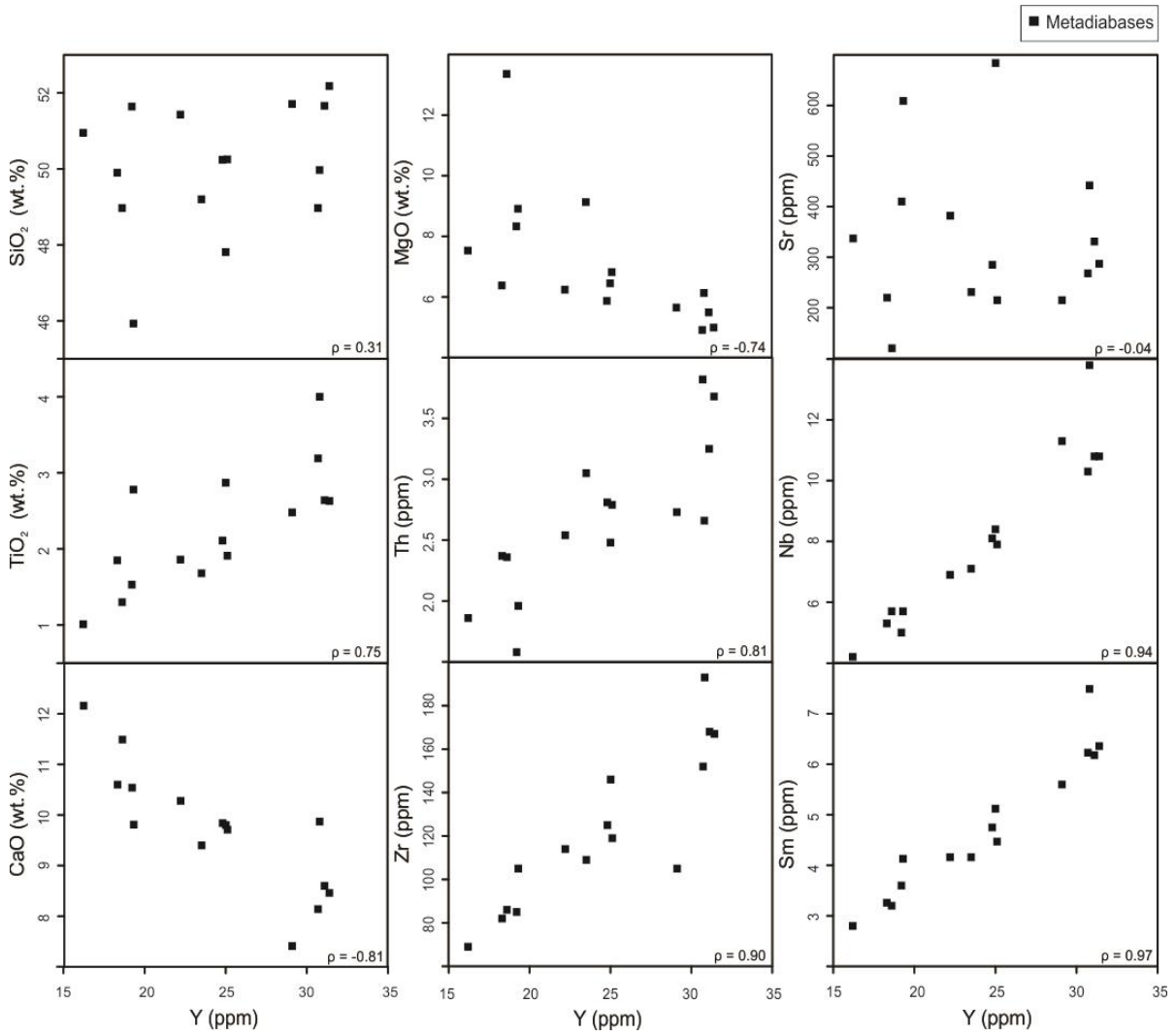

Figure 8 – Bivariate diagrams between selected elements and Y for evaluation of element mobility. Elements with very strong spearman rank-order correlation coefficients (ρ >0.7 or <-0.7) were considered immobile, whereas the others were considered immobile.

Table 2 – Whole-rock major and trace element data for the studied rocks.

	Leucodiabases		Diabases						Metadiabases														
Samples	DA-25	78-DA-04	17-DA-01	17-DA-02	78-DA-01	78-DA-02	78-DA-03	78-DA-05	DA-08	DA-09	DA-11	DA-12	DA-13	DA-15	DA-17	DA-18	DA-19	DA-20	DA-21	DA-22	DA-23	DA-24	DA-27
Major elements (w.t.%)																							
SiO_2	50.30	50.60	48.80	48.80	48.60	46.30	51.60	51.70	48.00	43.90	45.80	47.20	47.10	49.50	49.10	47.70	47.90	48.10	49.50	49.80	49.50	46.90	48.80
TiO_2	2.71	3.09	2.96	2.80	2.91	3.40	2.74	2.72	1.78	2.66	2.75	1.61	1.25	1.47	2.51	3.82	1.82	2.02	2.37	2.51	1.79	3.06	0.97
Al_2O_3	15.80	14.95	12.80	12.95	13.90	14.05	13.80	13.00	13.75	10.85	12.85	11.40	8.68	13.40	13.65	12.85	13.90	14.45	13.30	13.50	14.85	13.00	15.10
Fe_2O_3 (t)	13.05	14.55	16.95	16.20	15.80	15.50	15.90	16.10	13.05	16.60	14.55	13.55	13.15	10.40	12.85	12.85	12.45	13.35	13.45	12.90	10.45	15.30	10.20
MnO	0.21	0.21	0.24	0.23	0.19	0.22	0.21	0.23	0.18	0.21	0.20	0.21	0.20	0.19	0.18	0.16	0.19	0.21	0.19	0.20	0.16	0.21	0.16
MgO	2.86	3.34	5.95	6.10	4.55	5.00	4.91	6.03	6.14	8.52	6.18	8.76	12.85	7.99	5.22	5.85	6.50	5.62	5.41	4.76	6.01	4.70	7.21
CaO	8.25	7.95	9.88	9.95	9.59	9.49	9.66	9.85	10.20	9.38	9.39	9.02	11.05	10.10	8.17	9.42	9.26	9.42	7.09	8.07	9.89	7.80	11.65
Na_2O	3.18	3.18	2.40	2.35	2.57	2.54	2.53	2.39	2.71	2.38	3.31	2.16	1.47	2.56	2.39	2.36	2.77	2.68	2.37	2.91	2.45	2.49	2.20
K_2O	1.18	1.15	0.51	0.50	0.64	0.70	0.56	0.48	0.92	0.65	0.42	1.41	0.64	1.29	1.38	0.98	1.15	1.49	2.10	0.95	1.23	1.53	0.93
P_2O_5	0.79	0.65	0.26	0.27	0.28	0.39	0.28	0.28	0.10	0.15	0.23	0.16	0.11	0.14	0.28	0.29	0.18	0.19	0.22	0.28	0.18	0.24	0.09
LOI	2.57	1.16	1.18	1.12	0.91	0.47	0.74	0.42	3.84	4.40	4.20	4.04	3.83	4.19	4.99	4.58	4.72	4.33	4.28	4.58	3.77	4.20	4.29
Total	100.90	100.83	101.93	101.27	99.94	98.06	102.93	103.20	100.67	99.70	99.88	99.52	100.33	101.23	100.72	100.86	100.84	101.86	100.28	100.46	100.28	99.43	101.60
Mg#	30.24	31.27	41.02	42.73	36.31	38.98	37.97	42.57	48.23	50.40	45.69	56.16	65.94	60.33	44.58	47.43	50.85	45.48	44.34	42.24	53.23	37.85	58.35
Trace elements (ppm)																							
V	178	272	548	497	529	518	520	524	528	573	422	295	263	249	335	424	325	370	399	320	261	488	236
Cr	10	50	90	140	70	70	110	170	130	390	220	500	1080	220	50	110	150	70	10	20	70	<10	60
Co	26	32	46	47	45	42	47	45	48	71	53	62	71	41	41	43	47	42	43	38	38	50	47
Ni	20	25	67	83	40	61	61	74	59	231	144	268	337	94	44	127	101	75	47	32	59	24	64
Cu	638	635	341	381	343	532	320	349	61	79	75	123	148	63	39	169	79	78	51	37	51	57	77
Zn	140	147	130	126	123	145	118	111	90	119	116	112	89	75	96	101	99	88	113	103	87	120	68
Ga	31.5	29.5	25.3	23.9	27.5	27	25.9	24.6	24.7	25.7	29.3	21.6	16.4	21.5	27.7	25.9	23.5	24.3	23.4	26.1	24.5	28.6	21.6
Rb	34.4	35.2	12.4	12.4	16.7	20.2	14.1	11.4	33.6	16.8	14	45.7	23.1	38.9	40.6	25.1	38.1	55.2	79.9	37.5	41.5	55	29.6
Sr	344	356	248	242	287	221	268	233	220	609	684	231	120	410	331	442	215	285	215	287	382	268	337
Y	67.8	57.1	37.7	37.1	42.2	42.2	40.3	35.6	18.3	19.3	25	23.5	18.6	19.2	31.1	30.8	25.1	24.8	29.1	31.4	22.2	30.7	16.2
Zr	493	428	189	186	206	271	190	196	82	105	146	109	86	85	168	193	119	125	105	167	114	152	69
Nb	34.7	30.9	12.8	12.1	10.7	16.2	11.7	11.4	5.3	5.7	8.4	7.1	5.7	5	10.8	13.8	7.9	8.1	11.3	10.8	6.9	10.3	4.2
Cs	2.06	2.94	1.02	0.41	0.5	1.47	0.76	0.51	0.77	0.49	0.97	0.94	1.11	0.87	0.71	1.21	0.93	1.84	1.27	1.22	1.08	1.32	0.85
Ba	387	328	127	133.5	192	194	158	131	196.5	204	174	263	159	378	371	311	234	493	514	218	339	471	191.5
La	42	34.1	13.2	13.5	12.9	17.7	13.9	13.7	10.1	10.2	13.8	12.1	9.7	9.5	18.9	19.1	12.8	13	14.9	19.3	13.6	19.8	8.3
Ce	103	82	34.3	35.5	31.8	43	35.3	34.6	22.3	24	32.1	27.8	21.8	21.7	43.3	44.8	29	29.9	35	45	29.3	42.1	18.1
Pr	13.5	11.75	4.89	4.8	5.06	6.68	5.19	5.28	2.91	3.04	4.22	3.59	2.74	2.87	5.33	6.15	3.72	3.82	4.68	5.46	3.82	5.21	2.32
Nd	62.9	54.2	23.9	24.4	26.1	33.5	25.9	24.7	12.2	14.5	19.3	15.9	12.1	13	24.4	28.3	17.5	17.8	21.4	25.6	17.5	23.7	10.3
Sm	15.15	12.7	6.24	6.44	7.09	8.4	6.75	6.85	3.26	4.13	5.12	4.16	3.2	3.6	6.18	7.49	4.47	4.75	5.6	6.36	4.16	6.23	2.8
Eu	4.82	3.76	2.27	2.24	2.2	2.67	2.22	2.02	1.15	1.46	2.01	1.33	1.13	1.36	2.1	2.5	1.46	1.56	1.92	2.13	1.67	2	0.98
Gd	15.9	13.05	7.58	7.39	8.32	9.46	7.98	7.3	3.6	4.74	6.29	5.04	3.82	4.21	6.58	7.53	4.97	5.76	6.06	6.94	4.76	6.52	3.41
Tb	2.35	2	1.17	1.21	1.23	1.31	1.25	1.14	0.58	0.66	0.84	0.79	0.57	0.63	1.04	1.12	0.78	0.9	0.94	1.09	0.72	0.99	0.52
Dy	13.15	11.35	7.25	6.71	7.54	8.41	7.46	6.84	3.45	4.11	5.24	4.49	3.66	3.76	5.92	6.27	4.45	4.92	5.95	6.12	4.1	5.87	3.16
Ho	2.63	2.22	1.49	1.45	1.52	1.55	1.52	1.38	0.71	0.79	1.06	0.88	0.73	0.79	1.12	1.2	0.95	0.96	1.2	1.22	0.84	1.15	0.63
Er	7.18	6.43	3.75	3.59	4.32	4.53	4.06	4.15	1.82	1.8	2.6	2.26	1.99	1.85	2.96	3.02	2.4	2.65	2.99	3.02	2.24	3.02	1.68
Tm	0.86	0.75	0.56	0.51	0.59	0.67	0.58	0.59	0.23	0.26	0.36	0.29	0.23	0.22	0.39	0.4	0.33	0.36	0.39	0.4	0.29	0.39	0.19
Yb	5.4	5.17	3.5	3.37	3.6	3.85	3.47	3.19	1.46	1.48	2	2	1.56	1.51	2.47	2.27	2.16	2.27	2.53	2.75	1.72	2.39	1.38
Lu	0.85	0.64	0.48	0.5	0.54	0.55	0.45	0.44	0.25	0.22	0.29	0.29	0.26	0.23	0.37	0.35	0.34	0.34	0.38	0.41	0.29	0.35	0.2
Hf	12.3	10.6	5.3	5.4	5.6	7.3	4.9	5.2	2.5	3	4.3	3.4	2.5	2.6	4.9	5.3	3.5	3.4	3.2	4.9	3.3	4.4	2.1
Ta	2.2	2	0.8	0.8	1	1.4	0.9	0.9	0.4	0.4	0.6	0.5	0.4	0.4	0.8	0.9	0.6	0.5	0.8	0.8	0.5	0.7	0.4
Th	4.29	3.37	1.37	1.3	1.36	1.93	1.31	1.3	2.37	1.96	2.48	3.05	2.36	1.58	3.25	2.66	2.79	2.81	2.73	3.68	2.54	3.82	1.86
U	1.25	0.94	0.37	0.4	0.38	0.58	0.37	0.37	0.47	0.39	0.51	0.6	0.47	0.32	0.63	0.49	0.53	0.6	0.36	0.66	0.49	0.64	0.35
Eu/Eu*	0.95	0.90	1.01	1.00	0.88	0.92	0.93	0.88	1.03	1.01	1.09	0.89	0.99	1.07	1.01	1.02	0.95	0.92	1.01	0.99	1.15	0.96	0.97
$(La/Yb)_N$	5.19	4.40	2.51	2.67	2.39	3.06	2.67	2.86	4.61	4.59	4.60	4.03	4.15	4.19	5.10	5.61	3.95	3.82	3.93	4.68	5.27	5.52	4.01
$(Th/Nb)_N$	1.04	0.91	0.90	0.90	1.07	1.00	0.94	0.96	3.75	2.88	2.48	3.60	3.47	2.65	2.52	1.62	2.96	2.91	2.03	2.86	3.09	3.11	3.71

3.5.2 Major, minor and trace elements

A comparison of the distribution of elements among the leucodiabases, diabases and metadiabases is made in order to characterize the geochemistry of the studied dikes. Geochemical graphs were produced using the Geochemical Data Toolkit (GCDkit) version 5.0 (Janoušek et al., 2006). All major elements utilized for petrogenic interpretation and comparison were first recalculated to a volatile-free form to better account for post-magmatic changes, following the equation in Gill (2010). Harker diagrams have Zr as a differentiation index due to its immobile nature and broad distribution among the groups. Normalization values of Nakamura (1974) and Sun and McDonough (1989) were used for the chondrite-normalized REE spider diagram and the primitive mantle-normalized immobile elements spider diagram, respectively.

Leucodiabases have low MgO (2.93 – 3.38 wt.%; Fig. 9a), diabases have moderate MgO concentrations (4.59 – 6.17 wt.%; Fig. 9a) and metadiabases have MgO values varying from moderate to high (4.91 – 13.36 wt.%; Fig. 9a). This agrees with the modal content of the rocks given that metadiabases normally have a larger percentage of ferromagnesian minerals, such as clinopyroxene, than diabases and particularly leucodiabases, which have the smallest amount of ferromagnesian minerals among the studied rocks. CaO concentrations in the three groups (Fig. 9b) have a similar range: 8.04 to 8.47 wt.% in leucodiabases; 9.54 to 10.06 wt.% in diabases; and 7.41 to 12.16 wt.% in metadiabases. TiO_2 content in metadiabases varies from moderate to high (1.01 – 4.00 wt.%; Fig. 9c), unlike the consistently high concentrations in leucodiabases (2.78 – 3.13 wt.%; Fig. 9c) and diabases (2.73 – 3.42 wt.%; Fig. 9c). Moreover, leucodiabases are relatively more enriched in P_2O_5 (0.66 – 0.88 wt.%; Fig. 9d) compared to diabases (0.26 – 0.39 wt.%; Fig. 9d) and metadiabases (0.09 – 0.30 wt.%; Fig. 9d).

Leucodiabases have higher HFSE concentrations than both diabases and metadiabases. Diabases, in their turn, are generally more enriched in HFSE than metadiabases, except for similar values for U and Th. The following is the concentration span of selected HFSE for leucodiabases, diabases and metadiabases, respectively: a) Zr: 428 – 493, 186 – 271 and 69 – 193 ppm (Fig. 9; horizontal axis); b) U: 0.94 – 1.25, 0.37 – 0.58 and 0.32 – 0.66 ppm (Fig. 9e); c) Th: 3.37 – 4.29, 1.3 – 1.93 and 1.58 – 3.82 ppm (Fig. 9f); d) Hf: 10.6 – 12.3, 4.9 – 7.3 and 2.1 – 5.3 ppm (Fig. 9g); and e) Y: 57.1 – 67.8, 35.6 – 42.2 and 16.2 – 31.4 ppm (Fig. 9h).

Overall, the REE pattern in those rocks is not very different (Fig. 10a – Fig. 10d). All groups show light REE enrichment relative to heavy REE, though to different degrees. Diabases, for example, are less enriched in light REE than leucodiabases and metadiabases.

This is seen in the $(La/Yb)_N$ ratio for those rocks: 2.51 to 3.06 for diabases, whereas values for leucodiabases are between 4.40 and 5.19 and for metadiabases between 3.82 and 5.61. There is no significantly high Eu anomaly, only mildly negative Eu anomalies in leucodiabases (Eu/Eu* 0.90 – 0.95), absent to mildly negative in diabases (Eu/Eu* 0.88 – 1.01) and absent or either mildly positive or negative in metadiabases (Eu/Eu* 0.89 – 1.15).

Unlike patterns in the REE spider diagrams, there are three distinct patterns for each group in the primitive mantle-normalized immobile elements spider diagram (Fig. 10d). Metadiabases show a pronounced negative Nb anomaly and a negative P anomaly (Fig. 10e); diabases have only a negative P anomaly (Fig. 10f); and leucodiabases a negative P and Ti anomaly (Fig. 10g). The Nb anomaly in the metadiabases is also evidenced by the $(Th/Nb)_N$ ratio: while ratio values range from 1.62 to 3.75 in metadiabases, leucodiabases have values between 0.91 and 1.04 and diabases have values between 0.90 and 1.07.

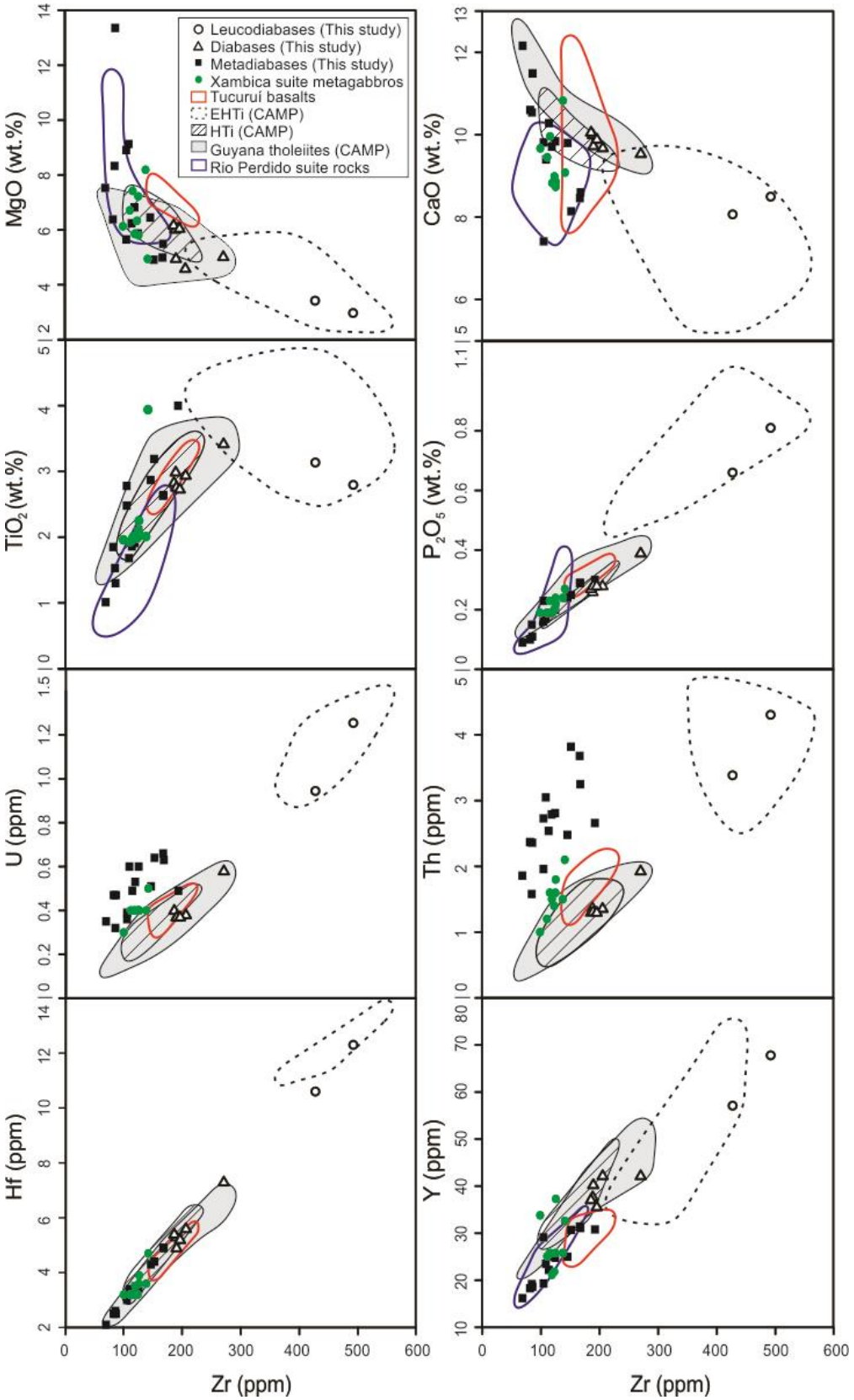

Figure 9 – Harker diagram for major, minor and trace elements of leucodiabases, diabases and metadiabases with Zr as the differentiation index. Data from metagabbros of the Xambica Instrusive Suite (Barros, 2010); Tucuruí basalts (Dutra, 2012); Guyana tholeiite dikes (Deckart et al., 2005); the evolved high-TiO_2 (EHTi) and high-TiO_2 (HTi) rocks from the Parnaíba Basin, São Luís Craton and Gurupi Belt (Fodor et al., 1990; Klein et al., 2013; Merle et al., 2011); and from the diabase dikes of the Rio Perdido Suite (Lima et al., 2017) were plotted for comparison.

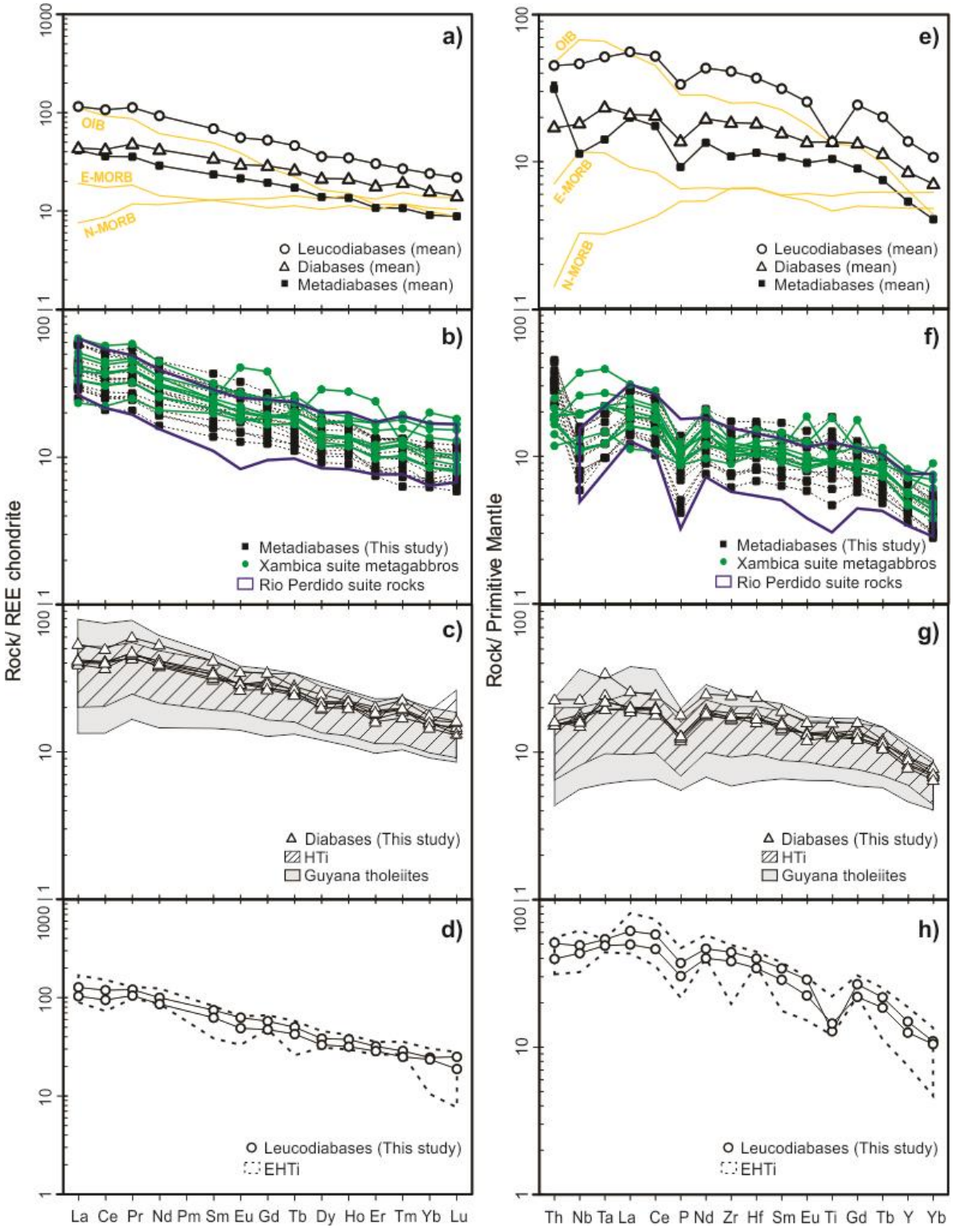

Figure 10 – Chondrite-normalized REE spider diagrams and primitive mantle-normalized immobile elements spider diagrams for metadiabases, diabases and leucodiabases samples. a) General REE pattern of the studied rocks; b) REE pattern of metadiabases; c) REE pattern of diabases; d) REE pattern of leucodiabases; e) General immobile elements patterns of the studied rocks; f) Immobile elements pattern of metadiabases; g) Immobile elements pattern of diabases; and h) Immobile elements pattern of leucodiabases. Chondrite normalization values of Nakamura (1974) and primitive mantle normalization values of Sun and McDonough (1989) were used. Data from metagabbros of the Xambica Instrusive Suite (Barros, 2010); Tucuruí basalts (Dutra, 2012); Guyana tholeiite dikes (Deckart et al., 2005); the evolved high-TiO_2 (EHTi) and high-TiO_2 (HTi) rocks from the Parnaíba Basin, São Luís Craton and Gurupi Belt (Fodor et al., 1990; Klein et al., 2013; Merle et al., 2011); and from the diabase dikes of the Rio Perdido Suite (Lima et al., 2017) were plotted for comparison.

3.5.3 Classification and magmatic affinity

According to the Zr/TiO_2 vs. Nb/Y classification diagram (Winchester and Floyd, 1977), the studied rocks can be compositionally classified as subalkaline basalts. The leucodiabases, however, are more alkaline, with two samples falling close to the boundary line of the basalt-andesite field (Fig. 11a). The Zr/Ti vs Nb/Y classification diagram (Pearce, 1996 after Winchester and Floyd, 1977) categorizes all the metadiabases and diabases as basalts and all leucodiabases fall within the andesite/basaltic andesite transition field (Fig. 11b). In the Y vs Zr diagram for determination of magmatic affinity (MacLean and Barrett, 1993), metadiabases and diabases plot between the tholeiitic and transitional field and leucodiabases plot slightly outside the transitional field. No sample shows a calc-alkaline affinity (Fig. 11c). All the rocks show tholeiitic affinity according to the Nb/Y vs. $Zr/(P_2O_5$ x 10,000) discrimination diagram (Fig. 11d; Rollinson, 1993 after Winchester and Floyd, 1976).

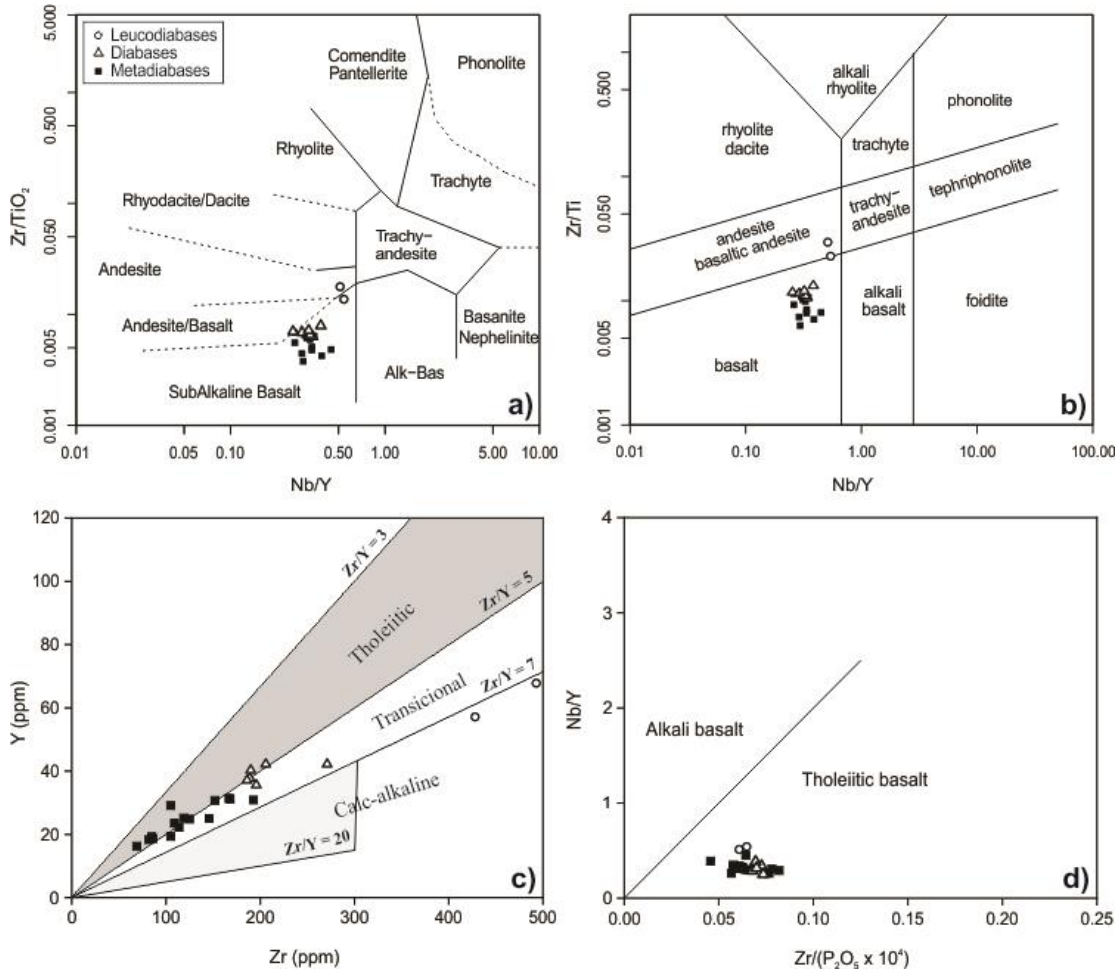

Figure 11 – a) Zr/TiO2 vs. Nb/Y classification diagram (Winchester and Floyd, 1977); b) Zr/Ti vs Nb/Y classification diagram (Pearce, 1996 after Winchester and Floyd, 1977); c) Y vs Zr diagram for determination of magmatic affinity; and d) Nb/Y vs. Zr/(P2O5 x 10,000) discrimination diagram (Rollinson, 1993 after Winchester and Floyd, 1976).

3.6 MINERAL CHEMISTRY

Quantitative chemical analyses of clinopyroxenes, plagioclases, amphiboles and biotites for the leucodiabases, diabases and metadiabases were carried out. In order to avoid transformed crystal rims – especially in the phenocrysts of the metadiabases – only data from crystals core was used.

3.6.1 Clinopyroxenes

Clinopyroxene structural formulas were calculated based on 4 cations and 6 oxygens and molar Fe^{+3} was estimated through stochiometric calculations. In Table 3, representative electron microprobe analyses are available. Apart from pigeonite in one diabase sample and diopside in one metadiabase sample, all the other clinopyroxenes are classified as augite according to the Wo-En-Fs classification diagram (Morimoto, 1988; Fig. 11). Augites from metadiabases are relatively more enriched in CaO (18.99 – 21.19 wt.%) than leucodiabase (17.35 – 18.74 wt.%) and diabase augites (15.63 – 18.42 wt.%). The analyzed pigeonite is composed of $Wo_{8.9}En_{56.7}Fs_{34.4}$ and the diopside of $Wo_{46.5}En_{33.8}Fs_{19.7}$.

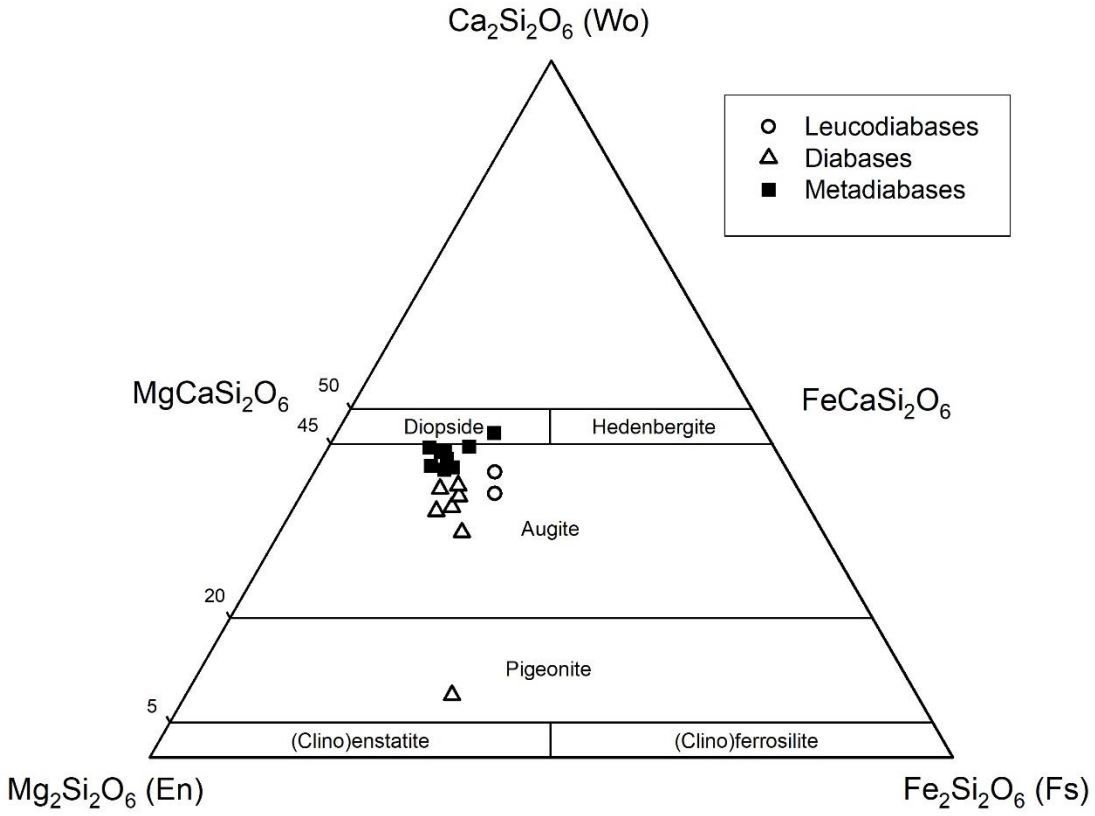

Figure 12 – Wo-En-Fs ternary classification diagram por clinopyroxenes of leucodiabases, diabases and metadiabases samples.

According to the Ti vs. Ca+Na diagram for determination of magmatic affinity (Fig. 13a; Leterrier et al., 1982), the clinopyroxenes compositions of the leucodiabases, diabases and metadiabases indicate they are derived from subalkaline rocks. They are further divided in the Ti+Cr vs. Ca diagram (Fig. 13b; Leterrier et al., 1982) as clinopyroxenes from non-orogenic tholeiites instead of from orogenic calc-alkaline rocks. This is in agreement with the immobile element geochemistry, which indicated subalkaline rocks with tholeiitic affinity (Fig. 11).

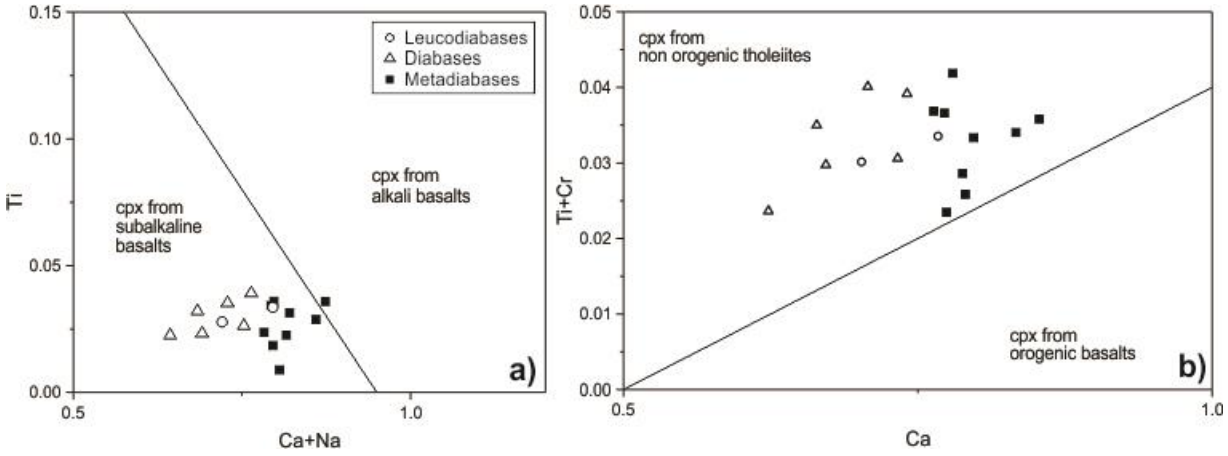

Figure 13 - a) Ti vs. Ca+Na diagram for determination of magmatic affinity based on clinopyroxene composition of the studied rocks (Leterrier et al., 1982). Samples falling in the subalkaline basalts field can be further plotted in the b) Ti +Cr vs. Ca diagram for discrimination between non-orogenic tholeiites and orogenic basalts (Leterrier et al., 1982).

.

Table 3 – Electron microprobe analyses of clinopyroxenes from leucodiabases, diabases and metadiabases samples.

Groups	Leucodiabases		Diabases							Metadiabases								
Samples	DA-25	78-DA-04	17-DA-01	17-DA-02	78-DA-02		78-DA-03	78-DA-05	78-DA-08	DA-01	DA-05	DA-09	DA-17	DA-19	DA-20		DA-21	DA-27
Concentrations in wt.%																		
SiO_2	51.20	53.25	53.02	52.00	50.92	52.45	50.23	51.59	51.52	54.85	55.10	52.53	51.81	51.55	52.51	52.53	52.44	53.21
TiO_2	1.17	0.98	1.14	0.81	1.39	0.51	1.25	0.83	0.93	0.31	0.84	1.22	1.04	0.80	1.13	1.26	1.25	0.67
Al_2O_3	2.04	1.68	2.42	1.92	2.69	0.74	3.40	2.51	2.62	2.57	2.97	2.84	2.95	2.77	3.12	4.07	2.44	2.81
Cr_2O_3	-	0.08	0.10	0.04	-	-	0.16	0.22	0.15	0.67	0.45	0.08	0.18	0.11	0.07	0.20	0.00	0.17
FeO (t)	13.17	14.11	11.60	14.09	11.43	21.03	11.84	10.95	10.27	7.15	8.26	10.10	8.89	8.53	9.39	9.59	11.35	9.85
MnO	0.51	0.30	0.25	0.26	0.28	0.54	0.31	0.27	0.26	0.23	0.01	0.16	0.27	0.25	0.39	0.35	0.25	0.18
MgO	12.02	12.56	14.71	15.64	14.27	19.48	14.40	15.89	15.23	13.59	12.88	13.87	14.53	14.96	14.07	11.70	10.94	14.65
CaO	18.74	17.35	16.57	15.63	18.42	4.25	17.55	16.76	18.32	19.59	18.99	19.37	21.19	19.73	20.19	19.13	20.96	19.72
Na_2O	0.39	0.25	0.28	0.28	0.31	0.06	0.29	0.26	0.28	0.24	0.26	0.28	0.37	0.35	0.33	0.24	0.28	0.30
Total	99.23	100.56	100.08	100.66	99.70	99.06	99.43	99.27	99.58	99.21	99.77	100.45	101.23	99.05	101.19	99.07	99.91	101.57
Formula units based on 6 oxygens																		
Si	1.9567	2.0119	1.9831	1.9347	1.9119	1.9893	1.8902	1.9308	1.9242	2.0591	2.0682	1.9563	1.9021	1.9276	1.9355	1.9983	1.9926	1.9508
Ti	0.0335	0.0278	0.0320	0.0225	0.0392	0.0146	0.0353	0.0233	0.0262	0.0088	0.0236	0.0342	0.0287	0.0226	0.0313	0.0359	0.0358	0.0184
Al	0.0918	0.0748	0.1068	0.0842	0.1191	0.0331	0.1507	0.1105	0.1154	0.1138	0.1316	0.1244	0.1277	0.1222	0.1354	0.1822	0.1091	0.1215
Cr	0.0000	0.0024	0.0030	0.0011	0.0000	0.0000	0.0048	0.0065	0.0044	0.0198	0.0133	0.0024	0.0053	0.0033	0.0020	0.0060	0.0001	0.0050
Fe^{+3}	0.0000	0.0000	0.0000	0.0207	0.0014	0.0000	0.0148	0.0000	0.0000	0.0000	0.0000	0.0000	0.0317	0.0000	0.0000	0.0000	0.0000	0.0000
Fe^{+2}	0.4209	0.4457	0.3629	0.4177	0.3575	0.6669	0.3579	0.3426	0.3209	0.2246	0.2594	0.3145	0.2411	0.2666	0.2895	0.3052	0.3607	0.3021
Mn	0.0165	0.0096	0.0080	0.0083	0.0087	0.0174	0.0099	0.0087	0.0082	0.0073	0.0004	0.0052	0.0085	0.0079	0.0122	0.0113	0.0081	0.0055
Mg	0.6845	0.7071	0.8200	0.8673	0.7986	1.1013	0.8078	0.8867	0.8480	0.7608	0.7209	0.7700	0.7950	0.8338	0.7731	0.6633	0.6198	0.8005
Ca	0.7673	0.7023	0.6641	0.6232	0.7410	0.1729	0.7076	0.6719	0.7329	0.7882	0.7636	0.7728	0.8334	0.7905	0.7975	0.7798	0.8532	0.7746
Na	0.0286	0.0185	0.0200	0.0204	0.0226	0.0046	0.0212	0.0191	0.0199	0.0176	0.0192	0.0202	0.0264	0.0256	0.0234	0.0179	0.0206	0.0215
Mg#	61.92	61.34	69.32	67.49	69.08	62.28	69.30	72.13	72.55	77.21	73.54	71.00	76.73	75.77	72.76	68.49	63.21	72.60
Wo	40.97	37.86	35.95	32.31	39.03	8.91	37.48	35.34	38.54	44.44	43.79	41.61	43.84	41.80	42.87	44.60	46.53	41.26
En	36.55	38.12	44.40	44.96	42.06	56.74	42.78	46.64	44.59	42.90	41.34	41.46	41.81	44.10	41.56	37.94	33.80	42.64
Fs	22.48	24.03	19.65	22.73	18.91	34.36	19.74	18.02	16.87	12.66	14.87	16.93	14.35	14.10	15.56	17.46	19.67	16.09

3.6.2 Plagioclases

The structural formulas of plagioclase were calculated based on 8 oxygens. The representative electron microprobe analyses are available in the Table 4. There is a clear distinction between the composition of plagioclases from metadiabases and the compositions from leucodiabases and diabases. For instance, while all plagioclases of metadiabase are albite ($An_{0.44 - 6}$), leucodiabase ($An_{51 - 54}$) and diabase plagioclases ($An_{60 - 66}$) are labradorites. Moreover, leucodiabase labradorites are more sodic compared to metadiabase labradorites. In figure 14, the plagioclase composition of the studied rocks is shown.

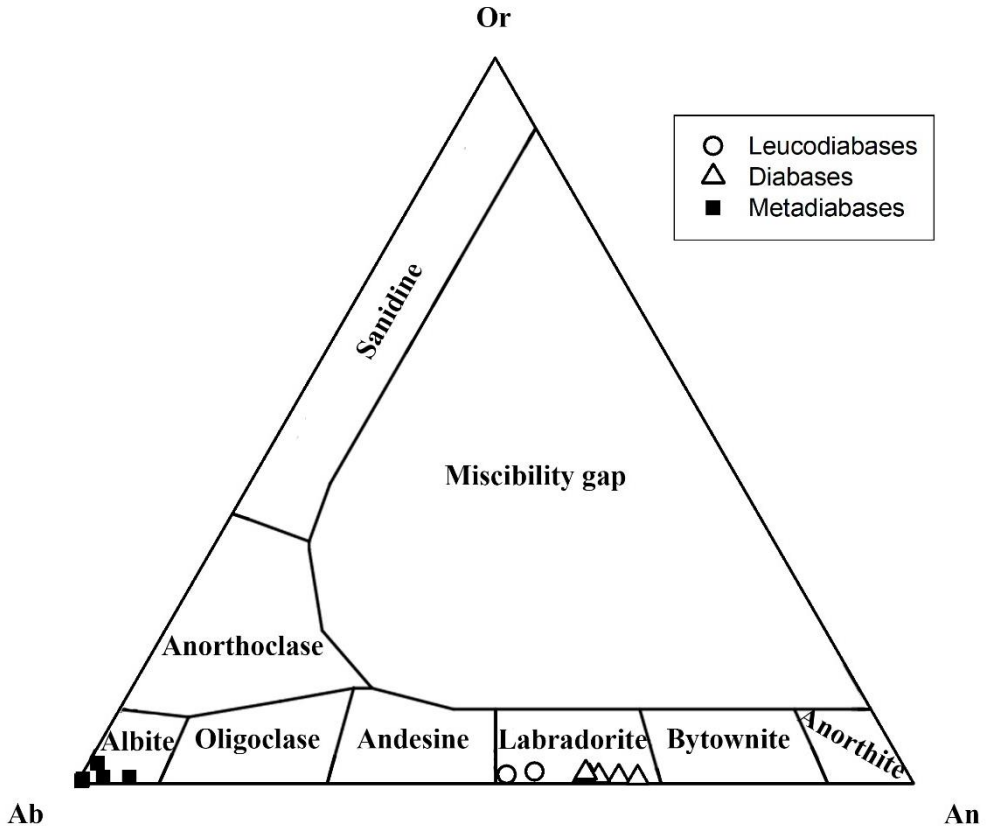

Figure 14 – Ab-Or-An ternary diagram showing the composition of the plagioclases from leucodiabases, diabases and metadiabases samples.

Table 4 - Electron microprobe analyses of plagioclases from leucodiabases, diabases and metadiabases samples.

Groups	Leucodiabases		Diabases						Metadiabases					
Samples	DA-25	78-DA-04	17-DA-01	17-DA-02	78-DA-02	78-DA-03	78-DA-05	78-DA-08	DA-05	DA-09	DA-17	DA-19	DA-20	DA-21
Concentrations in wt.%														
SiO_2	55.26	57.42	54.96	52.93	52.76	52.95	51.21	52.68	69.16	67.38	69.75	66.02	69.87	70.62
TiO_2	0.26	0.23	0.23	0.00	0.08	0.07	0.10	0.11	0.17	0.00	0.00	0.01	0.10	0.00
Al_2O_3	26.98	26.04	27.27	27.23	28.52	28.45	29.46	28.59	19.70	16.90	18.23	20.10	18.19	18.24
Cr_2O_3	0.00	0.00	0.09	0.00	-	-	-	-	0.07	0.04	0.00	-	0.00	0.00
FeO (t)	0.57	0.59	0.70	0.80	0.57	0.84	0.76	0.85	0.39	3.19	0.00	0.52	0.05	0.00
MnO	0.00	0.04	0.00	0.02	-	-	-	-	0.05	0.00	0.01	-	0.00	0.00
MgO	0.06	0.09	0.10	0.12	0.07	0.16	0.16	0.11	0.08	0.60	0.00	0.13	0.01	0.00
CaO	11.39	10.32	12.28	13.16	12.39	12.30	13.69	12.81	0.51	0.23	0.10	1.25	0.10	0.10
BaO	-	-	-	-	0.07	0.07	0.04	0.06	-	-	-	0.07	-	-
Na_2O	5.19	5.40	4.27	3.94	4.39	4.39	3.70	4.25	9.92	11.05	12.18	11.00	11.39	10.96
K2O	0.29	0.21	0.16	0.15	0.26	0.20	0.13	0.18	0.14	0.49	0.06	0.15	0.11	0.09
Total	100.00	100.33	100.06	98.35	99.11	99.41	99.24	99.64	100.18	99.87	100.33	99.26	99.82	100.00
Formula units based on 8 oxygens														
Si	2.5013	2.5930	2.5046	2.4548	2.4167	2.4193	2.3510	2.4040	3.0606	2.9767	3.0314	2.9151	3.0708	3.1086
Ti	0.0090	0.0078	0.0078	0.0000	0.0029	0.0023	0.0035	0.0036	0.0056	0.0000	0.0000	0.0003	0.0032	0.0000
Al	1.4395	1.3858	1.4648	1.4884	1.5399	1.5319	1.5940	1.5379	1.0272	0.8801	0.9337	1.0458	0.9421	0.9463
Cr	0.0000	0.0000	0.0034	0.0000	0.0000	0.0000	0.0000	0.0000	0.0025	0.0013	0.0000	0.0000	0.0000	0.0000
Fe	0.0216	0.0222	0.0265	0.0310	0.0218	0.0321	0.0291	0.0326	0.0145	0.1178	0.0000	0.0193	0.0019	0.0000
Mn	0.0000	0.0015	0.0000	0.0009	0.0000	0.0000	0.0000	0.0000	0.0018	0.0000	0.0003	0.0000	0.0000	0.0000
Mg	0.0040	0.0063	0.0065	0.0083	0.0045	0.0108	0.0106	0.0078	0.0051	0.0393	0.0000	0.0088	0.0009	0.0000
Ca	0.5524	0.4991	0.5996	0.6537	0.6083	0.6022	0.6736	0.6264	0.0242	0.0110	0.0045	0.0592	0.0045	0.0045
Ba	0.0000	0.0000	0.0000	0.0000	0.0012	0.0013	0.0006	0.0010	0.0000	0.0000	0.0000	0.0012	0.0000	0.0000
Na	0.4556	0.4724	0.3774	0.3538	0.3896	0.3888	0.3297	0.3761	0.8507	0.9464	1.0266	0.9417	0.9703	0.9354
K	0.0166	0.0119	0.0094	0.0091	0.0151	0.0114	0.0077	0.0106	0.0079	0.0274	0.0034	0.0086	0.0064	0.0052
An	53.92	50.75	60.79	64.30	60.04	60.07	66.62	61.83	2.74	1.12	0.44	5.86	0.46	0.48
Ab	44.46	48.04	38.26	34.80	38.46	38.79	32.61	37.12	96.36	96.10	99.24	93.28	98.89	98.97
Or	1.62	1.21	0.95	0.90	1.49	1.13	0.76	1.05	0.90	2.79	0.33	0.85	0.65	0.55

3.6.3 Amphiboles

The structural formulas of amphiboles were calculated with Probe-AMPH, a spreadsheet program developed by Tindle and Webb (1994). The formula units were based on 23 oxygens, stochiometric Fe^{2+}/Fe^{3+} estimation assumed 13 cations for calcic amphiboles and classification followed the nomenclatures of Leake et al. (1997). The chemical analyses of amphiboles are shown in Table 5. Amphiboles are restricted to the metadiabases group, where two types were identified in the petrographic analysis: dark brown hornblende and greenish actinolite. Mineral chemistry of the amphiboles also showed two main groups of minerals: magnesio-hornblendes, ferro-hornblendes and magnesio-hastingsites from the Hornblende Group and actinolites from the Tremolite-Actinolite Series Group (Fig. 15).

The TiO_2 content in the hornblendes is high (1.82 – 3.73 wt.%), which may account for their dark brown color, while the TiO_2 content in actinolites is relatively low (0.02 – 0.85 wt.%). In the Ca + Na + K vs Si discrimination diagram (Sial et al., 1998 after Leake and E., 1971; Fig. 16), Hornblende Group amphiboles plot inside the igneous field, whereas actinolites plot in the metamorphic field, which conforms with the petrographic analysis.

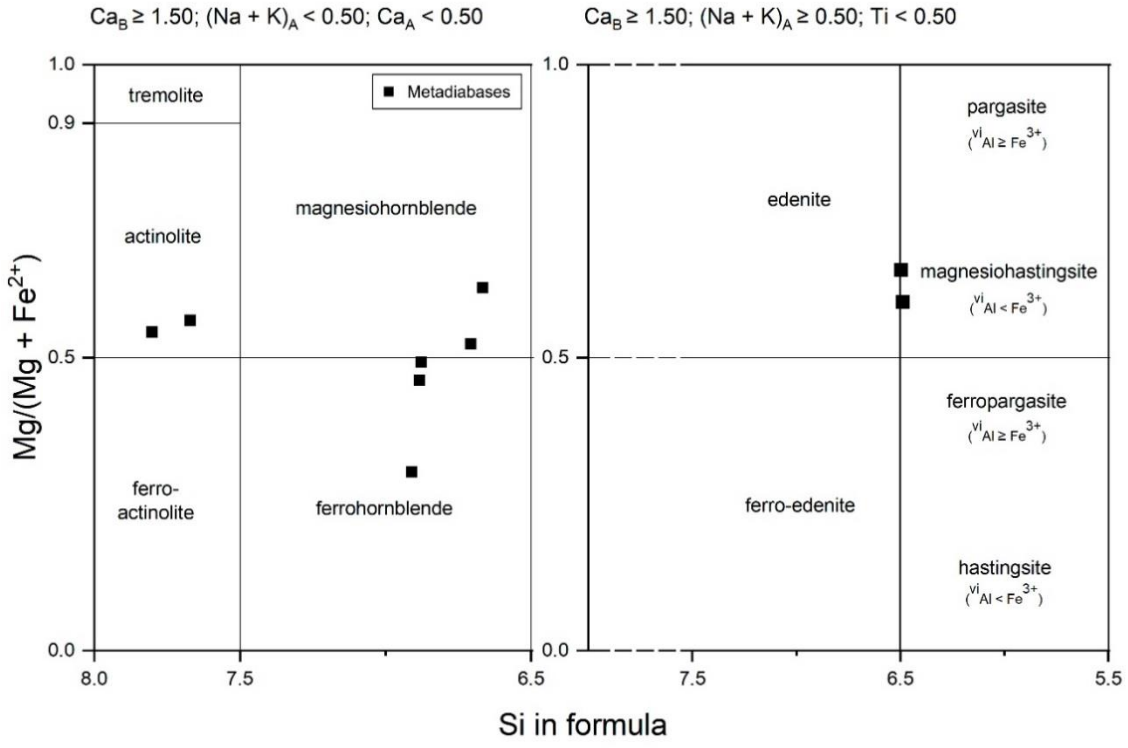

Figure 15 – Classification diagram for amphiboles from leucodiabases, diabases and metadiabases samples (Leake et al., 1997).

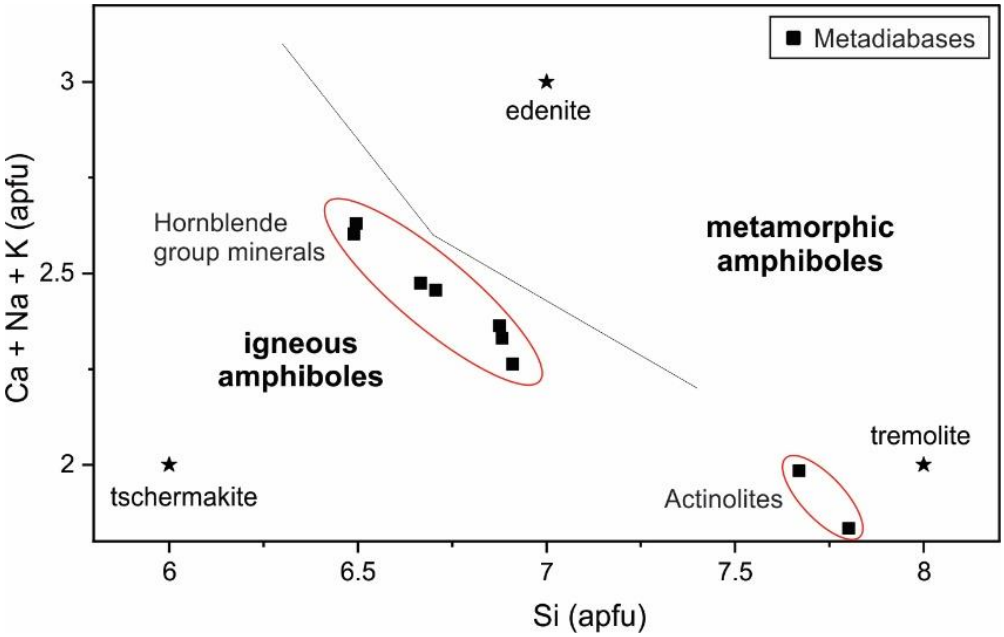

Figure 16 – Ca+Na+K vs. Si in atoms per formula unit (apfu) discrimination diagram for amphiboles of the studied rocks (Sial et al., 1998 after Leake and E., 1971). Hornblende group minerals fall within the igneous field and actinolites fall within the metamorphic field.

Table 5 – Electron microprobe analyses of amphiboles from metadiabases samples.

Group	Metadiabases								
Samples	DA-01		DA-05	DA-09		DA-20	DA-21	DA-27	
Concentrations in wt.%									
SiO_2	44.78	52.13	45.89	43.92	52.75	45.66	44.95	44.94	43.67
TiO_2	3.67	0.85	2.71	3.47	0.02	2.91	1.82	3.05	3.73
Al_2O_3	9.65	4.01	9.30	9.38	1.78	8.18	6.89	8.35	9.36
FeO	15.59	16.59	16.90	14.00	20.02	18.84	26.33	15.23	15.37
MnO	0.17	0.23	0.27	0.10	0.17	0.35	0.25	0.19	0.11
MgO	9.63	11.25	9.03	12.41	10.76	8.51	5.29	11.79	11.37
CaO	10.63	10.54	9.93	10.79	11.02	10.19	9.84	11.05	10.93
Na_2O	2.08	0.87	2.29	2.83	0.25	1.88	1.72	1.97	2.43
K_2O	0.76	0.40	0.54	0.59	0.08	0.69	0.66	0.79	0.85
F	0.07	0.04	0.24	0.27	-	0.21	0.28	-	0.27
Cl	0.06	0.07	0.04	0.04	0.02	0.05	0.45	0.06	0.04
Cr_2O_3	0.01	0.03	-	0.02	0.16	-	-	0.09	0.04
NiO	-	-	0.06	-	0.00	-	-	-	0.04
Total	97.10	97.00	97.19	97.81	97.02	97.49	98.49	97.53	98.21
Formula units based on 23 oxygens									
Si	6.7064	7.6700	6.8761	6.4960	7.8015	6.8834	6.9105	6.6664	6.4899
Al iv	1.2936	0.3300	1.1239	1.5040	0.1985	1.1166	1.0895	1.3336	1.5101
Al vi	0.4090	0.3652	0.5183	0.1316	0.1114	0.3372	0.1590	0.1270	0.1302
Ti	0.4134	0.0938	0.3058	0.3865	0.0026	0.3294	0.2101	0.3401	0.4167
Cr	0.0014	0.0040	0.0000	0.0027	0.0182	0.0000	0.0000	0.0110	0.0052
Fe^{3+}	0.0000	0.1278	0.0380	0.2569	0.4839	0.1437	0.6276	0.2848	0.1984
Fe^{2+}	1.9525	1.9139	2.0800	1.4749	1.9915	2.2322	2.7574	1.6051	1.7122
Mn	0.0218	0.0282	0.0338	0.0123	0.0208	0.0451	0.0331	0.0237	0.0142
Mg	2.1497	2.4671	2.0175	2.7351	2.3713	1.9124	1.2127	2.6082	2.5184
Ni	0.0000	0.0000	0.0066	0.0000	0.0002	0.0000	0.0000	0.0000	0.0047
Ca	1.7050	1.6609	1.5934	1.7094	1.7463	1.6466	1.6200	1.7564	1.7404
Na	0.6051	0.2490	0.6659	0.8101	0.0725	0.5501	0.5124	0.5678	0.7003
K	0.1456	0.0745	0.1034	0.1109	0.0147	0.1335	0.1302	0.1499	0.1619
F	0.0327	0.0186	0.1133	0.1244	0.0000	0.1006	0.1361	0.0000	0.1264
Cl	0.0150	0.0170	0.0094	0.0088	0.0038	0.0138	0.1183	0.0158	0.0103
OH*	1.9523	1.9644	1.8773	1.8668	1.9962	1.8856	1.7456	1.9842	1.8632
(Ca+Na) (B)	2.00	1.91	2.00	2.00	1.82	2.00	2.00	2.00	2.00
Na (B)	0.30	0.25	0.41	0.29	0.07	0.35	0.38	0.24	0.26
(Na+K) (A)	0.46	0.07	0.36	0.63	0.01	0.33	0.26	0.47	0.60
Mg/(Mg+Fe2)	0.52	0.56	0.49	0.65	0.54	0.46	0.31	0.62	0.60
Fe3/(Fe3+Alvi)	0.00	0.26	0.07	0.66	0.81	0.30	0.80	0.69	0.00

3.6.4 Biotites

Biotites only occur in the metadiabases group. Their structural formula was calculated based on 22 oxygens. The chemical analyses of the biotites from metadiabases are presented in Table 6. In the classification diagram of Deer et al. (1992), ~~they~~ fall within the biotite field with compositions close to the iron-end member annite (Fig. 17). Fe/(Fe+Mg) values in the studied biotites vary from 0.54 to 0.73. The ternary discrimination diagram of Nachit et al. (2005) indicates they are primary biotites instead of re-equilibrated or neoformed biotites. This corroborates the petrographic analysis.

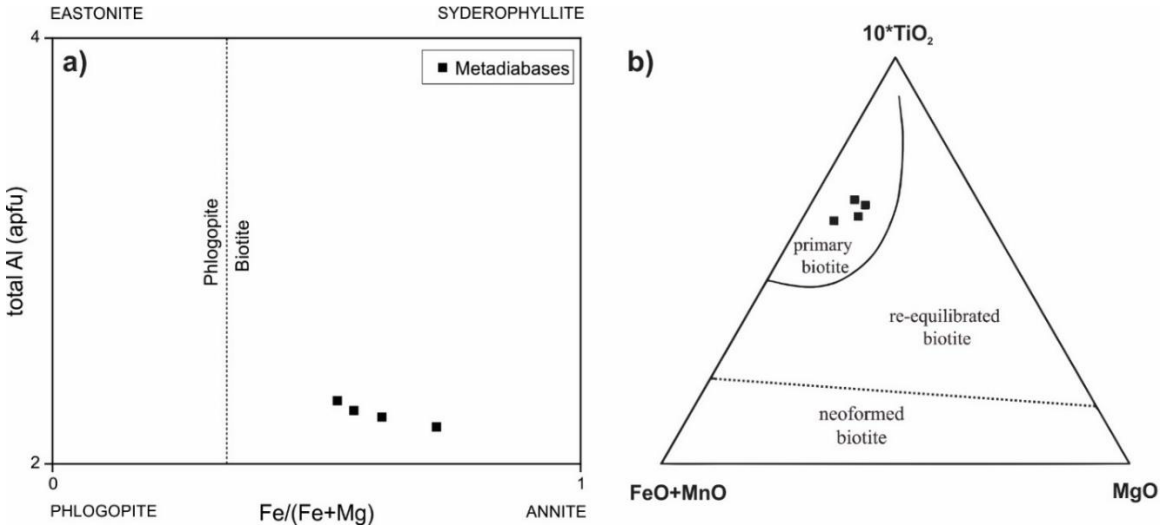

Figure 17 – a) Total Al vs. Fe(Fe+Mg) biotite classification diagram (Deer et al., 1992), showing the composition of the studied biotites from metadiabases; and b) 10*TiO2-Fe+MnO-MgO ternay discrimination diagram for biotites (Nachit et al., 2005).

Table 6 – Electron microprobe analyses of biotites from metadiabases.

Group	Metadiabases			
Samples	DA-01	DA-20	DA-27	
Concentrations in wt.%				
SiO_2	38.62	38.45	36.29	36.72
TiO_2	5.60	4.76	5.50	4.99
Al_2O_3	12.28	11.82	12.58	12.30
FeO	22.45	26.31	21.16	22.58
MnO	0.13	0.09	0.06	0.00
MgO	7.60	5.53	10.12	9.52
CaO	0.00	0.04	0.00	0.05
Na_2O	0.12	0.26	0.47	0.43
K_2O	8.92	8.32	8.73	8.53
Cl	0.07	0.16	0.07	0.10
F	0.10	0.01	0.05	0.05
O=F,Cl	0.06	0.04	0.04	0.04
Total	95.09	95.04	94.29	94.53
Formula units based on 22 oxygens				
Si	5.9235	5.9997	5.6224	5.6984
Al iv	2.0765	2.0003	2.2960	2.2499
Al vi	0.1433	0.1724	0.0000	0.0000
Ti	0.6456	0.5580	0.6403	0.5829
Fe^{2+}	2.8786	3.4321	2.7408	2.9296
Mn	0.0171	0.0114	0.0075	0.0000
Mg	1.7365	1.2872	2.3384	2.2028
Ca	0.0003	0.0065	0.0005	0.0088
Na	0.0360	0.0789	0.1424	0.1297
K	1.7456	1.6549	1.7253	1.6876
Cl	0.0174	0.0428	0.0192	0.0250
F	0.0466	0.0049	0.0225	0.0221
Fe/(Fe+Mg)	0.62374	0.72724	0.53961	0.57081

3.6.5 Olivines

Olivines only occur in the leucodiabases group. Their chemical analyses are shown in Table 7. Their structural formula was calculated based on 4 oxygens, molar Fe^{+3} was estimated through stochiometric calculations and classification followed the nomenclature in Deer et al. (1992). The olivines are iron-rich, with the forsterite component (Fo) varying from approximately 24 to 32%. Figure 18 shows that they range compositionally from hortonolite to ferrohortonolite, which are close to the iron-endmember fayalite. This is compatible with the petrographic analysis since those olivines are in equilibrium with quartz, which rules out the occurrence of more magnesium-rich olivines.

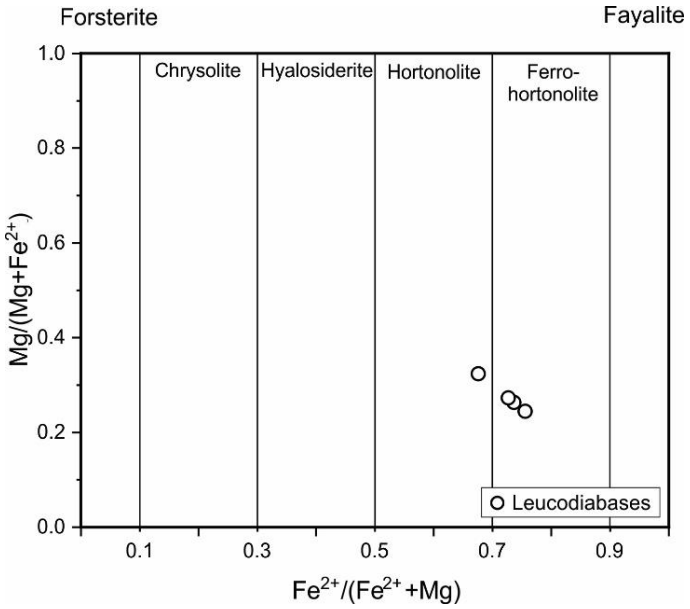

Figure 18 – $Mg(Mg+Fe^{+2})$ vs. $Fe^{+2}(Fe^{+2}+Mg)$ olivine classification diagram. The studied olivines range from hortonolite to ferrohortonolite.

Table 7 – Electron microprobe analyses of olivines from a leucodiabase sample.

Group	Leucodiabases			
Sample	DA-25			
Concentrations in wt.%				
SiO_2	32.123	32.305	32.768	33.35
TiO_2	0.03	-	0.099	-
Al_2O_3	0.035	0.026	-	0.006
FeO	57.07	56.213	55.467	52.746
MnO	0.973	1.046	0.877	1.135
MgO	10.351	11.212	11.676	14.175
CaO	0.243	0.297	0.327	0.332
Cr_2O_3	-	0.019	-	0.049
Total	100.825	101.118	101.214	101.793
Formula units based on 4 oxygens				
Si	0.9994	0.9963	1.0059	1.0009
Ti	0.0007	-	0.0023	-
Al	0.0013	0.0009	-	0.0002
Cr	-	0.0005	-	0.0012
Fe^{+3}	-	0.0061	-	-
Fe^{+2}	1.4848	1.4437	1.4239	1.3239
Mn	0.0256	0.0273	0.0228	0.0289
Mg	0.4801	0.5155	0.5343	0.6342
Ca	0.0081	0.0098	0.0108	0.0107
%Fo	24.02	25.74	26.83	31.75

3.7 DISCUSSIONS

3.7.1 Metamorphism and deformation

While diabases and leucodiabases are undeformed and unmetamorphosed, metadiabases show evidence that they have been affected by regional metamorphism. The metamorphic assemblage of metadiabases is originated mostly from the partial breakdown of clinopyroxene and plagioclase. In addition, chloritization of biotite and hornblende borders and replacement of titanomagnetite by titanite may also take place (Fig. 19a). This paragenesis of Ab + Chl + Act + Ep + Ttn + Ser ± Cal ± Qtz is typical of the greenschist facies (Best, 2003b). The absence of metamorphic biotite points to the lower temperature range of the greenschist facies. There is also signs of deformation in some minerals from metadiabases, such as: deformation twinning in calcite (Fig. 19b), sweeping undulose extinction in quartz (Fig. 19c) and kink bands in biotite (Figs. 19d). These microstructures are common in low-grade metamorphic conditions (Passchier and Trouw, 2005; Vernon, 2004). Quartz and calcite microveins (Fig. 19b) are also common in the metadiabases and may be a result of metamorphic segregation processes. Samples of metadiabases from the western section of the study area usually exhibit a minor degree of breakdown of primary phases and mineral deformation than samples from the eastern section.

The low-grade metamorphic condition of the metadiabases, based on their paragenesis and microstructures, as well as the increase of metamorphic grade from west to east suggest

that these rocks were affected by the Neoproterozoic regional metamorphism of the Araguaia Belt. Likewise, the lack of metamorphism and deformation in the diabases and leucodiabases indicates they succeed the metamorphic event and, thus, are relatively younger than the metadiabases.

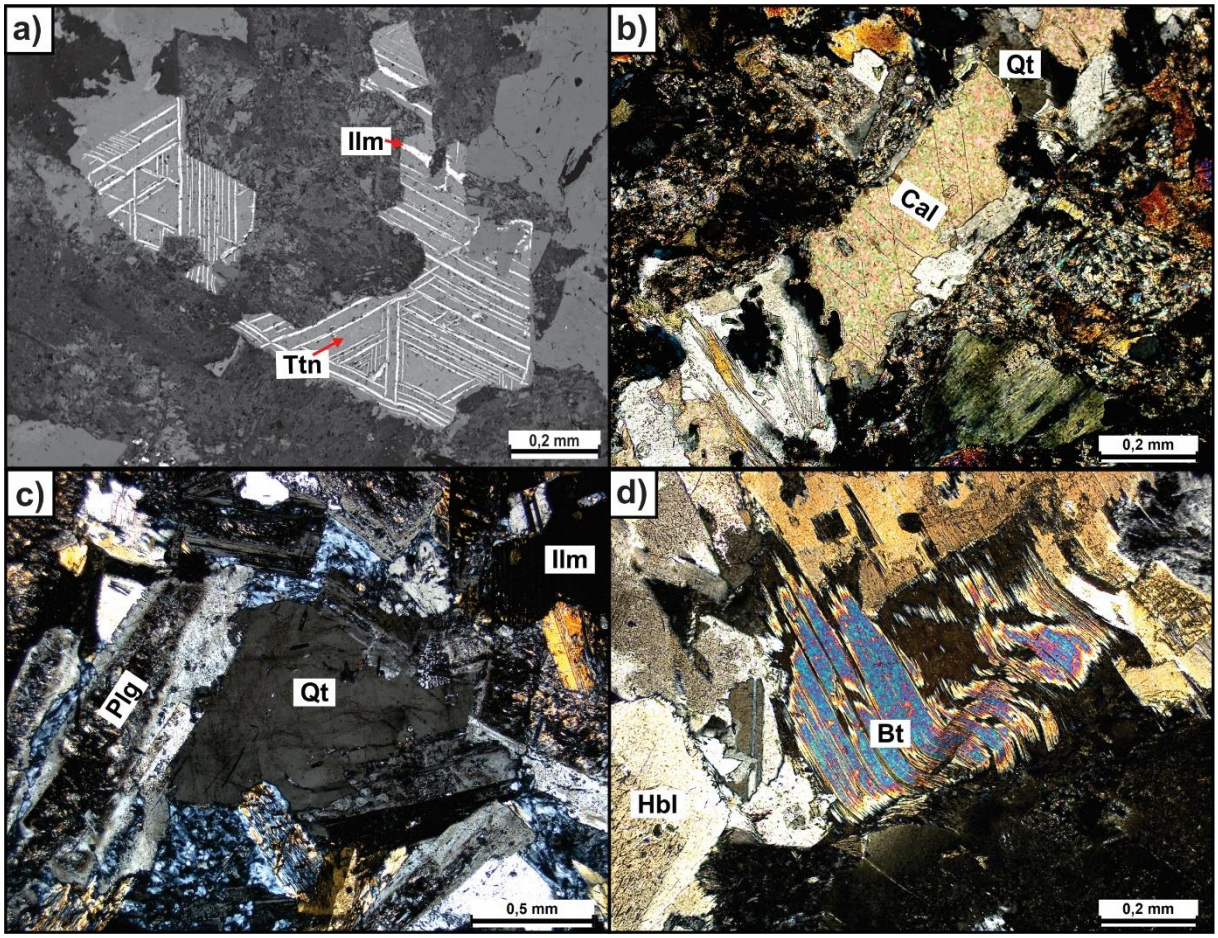

Figure 19 – a) Titanite (after titanomagnetite) with trellis-type ilmenite lamellae; b) thin deformation twinning in a calcite from a microvein; c) quartz cristal exhibiting sweeping undulose extinction; and d) kink bands in a biotite crystal.

3.7.2 Fractional crystallization processes

Metadiabases show a linear differentiation trend in the Hacker diagrams (Fig. 9). Besides, as mentioned earlier, these rocks occur near olivine cumulates containing magnetite and apatite. The origin of the more evolved metadiabases and the cumulates may be connected since fractional crystallization of a parental magma can generate both an evolved residual liquid and a cumulate.

Likewise, a linear trend is noticed between diabases and leucodiabases. A possible explanation is that these rocks are cogenetic and the diabases represent the parental melt that,

through fractional crystallization, generated the leucodiabases. Besides, the fact that the olivine crystals encountered in some leucodiabase samples are iron-rich may be due to fractionation of magnesium-rich olivines that left the residual liquid more enriched in iron.

Chemical data for the mafic dikes can provide insights on the processes that control their magmatic evolution. Thus, in order to assess the viability of the hypothesis above, two models were created by using the Rayleigh fractionation equation (1):

$$\frac{C_l}{C_0} = F^{(D-1)} \quad (1)$$

where C_l is the concentration of a given element in the residual liquid; C_0 is the concentration of the element in the original liquid; F is the fraction of remaining liquid; D is the bulk distribution coefficient. The bulk distribution coefficient was calculated by using the distribution coefficients available in Table 8 and the equation (2):

$$D = \sum W_A K_D^A \quad (2)$$

where W_A is the weight fraction of mineral A in the rock and K_D^A is the distribution coefficient for a given element in mineral A.

For the first model, it was assumed that sample DA-13, which has a high Mg content (Mg# = 66), represented the parental magma of the metadiabases. Sample DA-14 is a cumulative dunite which was collected close to sample DA-13 and is composed of olivine (95%), magnetite (5%) and apatite (1%). The concentration of elements in the residual liquid, therefore, was calculated by assuming that DA-13 represented the parental magma and that the cumulate was formed by olivine, magnetite and apatite at the same modal proportion as sample DA-14. It was found that 50% degree of fractional crystallization of the parental magma generated a liquid whose element concentrations are remarkably similar to the concentrations encountered in sample DA-24, which is the most evolved metadiabase (Mg# = 34). This indicates that fractional crystallization has played a role in the metadiabases differentiation.

For the second model, the diabase sample 17-DA-02 was chosen to represent the initial liquid composition. Then, the residual liquid was obtained by 65% of fractional crystallization of the initial liquid for a cumulate made up of olivine (98.5%) and apatite (1.5%). The element concentration of the calculated liquid is very similar to the concentration of the leucodiabase sample DA-25. This suggests that leucodiabases and diabases are cogenetic and that fractional crystallization can account for their differentiation.

Figure 20 show the element composition of the calculated residual liquids in the REE and multielement spidergrams. Element composition of selected samples are also shown for comparison.

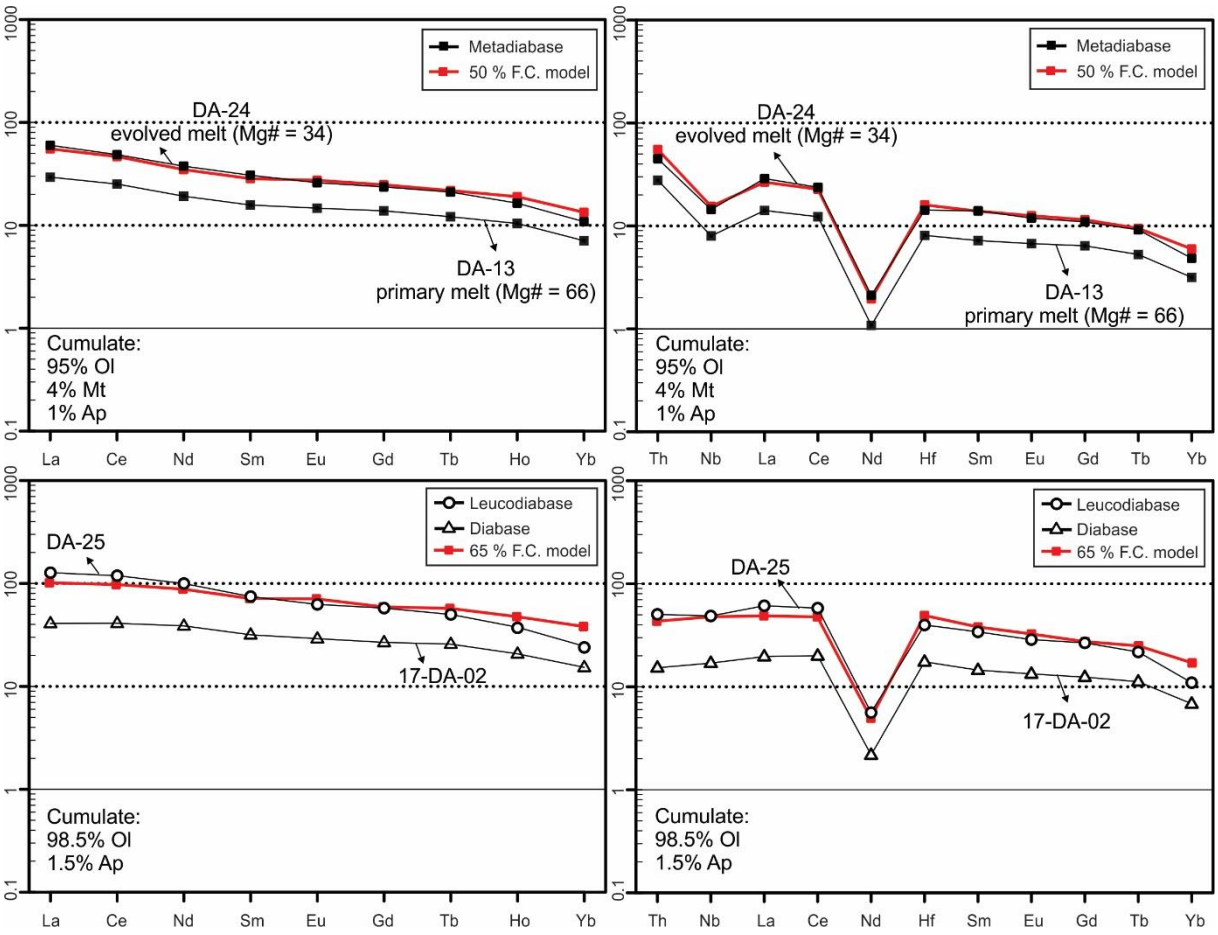

Figure 20 – Chondrite-normalized REE spider diagrams and primitive mantle-normalized immobile elements spider diagrams showing the element composition of the calculated residual liquid (in red) and selected studied samples. Samples DA-13 and 17-DA-02 represent the initial liquids. Samples DA-24 and DA-25 are compared with the obtained model.

Table 8 – Distribution coefficients (Kd) of selected elements in mafic parent rocks for the minerals olivine, magnetite and apatite.

	Olivine			Magnetite			Apatite		
Element	Kd	Rock Type	Ref.	Kd	Rock Type	Ref.	Kd	Rock Type	Ref.
Th	0.0001	Basalt	1	0.1	Basalt-Hawaiite	2	0.33	Basalt	4
Nb	0.01	Basalt	1	0.905*	Basalt	3	0.0012	Basalt	4
La	0.0004	Basalt	1	0.015	Basalt	2	8.6	Basalt	5
Ce	0.0005	Basalt	1	0.016	Basalt	2	11.2	Basalt	4
Nd	0.001	Basalt	1	0.026	Basalt	2	14	Basalt	4
Hf	0.01	Basalt	1	0.16	Basalt-Hawaiite	2	0.01	Basalt	4
Sm	0.0013	Basalt	1	0.024	Basalt	2	4.99	Basalt	4
Eu	0.0016	Basalt	1	0.025	Basalt	2	9.6	Basalt	5
Gd	0.0015	Basalt	1	0.018	Basalt	2	15.8	Basalt	5
Tb	0.0015	Basalt	1	0.019	Basalt	2	15.4	Basalt	5
Ho	0.0016	Basalt	1	0.017	Basalt	2	13.3	Basalt	5
Yb	0.0015	Basalt	1	0.018	Basalt	2	8.1	Basalt	5

Abbreviations: 1 = Mckenzie and O'Nions (1991); 2 = Lemarchand et al. (1987); 3 = Nielsen (1992); 4 = Prowatke and Klemme (2006); 5 = Paster et al. (1974); * = Average.

3.7.3 Tectonic setting and source of magmatism

There is a clear difference between the geochemical signature of metadiabases and the signature of diabases and leucodiabases. Metadiabases exhibit negative anomalies of HFSE (Fig. 10f), such as Nb and Ta, which is widely regarded as an arc-like signature, whereas leucodiabases and diabases lack a negative Nb-Ta anomaly and show a LREE-enriched pattern (Fig. 10g; Fig. 10h), which resembles the signatures of plume-generated basaltic rocks (Ernst et al., 2005).

Arc-like signatures are not restricted to subduction settings as many continental basaltic rocks also display enrichment of fluid-mobile elements and depletion of HFSE (Ernst, 2014). According to Wang et al. (2016), Ti–V, Zr–Zr/Y, Zr–Ti and Ti/V–Zr/Sm–Sr/Nd discrimination diagrams are tools that can be applied to distinguish true arc-basalts from arc-like continental basalts, whereas diagrams based on Nb and/or Ta should be avoided to classify the tectonic setting of ancient continental basalts. Most of the studied rocks fall inside the "Within-Plate Basalts" field in the Zr–Zr/Y (Pearce and Norry, 1979; Fig. 21a) and Zr–Ti (Pearce, 1996; Fig. 21b) discrimination diagrams. In the Ti/1000–V discrimination diagram (Rollinson, 1993 after Shervais, 1982; Fig. 21c), all rocks are classified as non-arc type, that is, they fall outside the

arc tholeiite field. The ternary Ti/V–Zr/Sm–Sr/Nd discrimination diagram proposed by Wang et al. (2016) was not used since Sr was evaluated as mobile in the studied metadiabases (Fig. 8). This suggests that theses rocks were formed in an intraplate setting.

The Zr/Nb–Nb/Th plot (Condie, 2005; Fig. 21cd) shows the mantle compositional components for volcanic rocks. It indicates an important contribution of enriched (EN) mantle components to metadiabases and significant contribution of primitive mantle (PM) to both leucodiabases and diabases. Thus, metadiabases derived from different sources than leucodiabases and diabases.

Arc-like signatures in basaltic rocks have been considered to derive from crustal contamination (Xia, 2014), from subduction-metasomatized mantle lithosphere (Ernst, 2014) and/or from the hydrous mantle transition zone (Wang et al., 2015, 2016). According to Condie (2005), the EN component, whose contribution was indicated in the metadiabases, includes upper continental crust and subcontinental lithosphere that may have inherited a subduction zone geochemical signature. This points to a subduction-metasomatized mantle lithosphere origin. However, the origin of arc-like continental basalts is still uncertain and no process can be ruled out for these rocks with the present available information.

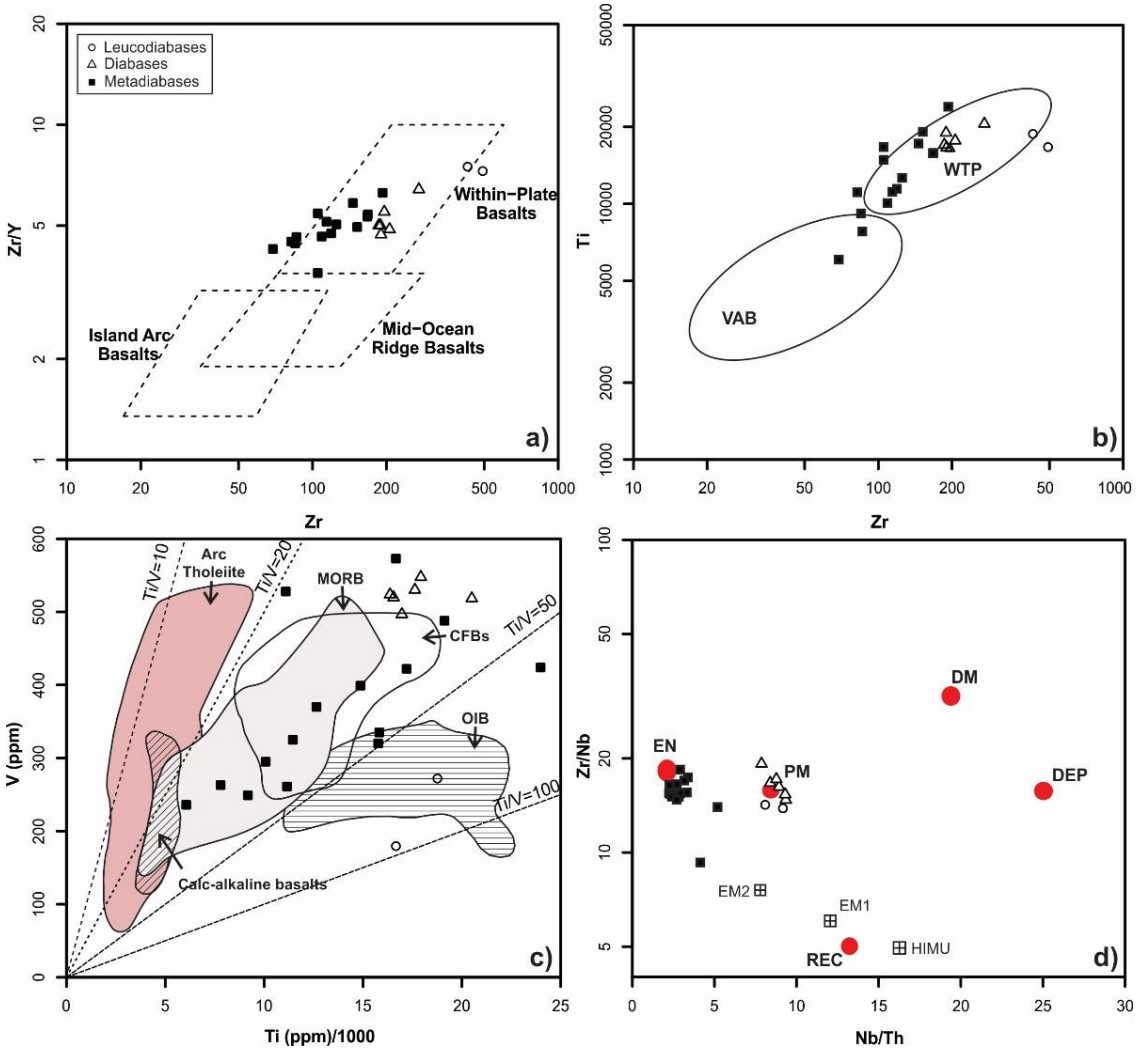

Figure 21 – Tectonic classification diagrams for the metadiabase, diabase and leucodiabase samples, indicating intraplate setting magmatism. a) Zr–Zr/Y diagram (Pearce and Norry, 1979); b) Zr–Ti diagram (Pearce, 1996); and c) Ti/1000–V diagram (Rollinson, 1993 after Shervais, 1982). Figure d) shows the Zr/Nb–Nb/Th diagram (Condie, 2005) to identify the mantle compositional components of the studied rocks. Abbreviations: UC, upper continental crust; PM, primitive mantle; DM, shallow depleted mantle; HIMU, high mu (U/Pb) source; EM1 and EM2, enriched mantle sources; DEP, deep depleted mantle; EN, enriched component; REC, recycled component.

3.7.4 Evolution model and comparison

In order to explain the petrographic, structural, mineralogical and geochemical differences between metadiabases and leucodiabases and diabases, we propose two different events of intracontinental mafic magmatism in the study area.

We suggest that the first magmatic event occurred during an extensional tectonic event related to the evolution of the Araguaia Belt and generated arc-like intracontinental flood basalts with tholeiitic affinity from the partial melting of a source with contribution of enriched mantle components. During their magmatic evolution, differentiation took place via fractional crystallization. The emplacement was facilitated by the presence of N-S trending regional lineaments and structures in the study area. In the Neoproterozoic, the volcanic rocks underwent

low-grade metamorphism in the greenschist facies. As time went by, these mafic bodies were eroded, exposing only the metadiabases dikes, which represent the volcanic plumbing system of the arc-like intracontinental basalts. The broad distribution of Neoproterozoic dates in the study area (Fig. 2) probably indicates partial resetting of the K-Ar system in the metadiabases due to the metamorphic event.

There is a similarity between the metadiabases from the study area and the Neoproterozoic Xambica Intrusive Suite metagabbros (~780 Ma) from the eastern domain of the Araguaia Belt. Both rocks show similar trend for immobile major and trace elements in the Harker diagram (Fig. 9) and similar immobile trace-element distribution patterns in the spidergrams (Fig. 10). The metadiabases also show a very similar immobile trace-element distribution pattern to the diabases of the Rio Perdido Suite, which are part of the 1110 Ma Rincón del Tigre-Huanchaca LIP event. For example, both dike swarms are characterized by the Nb-Ta negative anomaly. The Rio Perdido dikes have controversial geochemical signatures and have been considered either as intraplate (Lima et al., 2017) or subduction-related rocks (Remédio et al., 2014). We suggest the possibility that these rocks, like the metadiabases, are also derived from an arc-like intraplate continental magmatism. Thus, the metadiabases share similar geochemical features with nearby Neoproterozoic and Tonian mafic rocks, which suggest a possible link among these rocks that need to be studied further.

We suggest that the second magmatic event succeeded the Neoproterozoic metamorphism of the Araguaia Belt and generated intracontinental flood basalts with tholeiitic affinity in an extensional setting from the partial melting of a source with contribution of primitive mantle components. Their emplacement took advantage of the same regional structures and lineaments that the first magmatic event did, which explains the same trend directions for the two dike swarms. During their magmatic evolution, evolved rocks were generated by fractional crystallization processes. The diabases represent the exposed volcanic plumbing system of the rocks crystallized from juvenile melts, whereas the leucodiabases represent the exposed conduits of rocks crystallized from evolved melts. The Mesozoic K-Ar dates (~200 Ma) of mafic dikes of the study area probably indicate the crystallization ages of these rocks.

It is very likely that the second magmatic event is associated with the extensional event that lead to the breakup of the supercontinent Pangea. In the Harker diagrams (Fig. 9) and spidergrams (Fig. 10), both diabases and leucodiabases show a striking resemblance to the rocks of Central Atlantic Magmatic Province (CAMP). The diabases share similar geochemical signatures with Guyana tholeiite dikes (Deckart et al., 2005) and the high-TiO_2 basalts from the

Parnaíba Basin (Fodor et al., 1990; Merle et al., 2011) and the high-TiO_2 diabase dikes from the São Luís craton and Gurupi Belt (Klein et al., 2013). The leucodiabases are very similar to the evolved high-TiO_2 basalts from the Parnaíba Basin (Fodor et al., 1990; Merle et al., 2011) and the evolved high-TiO_2 diabase dikes from the São Luís cratonic fragment and Gurupi Belt (Klein et al., 2013).

3.8 CONCLUSIONS

The following conclusions and/or remarks may be drawn from our study:

i. The mafic dike swarms of the Santa Maria das Barreiras-Conceição do Araguaia region can be divided, based on petrography, into a group composed of metamorphosed diabases and another group consisting of unmetamorphosed and undeformed diabases and leucodiabases.
ii. The metadiabases were affected by the Neoproterozoic regional metamorphism that affected the Araguaia Belt.
iii. Fractional crystallization processes have played an important role in the metadiabases differentiation and leucodiabases origin.
iv. The metadiabases represent intracontinental arc-like basalts with tholeiitic affinity whose mantle source had enriched components. The diabases and leucodiabases represent intracontinental basalts with tholeiitic affinity whose mantle source had “primitive mantle” components.
v. There are two different events of intracontinental magmatism in the study area. The older event precedes the Neoproterozoic metamorphism and generated the metadiabases and the newer event succeeds the metamorphism and originated the diabases and leucodiabases.

ACKNOWLEDGMENTS

This work has been supported by the CNPq Project nº 427225/2016-7. Furthermore, the first author is very thankful do CNPq for granting a scholarship (nº 130794/2017-1) that allowed the development of this research.

REFERENCES

Abreu, F.A.M., 1978. O Super Grupo Baixo Araguaia, in: Anais Do 30º Congresso Brasileiro de Geologia. Sociedade Brasileira de Geologia, Recife, pp. 539–545.

Abreu, F.A.M., Gorayeb, P.S.S., 1994. Tectônica e inversão metamórfica no Cinturão Araguaia, in: Anais Do 4º Simpósio de Geologia Da Amazônia. Sociedade Brasileira de Geologia-NO, Belém, pp. 1–4.

Alkmim, F.F., 2015. Geological Background: A Tectonic Panorama of Brazil, in: Vieira, B.C., Salgado, A.A.R., Santos, L.J.C. (Eds.), Landscapes and Landforms of Brazil. Springer Netherlands, Dordrecht, pp. 9–17. https://doi.org/10.1007/978-94-017-8023-0_2

Almeida, F.F.M., Hasui, Y., Brito Neves, B.B., Fuck, R.A., 1981. Brazilian structural provinces: An introduction. Earth-Science Reviews 17, 1–29. https://doi.org/10.1016/0012-8252(81)90003-9

Alvarenga, C.J.S., Moura, C.A.V., Gorayeb, P.S.S., Abreu, F.A.M., 2000. Paraguay and Araguaia belts, in: Cordani, U.G., Milani, E.J., Thomaz Filho, A., Campos, D.A. (Eds.), Tectonic Evolution of South America. 31st International Geological Congress, Rio de Janeiro, pp. 183–193.

Barbosa, O., Ramos, J.A., Gomes, F.A., Helmbold, R., 1966. Geologia estratigráfica, estrutural e econômica da área do Projeto Araguaia. DNPM/Divisão de Geologia e Mineralogia, Rio de Janeiro.

Barros, G.S., 2010. Petrografia, geoquímica e geocronologia dos metagabros da região de Xambioá-Araguanã-TO. Universidade Federal do Pará.

Barros, L.D., Gorayeb, P.S.S., 2013. Metabasaltos almofadados do sul da Serra do Tapa, SE do Pará - Cinturão Araguaia, in: Anais Do 13º Simpósio de Geologia Da Amazônia. Sociedade Brasileira de Geologia-NO, Belém, pp. 322–325.

Best, M.G., 2003. Igneous and metamorphic petrology. Blackwell Publishers, Malden.

Cann, J.R., 1970. Rb, Sr, Y, Zr and Nb in some ocean floor basaltic rocks. Earth and Planetary Science Letters 10, 7–11. https://doi.org/10.1016/0012-821X(70)90058-0

Condie, K.C., 2005. High field strength element ratios in Archean basalts: a window to evolving sources of mantle plumes? Lithos 79, 491–504. https://doi.org/10.1016/j.lithos.2004.09.014

Cunha, B.C.C., Potiguar, L.A.T., Ianhez, A.C., Bezerra, P.E.L., Pitthan, J.H.L., Souza Jr., J.J., Montalvão, R.M.G., Sousa, A.M.S., Hildred, P.R., Tassinari, C.C.., 1981. Geologia, in: Folha SC.22 Tocantins. Projeto RADAMBRASIL, Rio de Janeiro, pp. 21–196.

Dall'Agnol, R., Teixeira, N.P., Macambira, J.B., Kotschoubey, B., Gorayeb, P.S.S., Santos, M.D., 1988. Petrologia dos gnaisses e micaxistos da porção norte da faixa de dobramentos Araguaia-Goiás-Brasil, in: Anais Do 7º Congresso Latino-Americano de Geologia. Sociedade Brasileira de Geologia-NO, Belém, pp. 1–19.

Deckart, K., Bertrand, H., Liégeois, J.-P., 2005. Geochemistry and Sr, Nd, Pb isotopic composition of the Central Atlantic Magmatic Province (CAMP) in Guyana and Guinea. Lithos 82, 289–314. https://doi.org/10.1016/J.LITHOS.2004.09.023

Deer, W.A., Howie, R.A., Zussman, J., 1992. An introduction to the rock-forming minerals. Longman Scientific & Technical, London.

Dutra, A.C.S., 2012. Magmatismo basáltico na sucessão sedimentar do Grupo Tucuruí-Cinturão Araguaia, nordeste do Pará. Universidade Federal do Pará.

Dutra, A.C.S., Gorayeb, P.S.S., Nogueira, A.C.R., 2014. Geologia USP: Série Científica, Geologia USP. Série Científica. Instituto de Geociências da Universidade de São Paulo.

Ernst, R.E., 2014. Large Igneous Provinces. Cambridge University Press, Cambridge. https://doi.org/10.1017/CBO9781139025300

Ernst, R.E., Buchan, K.L., Campbell, I.H., 2005. Frontiers in Large Igneous Province research. Lithos 79, 271–297. https://doi.org/10.1016/j.lithos.2004.09.004

Figueiredo, A.J.A., Souza, J.O., 2001. Carta geológica - Folha Conceição do Araguaia - SB.22-X-B - Escala 1:250.000, in: Figueiredo, A.J.A., Souza, J.O., Olivatti, O. (Eds.), Conceição Do Araguaia - Folha SB.22-X-B - Estados Do Tocantins/Pará. Programa Levantamentos Geológicos Básicos do Brasil. CPRM, Brasília.

Fodor, R. V., Sial, A.N., Mukasa, S.B., McKee, E.H., 1990. Petrology, isotope characteristics, and K-Ar ages of the Maranhão, northern Brazil, Mesozoic basalt province. Contributions to Mineralogy and Petrology 104, 555–567. https://doi.org/10.1007/BF00306664

Fuck, R.A., Dantas, E.L., Pimentel, M.M., Botelho, N.F., Armstrong, R., Laux, J.H., Junges, S.L., Soares, J.E., Praxedes, I.F., 2014. Paleoproterozoic crust-formation and reworking events in the Tocantins Province, central Brazil: A contribution for Atlantica supercontinent reconstruction. Precambrian Research 244, 53–74. https://doi.org/10.1016/J.PRECAMRES.2013.12.003

Giovanardi, T., Girardi, V.A.V., Teixeira, W., Mazzucchelli, M., 2019. Mafic dyke swarms at 1882, 535 and 200 Ma in the Carajás region, Amazonian Craton: Sr-Nd isotopy, trace element geochemistry and inferences on their origin and geological settings. Journal of South American Earth Sciences 92, 197–208. https://doi.org/10.1016/J.JSAMES.2019.02.017

Gorayeb, P.S.S., 1989. Corpos serpentiníticos da Faixa Araguaia na região de Araguacema-Pequizeiro-Conceição do Araguaia. Revista Brasileira de Geociências 19, 51–62.

Gorayeb, P.S.S., 1981. Evolução geológica da região de Araguacema Pequizeiro. Universidade Federal do Pará.

Gorayeb, P.S.S., Costa, J.R.C., Cruz, D.J.N., 2017. A suíte máfica Conceição do Araguaia-Santa Maria das Barreiras (feixe de diques de diabásio e gabro): Fronteira Pará-Tocantins, in: Gorayeb, P.S.S., Teixeira, S.G. (Eds.), Anais Do 15º Simpósio de Geologia Da Amazônia. Sociedade Brasileira de Geologia-NO, Belém, pp. 492–496.

Gorayeb, P.S.S., Moura, C.A.V., Abreu, F.A.M., 2008. Geologia do Parque Estadual da Serra dos Martírios-Andorinhas e região adjacente, in: Gorayeb, P.S.S. (Ed.), Parque Martírios-Andorinhas: Conhecimento, História e Preservação. EDUFPA, Belém, pp. 53–75.

Gorayeb, P.S.S., Moura, C.A. V., Arcanjo, S.H.S., 2000. Granitogenesis events in the Porto Nacional - Palmas - Paraíso do Tocantins region, Tocantins Province, Brazil, in: 31st International Geological Congress. Rio de Janeiro.

Gorayeb, P.S.S., Moura, C.A. V., Calado, W.M., 2004. Suíte Intrusiva Xambica: um magmatismo toleítico Neoproterozoico, pré-tectônico, no Cinturão Araguaia, in: Anais Do 42º Congresso Brasileiro de Geologia. Sociedade Brasileira de Geologia, Axará, p. 35.

Gorayeb, P.S.S., Santos, W.P., Moura, C.A.V., Sousa, L.H., 2019. Petrologia, geoquímica e

geocronologia do Granodiorito Presidente Kennedy: contextualização na evolução do Cinturão Araguaia. Geologia USP. Série Científica 19, 89–116. https://doi.org/10.11606/issn.2316-9095.v19-137160

Hasui, Y., Costa, J.B.S., Abreu, F.A.M., 1984. Província Tocantins, Setor Setentrional, in: Almeida, F.F.M., Hasui, Y. (Eds.), O Pré-Cambriano Do Brasil. Ed. Edgard Blücher, São Paulo, pp. 187–204.

Hasui, Y., Tassinari, C.C.G., Siga Jr., O., Teixeira, W., Almeida, F.F.M., Kawashita, K., 1980. Datações Rb-Sr e K-Ar do centro-norte do Brasil e seu significado geológico-geotectônico, in: Anais Do 31º Congresso Brasileiro de Geologia. Sociedade Brasileira de Geologia, Balneário Camboriú, pp. 2659–2676.

Hodel, F., Trindade, R.I.F., Macouin, M., Meira, V.T., Dantas, E.L., Paixão, M.A.P., Rospabé, M., Castro, M.P., Queiroga, G.N., Alkmim, A.R., Lana, C.C., 2019. A Neoproterozoic hyper-extended margin associated with Rodinia's demise and Gondwana's build-up: The Araguaia Belt, central Brazil. Gondwana Research 66, 43–62. https://doi.org/10.1016/J.GR.2018.08.010

Hughes, C.J., 1972. Spilites, keratophyres, and the igneous spectrum. Geological Magazine 109, 513. https://doi.org/10.1017/S0016756800042795

Klein, E.L., Angélica, R.S., Harris, C., Jourdan, F., Babinski, M., 2013. Mafic dykes intrusive into Pre-Cambrian rocks of the São Luís cratonic fragment and Gurupi Belt (Parnaíba Province), north-northeastern Brazil: Geochemistry, Sr-Nd-Pb-O isotopes, 40Ar/39Ar geochronology, and relationships to CAMP magmatism. Lithos 172–173, 222–242. https://doi.org/10.1016/j.lithos.2013.04.015

Kotschoubey, B., Hieronymus, B., Albuquerque, C.A.R., 2005. Disrupted peridotites and basalts from the Neoproterozoic Araguaia belt (northern Brazil): Remnants of a poorly evolved oceanic crust? Journal of South American Earth Sciences 20, 211–230. https://doi.org/10.1016/J.JSAMES.2005.05.007

Le Maitre, R.W., Streckeisen, A., Zanettin, B., Le Bas, M.J., Bonin, B., Bateman, P., 2002. Igneous Rocks: A Classification and Glossary of Terms (Recommendations of the IUGS Subcommission on the Systematics of Igneous Rocks), Cambridge University Press. https://doi.org/10.2113/gscanmin.40.6.1737

Leake, B.E., E., B., 1971. On aluminous and edenitic hornblendes. Mineralogical Magazine 38, 389–407. https://doi.org/10.1180/minmag.1971.038.296.01

Leake, B.E., Woolley, A.R., Arps, C.E.S., Birch, W.D., Gilbert, M.C., Grice, J.D., Hawthorne, F.C., Kato, A., Kisch, H.J., Krivovichev, V.G., Linthout, K., Laird, J., Mandarino, J.A., Maresch, W. V., Nickel, E.H., Rock, N.M.S., Schumacher, J.C., Smith, D.C., Stephenson, N.C.N., Ungaretti, L., Whittaker, E.J.W., Youzhi, G., 1997. Nomenclature of amphiboles: Report of the subcommittee on amphiboles of the international mineralogical association, commission on new minerals and mineral names. American Mineralogist.

Lemarchand, F., Villemant, B., Calas, G., 1987. Trace element distribution coefficients in alkaline series. Geochimica et Cosmochimica Acta 51, 1071–1081. https://doi.org/10.1016/0016-7037(87)90201-8

Leterrier, J., Maury, R.C., Thonon, P., Girard, D., Marchal, M., 1982. Clinopyroxene composition as a method of identification of the magmatic affinities of paleo-volcanic series. Earth and Planetary Science Letters 59, 139–154. https://doi.org/10.1016/0012-821X(82)90122-4

Lima, G.A., Macambira, M.J.B., Sousa, M.Z.A., Ruiz, A.S., 2017. Suíte Intrusiva Rio Perdido: magmatismo intraplaca no sul do Cráton Amazônico – Bloco Rio Apa. Geologia USP. Série Científica 17, 79. https://doi.org/10.11606/issn.2316-9095.v17-454

MacLean, W.H., Barrett, T.J., 1993. Lithogeochemical techniques using immobile elements. Journal of Geochemical Exploration 48, 109–133. https://doi.org/10.1016/0375-6742(93)90002-4

Marzoli, A., Renne, P.R., Piccirillo, E.M., Ernesto, M., Bellieni, G., De Min A, A. De, 1999. Extensive 200-million-year-Old continental flood basalts of the central atlantic magmatic province. Science 284, 616–8. https://doi.org/10.1126/science.284.5414.616

Mckenzie, D., O'nions, R.K., 1991. Partial melt distributions from inversion of rare earth element concentrations. Journal of Petrology 32, 1021–1091. https://doi.org/10.1093/petrology/32.5.1021

Merle, R., Marzoli, A., Bertrand, H., Reisberg, L., Verati, C., Zimmermann, C., Chiaradia, M., Bellieni, G., Ernesto, M., 2011. Lithos Ar / 39 Ar ages and Sr – Nd – Pb – Os geochemistry of CAMP tholeiites from Western Maranhão basin (NE Brazil). LITHOS 122, 137–151. https://doi.org/10.1016/j.lithos.2010.12.010

Miyagawa, L.J.P.P., Gorayeb, P.S.S., 2013. Basaltos almofadados da Suíte Ofiolítica Morro do Agostinho: registros de fundo oceânico na porção centro-oeste do Cinturão Araguaia. Geologia USP. Série Científica 13, 111–124. https://doi.org/10.5327/Z1519-874X201300040006

Morimoto, N., 1988. Nomenclature of Pyroxenes. Mineralogy and Petrology 39, 55–76. https://doi.org/10.1007/BF01226262

Moura, C.A. V., Gaudette, H.E., 1993. Evidence of brasiliano/panafrican deformation in the Araguaia belt: implication for Gondwana evolution. Revista Brasileira de Geociências 23, 117–123. https://doi.org/10.25249/0375-7536.1993232117123

Nachit, H., Ibhi, A., Abia, E.H., Ben Ohoud, M., 2005. Discrimination between primary magmatic biotites, reequilibrated biotites and neoformed biotites. Comptes Rendus Geoscience 337, 1415–1420. https://doi.org/10.1016/J.CRTE.2005.09.002

Nakamura, N., 1974. Determination of REE, Ba, Fe, Mg, Na and K in carbonaceous and ordinary chondrites. Geochimica et Cosmochimica Acta 38, 757–775. https://doi.org/10.1016/0016-7037(74)90149-5

Nascimento, R.S., Dutra, A.C.S., Gorayeb, P.S.S., Moura, C.A. V., 2011. Aspectos petrográficos e geoquímicos do Diabásio Penatecaua na região de Monte Alegre-PA, borda nordeste da Bacia do Amazonas., in: Nascimento, R.S.C., Horbe, A.M.C., Almeida, C.M. (Eds.), Contribuições à Geologia Da Amazônia (Vol. 7). Sociedade Brasileira de Geologia-NO, Belém, pp. 45–46.

Neves, A.P., Vale, A.G., 1999. Carta geológica - Folha Redenção - SC.22-X-A - Escala 1:250.000, in: Neves, A.P., Vale, A.G. (Eds.), Folha Redenção SC.22-X-A. Programa Levantamentos Geológicos Básicos do Brasil. CPRM., Brasília.

Nielsen, R.L., 1992. BIGD.FOR: A FORTRAN program to calculate trace-element partition coefficients for natural mafic and intermediate composition magmas. Computers and Geosciences 18, 773–788. https://doi.org/10.1016/0098-3004(92)90024-L

Olivatti, O., Souza, J.O., Figueiredo, A.J.A., 2001. Estratigrafia, in: Figueiredo, A.J.A., Souza, J.O., Olivatti, O. (Eds.), Conceição Do Araguaia - Folha SB.22-X-B - Estados Do

Tocantins/Pará. Programa Levantamentos Geológicos Básicos do Brasil. CPRM., Brasília, pp. 19–51.

Paixão, M.A.P., Gorayeb, P.S.S., 2014. Metalogênese do Cinturão Araguaia, in: Silva, M.G., Rocha Neto, M.B., Jost, H., Kuyumjian, R.M. (Eds.), Metalogênese Das Províncias Tectônicas Brasileiras. CPRM, Rio de Janeiro, pp. 467–488.

Paixão, M.A.P., Nilson, A.A., Dantas, E.L., 2008. The Neoproterozoic Quatipuru ophiolite and the Araguaia fold belt, central-northern Brazil, compared with correlatives in NW Africa, in: Pankhurst, R.J., Trouw, R.A.J., Brito Neves, B.B., Wit, M.. (Eds.), West Gondwana: Pre-Cenozoic Correlations across the South Atlantic Region. Geological Society of London, pp. 297–318. https://doi.org/10.1144/SP294.16

Passchier, C.W., Trouw, R.A.J., 2005. Microtectonics. Springer, New York. https://doi.org/10.1007/3-540-29359-0

Paster, T.P., Schauwecker, D.S., Haskin, L.A., 1974. The behavior of some trace elements during solidification of the Skaergaard layered series. Geochimica et Cosmochimica Acta 38, 1549–1577. https://doi.org/10.1016/0016-7037(74)90174-4

Pearce, J.A., 1996. A User's Guide to Basalt Discrimination Diagrams, in: Wyman, D.A. (Ed.), Trace Element Geochemistry of Volcanic Rocks: Applications for Massive Sulphide Exploration. Geological Association of Canada, Short Course Notes, pp. 79–113.

Pearce, J.A., Norry, M.J., 1979. Petrogenetic implications of Ti, Zr, Y, and Nb variations in volcanic rocks. Contributions to Mineralogy and Petrology 69, 33–47. https://doi.org/10.1007/BF00375192

Pimentel, M.M., Fuck, R.A., Jost, H., Ferreira Filho, C.R., Araújo, S.M., 2000. The basement of the Brasília Fold Belt and the Goiás Magmatic Arc, in: Cordani, U.G., Milani, E.J., Thomaz Filho, A., Campos, D.A. (Eds.), Tectonic Evolution of South America. 31st International Geological Congress, Rio de Janeiro, pp. 195–229.

Prowatke, S., Klemme, S., 2006. Trace element partitioning between apatite and silicate melts. Geochimica et Cosmochimica Acta 70, 4513–4527. https://doi.org/10.1016/j.gca.2006.06.162

Remédio, M.J., Faleiros, F.M., Brumatti, M., Almeida, V.V., Costa, V.C., 2014. Unidades litoestratigráficas, in: Remédio, M.J., Faleiros, F.M. (Eds.), Geologia e Recursos Minerais Da Folha Fazenda Margarida — SF.21-X-C-IV. CPRM, São Paulo, pp. 29–62.

Rollinson, H.R., 1993. Using geochemical data: evaluation, presentation, interpretation. Longman Scientific & Technical.

Rosa-Costa, L.T., 2014. Unidades Estatigráficas, in: Rosa-Costa, L.T., Chaves, C.L., Klein, E.L. (Eds.), Geologia e Recursos Minerais Da Folha Rio Araguari – NA.22-Y-B. CPRM, Belém, pp. 25–94.

Shervais, J.W., 1982. Ti-V plots and the petrogenesis of modern and ophiolitic lavas. Earth and Planetary Science Letters 59, 101–118. https://doi.org/10.1016/0012-821X(82)90120-0

Sial, A.N., Ferreira, V.P., Fallick, A.E., Jerônimo M. Cruz, M., 1998. Amphibole-rich clots in calc-alkalic granitoids in the Borborema province, northeastern Brazil. Journal of South American Earth Sciences 11, 457–471. https://doi.org/10.1016/S0895-9811(98)00034-0

Silva, J.M.R., 1980. Metamorfismo das rochas pelíticas do segmento setentrional da faixa Paraguai-Araguaia. Universidade Federal do Pará.

Streckeisen, A., 1976. To each plutonic rock its proper name. Earth Science Reviews. https://doi.org/10.1016/0012-8252(76)90052-0

Sun, S.S., McDonough, W.F., 1989. Chemical and isotopic systematics of oceanic basalts: implications for mantle composition and processes. Geological Society, London, Special Publications 42, 313–345. https://doi.org/10.1144/GSL.SP.1989.042.01.19

Teixeira, W., Hamilton, M.A., Girardi, V.A.V., Faleiros, F.M., Ernst, R.E., 2019. U-Pb baddeleyite ages of key dyke swarms in the Amazonian Craton (Carajás/Rio Maria and Rio Apa areas): Tectonic implications for events at 1880, 1110 Ma, 535 Ma and 200 Ma. Precambrian Research 329, 138–155. https://doi.org/10.1016/j.precamres.2018.02.008

Teixeira, W., Hamilton, M.A., Lima, G.A., Ruiz, A.S., Matos, R., Ernst, R.E., 2015. Precise ID-TIMS U–Pb baddeleyite ages (1110–1112Ma) for the Rincón del Tigre–Huanchaca large igneous province (LIP) of the Amazonian Craton: Implications for the Rodinia supercontinent. Precambrian Research 265, 273–285. https://doi.org/10.1016/j.precamres.2014.07.006

Tindle, A.G., Webb, P.C., 1994. Probe-AMPH—A spreadsheet program to classify microprobe-derived amphibole analyses. Computers & Geosciences 20, 1201–1228. https://doi.org/10.1016/0098-3004(94)90071-X

Vale, A.G., Neves, A.P., 1999. Geologia, in: Neves, A.P., Vale, A.G. (Eds.), Folha Redenção SC.22-X-A. Programa Levantamentos Geológicos Básicos do Brasil. CPRM., pp. 15–100.

Vernon, R.H., 2004. A Practical Guide to Rock Microstructure. Cambridge University Press, Cambridge. https://doi.org/10.1017/CBO9780511807206

Wang, X.-C., Wilde, S.A., Li, Q.-L., Yang, Y.-N., 2015. Continental flood basalts derived from the hydrous mantle transition zone. Nature Communications 6, 7700. https://doi.org/10.1038/ncomms8700

Wang, X., Wilde, S.A., Xu, B., Pang, C., 2016. Origin of arc-like continental basalts: Implications for deep-Earth fluid cycling and tectonic discrimination. LITHOS 261, 5–45. https://doi.org/10.1016/j.lithos.2015.12.014

Winchester, J.A., Floyd, P.A., 1977. Geochemical discrimination of different magma series and their differentiation products using immobile elements. Chemical Geology 20, 325–343. https://doi.org/10.1016/0009-2541(77)90057-2

Winchester, J.A., Floyd, P.A., 1976. Geochemical magma type discrimination: application to altered and metamorphosed basic igneous rocks. Earth and Planetary Science Letters 28, 459–469. https://doi.org/10.1016/0012-821X(76)90207-7

Xia, L.Q., 2014. The geochemical criteria to distinguish continental basalts from arc related ones. Earth-Science Reviews 139, 195–212. https://doi.org/10.1016/j.earscirev.2014.09.006

CAPÍTULO 4 CONSIDERAÇÕES FINAIS

A fim de explicar as diferenças petrográficas, estruturais, mineralógicas e geoquímicas entre metadiabásios e leucodiabásios e diabásios, sugeriu-se dois diferentes eventos de magmatismo máfico intracontinental na área de estudo.

Considera-se que o primeiro evento ocorreu durante um evento tectônico extensional relacionado à evolução do Cinturão Araguaia e gerou um sistema de rochas vulcânicas com afinidade toleítica provenientes da fusão parcial de fontes mantélicas com componentes enriquecidos. Durante a evolução magmática dessas rochas, diferenciação ocorreu por processos de cristalização fracionada. A colocação desses corpos foi provavelmente facilitada pela presença na área de estudo de grandes lineamentos e estruturas regionais de direção N-S. No Neoproterozoico, essas rochas vulcânicas sofreram metamorfismo de baixo grau na fácies xisto-verde. Com o tempo, esses corpos foram erodidos, expondo apenas os diques de metadiabásios, que representam o sistema de condutos dos basaltos intracontinentais com assinatura de arco. A grande distribuição de idades neoproterozoicas na área de estudo indica que houve *reset* do sistema K-Ar nos metadiabásios durante o metamorfismo.

Assinaturas de arco em basaltos vem sendo consideradas como provenientes de contaminação crustal (Xia, 2014), de fusão do manto litosférico previamente metasomatizado durante subducção (Ernst, 2014) e/ou da zona hidrata de transição do manto (Wang *et al*. 2015, 2016). De acordo com Condie (2005), o componente enriquecido (EN) - cuja contribuição foi sugerida nos metadiabásios – inclui a crosta continental superior e a litosfera subcontinental que podem ter herdado uma assinatura geoquímica de zona de subducção. Isso aponta para uma fusão de um manto que foi afetado previamente pela subducção. No entanto, a origem de basaltos com características de arco é ainda incerta e nenhum processo pode ser descartado para essas rochas com as informações que se tem disponíveis no momento.

Há uma similaridade entre os metadiabásios da área de estudo com os metagabros da Suíte Intrusiva Xambica (~780 Ma), que se situa no domínio leste do Cinturão Araguaia. Ambos grupos de rochas demonstram *trends* similares de elementos maiores e traços no diagram Hacker e padrões similares de distribuição de elementos traços imóveis nos diagramas de multi-elementos. Os metadiabásios também apresentam um padrão de distribuição de elementos traços imóveis bastante similar com os dos diques de diabásios da Suíte Rio Perdido, que faz parte da LIP Rincón del Tigre-Huanchaca de 1100 Ma. Por exemplo, ambos os enxames de diques são caracterizados pela anomalia negativa de Nb-Ta. Os diques de Rio Perdido apresentam uma assinatura geoquímica controversa que sugere tanto um ambiente tectônico

intraplaca (Lima *et al*. 2017) quanto um ambiente de subducção (Remédio *et al.* 2014). Desse modo, sugere-se que devido as semelhanças, pode haver uma conexão entre os metadiabásios e as rochas máficas próximas do Neoproterozoico e/ou Toniano.

O segundo evento magmático proposto sucedeu o metamorfismo regional do Cinturão Araguaia e gerou um sistema de rochas vulcânicas de afinidade toleítica em um ambiente tectônico intracontinental. A colocação dessas rochas provavelmente aproveitou os mesmos lineamentos e estruturas regionais que foram facilitaram a colocação do primeiro evento magmático, o que explicaria como estes dois enxames distinto apresentam a mesma direção. Durante a evolução magmática desses corpos, rochas mais evoluídas foram geradas por processos de cristalização fracionada, como sugere os *trends* lineares de diabásio e leucodiabásios nos diagramas Hacker. Assim, os diabásios representariam os condutos expostos de basaltos menos evoluídos, enquanto os leucodiabásios representariam os condutos expostos de basaltos mais evoluídos. As datações K-Ar do Mesozoico (-200 Ma) de diques máficos da área de estudo provavelmente representam a idade de cristalização dos diabásios e leucodiabásios.

É provável que o segundo evento magmático esteja associado com o evento extensional que resultou na quebra do supercontinente Pangea. Nos diagramas Harker, tanto os diabásios como os leucodiabásios apresentam uma semelhança bastante clara com as rochas da Província Magmática Atlântico Central (CAMP). Os diabásios compartilham assinaturas geoquímicas similares com os dos diques da Guiana (Deckart *et al*. 2005), com os basaltos de alto-TiO_2 da Bacia do Parnaíba (Fodor *et al*. 1990, Merle *et al*. 2011) e com os diques de diabásio de alto TiO_2 do Cráton São Luís e do Cinturão Gurupi (Klein *et al*. 2013). Os leucodiabásios são bastante similares com as rochas evoluídas de alto TiO_2 da bacia do Parnaíba (Fodor *et al*. 1990, Merle *et al*. 2011) e com os diques de diabásio evoluído de alto TiO_2 do Cráton São Luís e do Cinturão Gurupi (Klein *et al*. 2013).

Portanto, as conclusões que podem ser feitas a partir do presente trabalho são as seguintes:

i. Os diques máficos da região de Santa-Maria das Barreiras-Conceição do Araguaia podem ser divididos petrograficamente em dois grupos: um consistindo de diabásios metamorfizados e outro composto de diabásios e leucodiabásios sem metamorfismo e deformação
ii. Os metadiabásios foram afetados pelo metamorfismo regional que afetou o Cinturão Araguaia no Neoproterozoico.

iii. Processos de cristalização fracionada tiveram um papel importante na diferenciação dos metadiabásios e na gênese dos leucodiabásios.

iv. Os metadiabásios representam basaltos intracontinentais de afinidade toleítica e assinatura de arco cuja fonte mantélica tinha componentes enriquecidos. Os diabásios e leucodiabásios representam basaltos intracontinentais de afinidade toleítica cuja fonte mantélica tinha componentes do manto primitivo.

v. Há dois eventos de magmatismo intracontinental na área de estudo. O evento mais antigo precede o metamorfismo regional do Neoproterozoico e gerou os metadiabásios, enquanto que o evento mais antigo sucede o metamorfismo e deu origem aos diabásios e leucodiabásios.

REFERÊNCIAS

Abreu F.A.M. 1978. O Super Grupo Baixo Araguaia. *In*: SBG, 30° Congresso Brasileiro de Geologia, Recife. *Anais...* p. 539–545.

Abreu F.A.M. & Gorayeb P.S.S. 1994. Tectônica e inversão metamórfica no Cinturão Araguaia. *In:* SBG-NO, 4º Simpósio de Geologia da Amazônia, Belém. *Anais...* p. 1–4.

Almeida F.F.M., Hasui Y., Brito Neves B.B., Fuck R.A. 1981. Brazilian structural provinces: an introduction. *Earth-Science Reviews* **17** (1-2): 1–29. https://doi.org/10.1016/0012-8252(81)90003-9

Alvarenga C.J.S., Moura C.A.V., Gorayeb P.S.S., Abreu F.A.M. 2000. Paraguay and Araguaia belts. *In*: Cordani U.G., Milani E.J., Thomaz Filho A., Campos D.A. (ed.). *Tectonic Evolution of South America*. Rio de Janeiro, 31st International Geological Congress, p. 183–193.

Arcanjo S.H.S. 2002. *Evolução Geológica das sequências do Embasamento na porção sul do Cinturão Araguaia–Região de Paraíso do Tocantins*. PhD Thesis, Instituto de Geociências, Universidade Federal do Pará, Belém, 181 p.

Arcanjo S.H.S., Abreu F.A.M., Moura C.A.V. 2013. Evolução geológica das sequências do embasamento do Cinturão Araguaia na região de Paraíso do Tocantins (TO), Brasil. *Brazilian Journal of Geology*, São Paulo, **43** (3): 501–514. https://doi.org/10.5327/Z2317-48892013000300007

Arcanjo S.H.S. & Moura C.A.V. 2000. Geocronologia Pb-Pb em zircão (método de evaporação) das rochas do embasamento do sertor meridional do Cinturão Araguaia - Região de Paraíso do Tocantins (TO). *Revista Brasileira de Geociências*, São Paulo, **30** (4): 665–670. https://doi.org/10.25249/0375-7536.2000304665670

Barbosa O., Ramos J.A., Gomes F.A., Helmbold R. 1966. *Geologia estratigráfica, estrutural e econômica da área do Projeto Araguaia*. Rio de Janeiro, DNPM/Divisão de Geologia e Mineralogia. Monografia.

Barreira C.F. & Dardenne M.A. 1981. Sequência vulcano-sedimentar do Rio do Coco. *In:* SBG, 1º Simpósio de Geologia do Centro-Oeste, Goiânia. *Anais...* p. 241–264.

Barros G.S. 2010. *Petrografia, geoquímica e geocronologia dos metagabros da região de Xambioá-Araguanã-TO*. MS Dissertation, Instituto de Geociências, Universidade Federal do Pará, Belém, 103 p.

Barros L.D. & Gorayeb P.S.S. 2013. Metabasaltos almofadados do sul da Serra do Tapa, SE do Pará - Cinturão Araguaia. *In:* SBG-NO, 13º Simpósio de Geologia da Amazônia, Belém. Anais... p. 322–325.

Best M.G. 2003. *Igneous and metamorphic petrology*. Malden, Blackwell Publishing.

Condie K.C. 2005. High field strength element ratios in Archean basalts: a window to evolving sources of mantle plumes? *Lithos*, **79** (3-4)**:** 491–504. https://doi.org/10.1016/j.lithos.2004.09.014

Costa J.B.S. 1980. Estratigrafia da Região de Colmeia. *In*: SBG, 31º Congresso Brasileiro de Geologia, Camboriu. *Anais...* p. 720–728.

Costa J.B.S., Gorayeb, P.S.S., Bemergury, R.L., Gama Jr., T., Kotschoubey, B., Lemos, R.L. 1983. *Projeto Paraíso do Norte*. Belém, DNPM/UFPA. Relatório Final.

Cunha B.C.C., Potiguar L.A.T., Ianhez A.C., Bezerra P.E.L., Pitthan J.H.L., Souza Jr. J.J., Montalvão R.M.G., Sousa A.M.S., Hildred P.R., Tassinari C.C.G. Geologia. *In:* Projeto Radam Brasil. *Folha SC.22 Tocantins*. Rio de Janeiro, MME. p. 21-196. (Levantamento de Recursos Naturais, 22).

Dall'Agnol R., Teixeira N.P., Macambira J.B., Kotschoubey B., Gorayeb P.S.S., Santos M.D. 1988. Petrologia dos gnaisses e micaxistos da porção norte da faixa de dobramentos Araguaia-Goiás-Brasil. *In*: SBG-NO, 7° Congresso Latino-Americano de Geologia, Belém. *Anais...* p. 1–19.

Deckart K., Bertrand H., Liégeois J.-P. 2005. Geochemistry and Sr, Nd, Pb isotopic composition of the Central Atlantic Magmatic Province (CAMP) in Guyana and Guinea. *Lithos*, **82** (3-4), 289–314. https://doi.org/10.1016/J.LITHOS.2004.09.023

Deer W.A., Howie R.A., Zussman J. 2013. *An Introduction to the Rock-Forming Minerals*. London, Mineralogical Society of Great Britain and Ireland.

Dutra A.C.S. 2012. *Magmatismo basáltico na sucessão sedimentar do Grupo Tucuruí-Cinturão Araguaia, nordeste do Pará*. MS dissertation, Instituto de Geociências, Universidade Federal do Pará, Belém, 111 p.

Dutra A.C.S., Gorayeb P.S.S., Nogueira A.C.R. 2014. *Geologia USP: Série Científica*, São Paulo, **14** (1): 21–36.

Ernst R.E. 2014. *Large Igneous Provinces*. Cambridge, Cambridge University Press.

Ernst R.E., Buchan K.L., Campbell I.H. 2005. Frontiers in Large Igneous Province research. *Lithos*, **79** (3-4): 271–297. https://doi.org/10.1016/j.lithos.2004.09.004

Fettes D.J., Desmons J., Árkai P., Brodie K., Bryhni I. 2007. *Metamorphic rocks: a classification and glossary of terms. Recommendations of the International Union of Geological Sciences Subcommission on the Systematics of Metamorphic Rocks*. Cambridge, Cambridge University Press.

Figueiredo A.J.A. & Souza J.O. Carta geológica – Folha Conceição do Araguaia – SB.22-X-B. Belém, MME, CPRM. 1 mapa. Escala 1:250.000. (Programa Levantamentos Geológicos Básicos do Brasil – PLGB).

Fodor R. V., Sial A.N., Mukasa S.B., McKee E.H. 1990. Petrology, isotope characteristics, and K-Ar ages of the Maranhão, northern Brazil, Mesozoic basalt province. *Contributions to Mineralogy and Petrology*, **104** (5): 555–567. https://doi.org/10.1007/BF00306664

Gill R. 2010. *Igneous Rocks and Processes: a practical guide*. West Sussex, Wiley-Blackwell.

Giovanardi T., Girardi V.A.V., Teixeira W., Mazzucchelli M. 2019. Mafic dyke swarms at 1882, 535 and 200 Ma in the Carajás region, Amazonian Craton: Sr-Nd isotopy, trace element geochemistry and inferences on their origin and geological settings. *Journal of South American Earth Sciences*, **92** (2019): 197–208. https://doi.org/10.1016/J.JSAMES.2019.02.017

Gorayeb P.S.S. 1996. *Petrologia e evolução crustal das rochas de alto grau de Porto Nacional – TO*. PhD Thesis, Centro de Geociências, Universidade Federal do Pará, Belém, 258 p.

Gorayeb P.S.S. 1989. Corpos serpentiníticos da Faixa Araguaia na região de Araguacema-Pequizeiro-Conceição do Araguaia. *Revista Brasileira de Geociências*, Belém, **19** (1): 51–62.

Gorayeb P.S.S., 1981. *Evolução geológica da região de Araguacema Pequizeiro*. MS dissertation, Centro de Geociências, Universidade Federal do Pará, Belém, 111 p.

Gorayeb P.S.S., Barros G.S., Nascimento R.S. 2010. Petrologia e geocronologia dos escapolita metagabros e anfibolitos do Cinturão Araguaia na região de Xambioá-Araguanã. *In:* SBG-NO, 45° Congresso Brasileiro de Geologia, Belém. *Anais...* 1 CD-ROM.

Gorayeb P.S.S., Costa J.R.C., Cruz D.J.N. 2017. A suíte máfica Conceição do Araguaia-Santa Maria das Barreiras (feixe de diques de diabásio e gabro): fronteira Pará-Tocantins. *In:* SBG-NO, 15º Simpósio de Geologia da Amazônia, Belém, p 492–496.

Gorayeb P.S.S., Moura C.A.V., Abreu F.A.M. 2008. Geologia do Parque Estadual da Serra dos Martírios-Andorinhas e região adjacente. *In:* Gorayeb P.S.S. (ed.). *Parque Martírios-Andorinhas: conhecimento, história e preservação*. Belém, EDUFPA, p. 53–75.

Gorayeb P.S.S., Moura C.A. V., Calado W.M. 2004. Suíte Intrusiva Xambica: um magmatismo toleítico Neoproterozoico, pré-tectônico, no Cinturão Araguaia *In:* SBG, 42º Congresso Brasileiro de Geologia, Axará. *Anais...* p. 35.

Gorayeb P.S.S., Santos W.P., Moura C.A.V., Sousa L.H. 2019. Petrologia, geoquímica e geocronologia do Granodiorito Presidente Kennedy: contextualização na evolução do Cinturão Araguaia. *Geologia USP Série Científica*, São Paulo, **19** (2): 89–116. https://doi.org/10.11606/issn.2316-9095.v19-137160

Hasui Y., Costa J.B.S., Abreu F.A.M. 1984. Província Tocantins, Setor Setentrional. In: Almeida, F.F.M. & Hasui, Y. (ed.). *O Pré-Cambriano do Brasil*. São Paulo, Ed. Edgard Blücher, p. 187–204.

Hasui Y., Tassinari C.C.G., Siga Jr. O., Teixeira W., Almeida F.F.M., Kawashita K. 1980. Datações Rb-Sr e K-Ar do centro-norte do Brasil e seu significado geológico-geotectônico. *In:* SBG, 31º Congresso Brasileiro de Geologia, Balneário Camboriú. *Anais...* p. 2659–2676.

Hodel F., Trindade R.I.F., Macouin M., Meira V.T., Dantas E.L., Paixão M.A.P., Rospabé M., Castro M.P., Queiroga G.N., Alkmim A.R., Lana C.C. 2019. A Neoproterozoic hyper-extended margin associated with Rodinia's demise and Gondwana's build-up: the Araguaia Belt, central Brazil. *Gondwana Research,* **66** (2019): 43–62. https://doi.org/10.1016/J.GR.2018.08.010

Klein E.L., Angélica R.S., Harris C., Jourdan F., Babinski M. 2013. Mafic dykes intrusive into Pre-Cambrian rocks of the São Luís cratonic fragment and Gurupi Belt (Parnaíba Province), north-northeastern Brazil: Geochemistry, Sr-Nd-Pb-O isotopes, 40Ar/39Ar geochronology, and relationships to CAMP magmatism. *Lithos*, **172–173** (2013): 222–242. https://doi.org/10.1016/j.lithos.2013.04.015

Kotschoubey B., Hieronymus B., Albuquerque C.A.R. 2005. Disrupted peridotites and basalts from the Neoproterozoic Araguaia belt (northern Brazil): remnants of a poorly evolved oceanic crust? *Journal of South American Earth Sciences*, **20** (3): 211–230. https://doi.org/10.1016/J.JSAMES.2005.05.007

Le Maitre R.W., Streckeisen A., Zanettin B., Le Bas M.J., Bonin B., Bateman P. 2002. *Igneous Rocks:* a classification and glossary of terms (recommendations of the IUGS subcommission on the systematics of igneous rocks). Cambridge, Cambridge University Press. https://doi.org/10.2113/gscanmin.40.6.1737

Lima G.A., Macambira M.J.B., Sousa M.Z.A., Ruiz A.S. 2017. Suíte Intrusiva Rio Perdido: magmatismo intraplaca no sul do Cráton Amazônico – Bloco Rio Apa. *Geologia USP Série Científica*, São Paulo, **17** (3): 79. https://doi.org/10.11606/issn.2316-9095.v17-454

Marzoli A., Renne P.R., Piccirillo E.M., Ernesto M., Bellieni G., De Min A A. De. 1999. Extensive 200-million-year-Old continental flood basalts of the Central Atlantic Magmatic Province. *Science*, **284** (5414): 616–618. https://doi.org/10.1126/science.284.5414.616

Merle R., Marzoli A., Bertrand H., Reisberg L., Verati C., Zimmermann C., Chiaradia M., Bellieni G., Ernesto M. 2011. Lithos Ar / 39 Ar ages and Sr – Nd – Pb – Os geochemistry of CAMP tholeiites from Western Maranhão basin (NE Brazil). *Lithos*, **122** (3-4): 137–151. https://doi.org/10.1016/j.lithos.2010.12.010

Miyagawa L.J.P.P. & Gorayeb P.S.S. 2013. Basaltos almofadados da Suíte Ofiolítica Morro do Agostinho: registros de fundo oceânico na porção centro-oeste do Cinturão Araguaia. *Geologia USP Série Científica*, São Paulo, **13** (4): 111–124. https://doi.org/10.5327/Z1519-874X201300040006

Moura C.A.V. & Gaudette H.E. 1999. Zircon Ages of Basement Orthogneisses from the Northern Segment of the Araguaia Belt, Brazil. *In:* Sinha A.K. (ed.). *Basement Tectonics 13*. Blacksburg, Springer, p. 155–178. https://doi.org/10.1007/978-94-011-4800-9_10

Moura C.A.V. & Gaudette H.E. 1994. Geochemistry of the basement orthogneisses of the Araguaia Belt, Tocantins-Brazil. *In:* SBG, 38° Congresso Brasileiro de Geologia, Camboriú. *Anais...* pp. 240–241.

Moura C.A.V. & Gaudette H.E. 1993. Evidence of brasiliano/panafrican deformation in the Araguaia belt: implication for Gondwana evolution. *Revista Brasileira de Geociências*, São Paulo, **23** (2): 117–123. https://doi.org/10.25249/0375-7536.1993232117123

Moura C.A.V. & Souza S.H.P. 1996. Síntese dos dados Geocronológicos das rochas do Embasamento do Cinturão Araguaia e suas Implicações Estratigráficas. *In:* SBG, 39° Congresso Brasileiro de Geologia, Salvador. *Anais...* p. 31–34.

Nascimento R.S., Dutra A.C.S., Gorayeb P.S.S., Moura C.A.V. 2011. Aspectos petrográficos e geoquímicos do Diabásio Penatecaua na região de Monte Alegre-PA, borda nordeste da Bacia do Amazonas *In:* Nascimento R.S.C., Horbe A.M.C., Almeida C.M. (ed.). *Contribuições à Geologia da Amazônia (Vol. 7)*. Belém, SBG, p. 45–46.

Nesse W.D., 2013. *Introduction to optical mineralogy*. Oxford, Oxford University Press.

Neves A.P. & Vale A.G. 1999. Carta geológica – Folha Redenção – SB.22-X-A. Belém, MME, CPRM. 1 mapa. Escala 1:250.000. (Programa Levantamentos Geológicos Básicos do Brasil – PLGB).

Olivatti O., Souza J.O., Figueiredo A.J.A. 2001. Estratigrafia. *In:* Figueiredo A.J.A., Souza J.O., Olivatti O. (ed.). *Folha Conceição do Araguaia - SB.22-X-B.* Belém, CPRM, p. 19–51. (Programa Levantamentos Geológicos Básicos do Brasil)

Paixão M.A.P. & Gorayeb P.S.S. 2014. Metalogênese do Cinturão Araguaia. *In*: Silva, M.G., Rocha Neto M.B., Jost H., Kuyumjian R.M. (ed.). *Metalogênese das províncias tectônicas brasileiras*. Rio de Janeiro, CPRM, p. 467–488.

Paixão M.A.P., Nilson A.A., Dantas E.L. 2008. The Neoproterozoic Quatipuru ophiolite and the Araguaia fold belt, central-northern Brazil, compared with correlatives in NW Africa. In: Pankhurst R.J., Trouw R.A.J., Brito Neves B.B., Wit M.J (ed.). *West Gondwana: Pre-Cenozoic*

correlations across the South Atlantic Region. London, Geological Society of London, p. 297–318. (Special Publications 294) https://doi.org/10.1144/SP294.16

Passchier C.W. & Trouw R.A.J. 2005. *Microtectonics*. New York, Springer. https://doi.org/10.1007/3-540-29359-0

Remédio M.J., Faleiros F.M., Brumatti M., Almeida V.V., Costa V.C. 2014. Unidades litoestratigráficas. *In:* Remédio M.J., Faleiros F.M. (ed.). *Geologia e Recursos Minerais Da Folha Fazenda Margarida — SF.21-X-C-IV*. São Paulo, CPRM, p. 29–62.

Rosa-Costa L.T. 2014. Unidades Estatigráficas. *In:* Rosa-Costa L.T., Chaves C.L., Klein E.L. (ed.). *Geologia e recursos minerais da Folha Araguari - NA.22-Y-B*. Belém, CPRM, p. 25–94.

Silva J.M.R. 1980. *Metamorfismo das rochas pelíticas do segmento setentrional da faixa Paraguai-Araguaia*. MS dissertation, Centro de Geociências, Universidade Federal do Pará, Belém, 48 p.

Spear F.S. 1995. *Metamorphic phase equilibria and pressure-temperature-time paths*. Washington D.C., Mineralogical Society of America.

Teixeira W., Hamilton M.A., Girardi V.A.V., Faleiros F.M., Ernst R.E. 2019. U-Pb baddeleyite ages of key dyke swarms in the Amazonian Craton (Carajás/Rio Maria and Rio Apa areas): Tectonic implications for events at 1880, 1110 Ma, 535 Ma and 200 Ma. *Precambrian Research*, **329** (2019): 138–135. https://doi.org/10.1016/j.precamres.2018.02.008

Teixeira W., Hamilton M.A., Lima G.A., Ruiz A.S., Matos R., Ernst R.E. 2014. Precise ID-TIMS U-Pb baddeleyite ages (1110-1112 Ma) for the Rincón del Tigre-Huanchaca large igneous province (LIP) of the Amazonian Craton: Implications for the Rodinia supercontinent. *Precambrian Research*, **265** (2014): 273-285. https://doi.org/10.1016/j.precamres.2014.07.006

Vale A.G., Neves A.P., 1999. Geologia, in: Neves A.P., Vale A.G. (ed.), *Folha Redenção SC.22-X-A*. Brasília, CPRM., p. 15–100. (Programa Levantamentos Geológicos Básicos do Brasil - PLGB)

Vernon R.H. 2004. *A practical guide to rock microstructure*. Cambridge, Cambridge University Press. https://doi.org/10.1017/CBO9780511807206

Wang X.-C., Wilde S.A., Li Q.-L., Yang Y.-N. 2015. Continental flood basalts derived from the hydrous mantle transition zone. *Nature Communications*, **6** (1): 7700. https://doi.org/10.1038/ncomms8700

Wang X., Wilde S.A., Xu B., Pang C. 2016. Origin of arc-like continental basalts: Implications for deep-Earth fluid cycling and tectonic discrimination. *Lithos*, **261** (2016): 5–45. https://doi.org/10.1016/j.lithos.2015.12.014

Winter J.D. 2010. *Principles of igneous and metamorphic petrology*. New York, Prentice Hall.

Xia L.Q. 2014. The geochemical criteria to distinguish continental basalts from arc related ones. *Earth-Science Reviews*, **139** (2014): 195–212. https://doi.org/10.1016/j.earscirev.2014.09.006

ANEXO A - MAPA AEROGEOFÍSCO

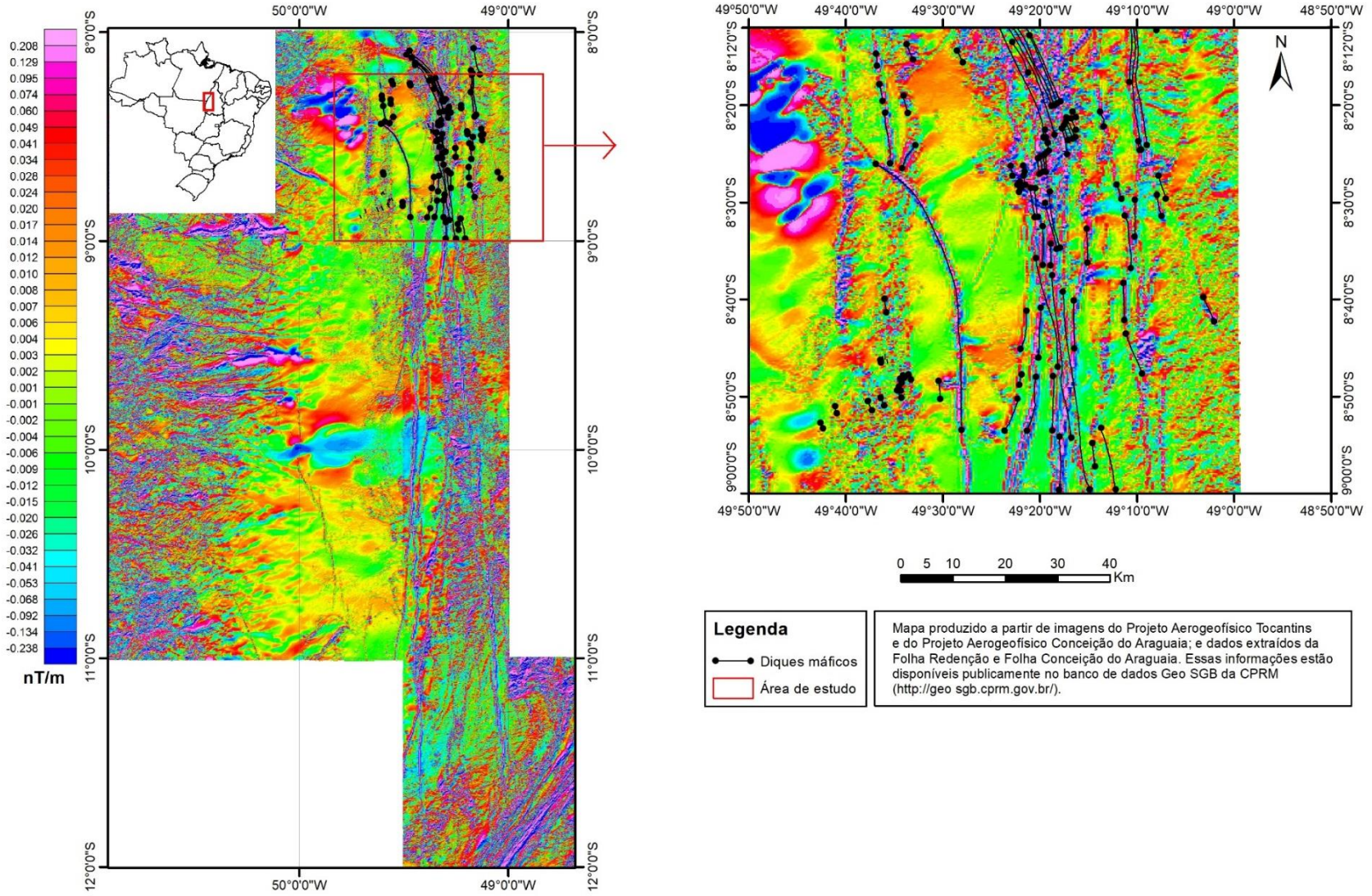

ANEXO B - TABELA DE AMOSTRAS

Amostra	Litotipo	Coordenada X	Coordenada Y	Petrografia	Litogeoquímica	WDS
DA-01	Metadiabásio	-49.3265991	-8.2624197	X		X
DA-05	Metadiabásio	-49.3457985	-8.26544	X		X
DA-07	Metadiabásio	-49.2752991	-8.3491697	X		
DA-08	Metadiabásio	-49.5597	-8.79667	SAM	X	
DA-09	Metadiabásio	-49.2792015	-8.3699999	X	X	X
DA-11	Metadiabásio	-49.2860985	-8.3800001	SAM	X	
DA-12	Metadiabásio	-49.2921982	-8.3880596	X	X	
DA-13	Metadiabásio	-49.3189011	-8.4008303	X	X	
DA-14	Dunito cumulático	-49.3711014	-8.4758301	X	X	
DA-15	Metadiabásio	-49.3692017	-8.4694405	X	X	
DA-16	Metadiabásio	-49.3600006	-8.4572201	X		
DA-17	Metadiabásio	-49.3608017	-8.4411097	X	X	X
DA-18	Metadiabásio	-49.7085991	-8.8747196	X	X	
DA-19	Metadiabásio	-49.6847	-8.8555603	X	X	X
DA-20	Metadiabásio	-49.6239014	-8.8488903	X	X	X
DA-21	Metadiabásio	-49.6035995	-8.8424997	X	X	X
DA-22	Metadiabásio	-49.5764008	-8.82833	SAM	X	
DA-23	Metadiabásio	-49.573101	-8.8080597	X	X	
DA-24	Metadiabásio	-49.5653	-8.8030596	X	X	
DA-25	Leucodiabásio	-49.4738998	-8.6636105	X	X	X
DA-27	Metadiabásio	-49.5597	-8.79667	X	X	X
17-DA-01	Diabásio	-49.2402	-8.9373302	X	X	X
17-DA-02	Diabásio	-49.160099	-8.7868404	X	X	X
78-DA-01	Diabásio	-49.2669983	-8.6804504	X	X	
78-DA-02	Diabásio	-49.2453003	-8.5514097	X	X	X
78-DA-03	Diabásio	-49.5047989	-8.8188601	X	X	X
78-DA-04	Leucodiabásio	-49.4575005	-8.7671604	X	X	X
78-DA-05	Diabásio	-49.3404007	-8.4917498	X	X	X
78-DA-08	Diabásio	-49.4430008	-8.8431597	X		X

Legenda:

X – Método implementado na amostra.

SAM - Somente amostra de mão.

Referência das coletas de amostras:

Siglas DA e 17-DA – Coletada para esta dissertação.

Sigla 78-DA – Coletada para dissertação de mestrado de Paulo Gorayeb.

ANEXO C - MAPA DE AMOSTRAGEM

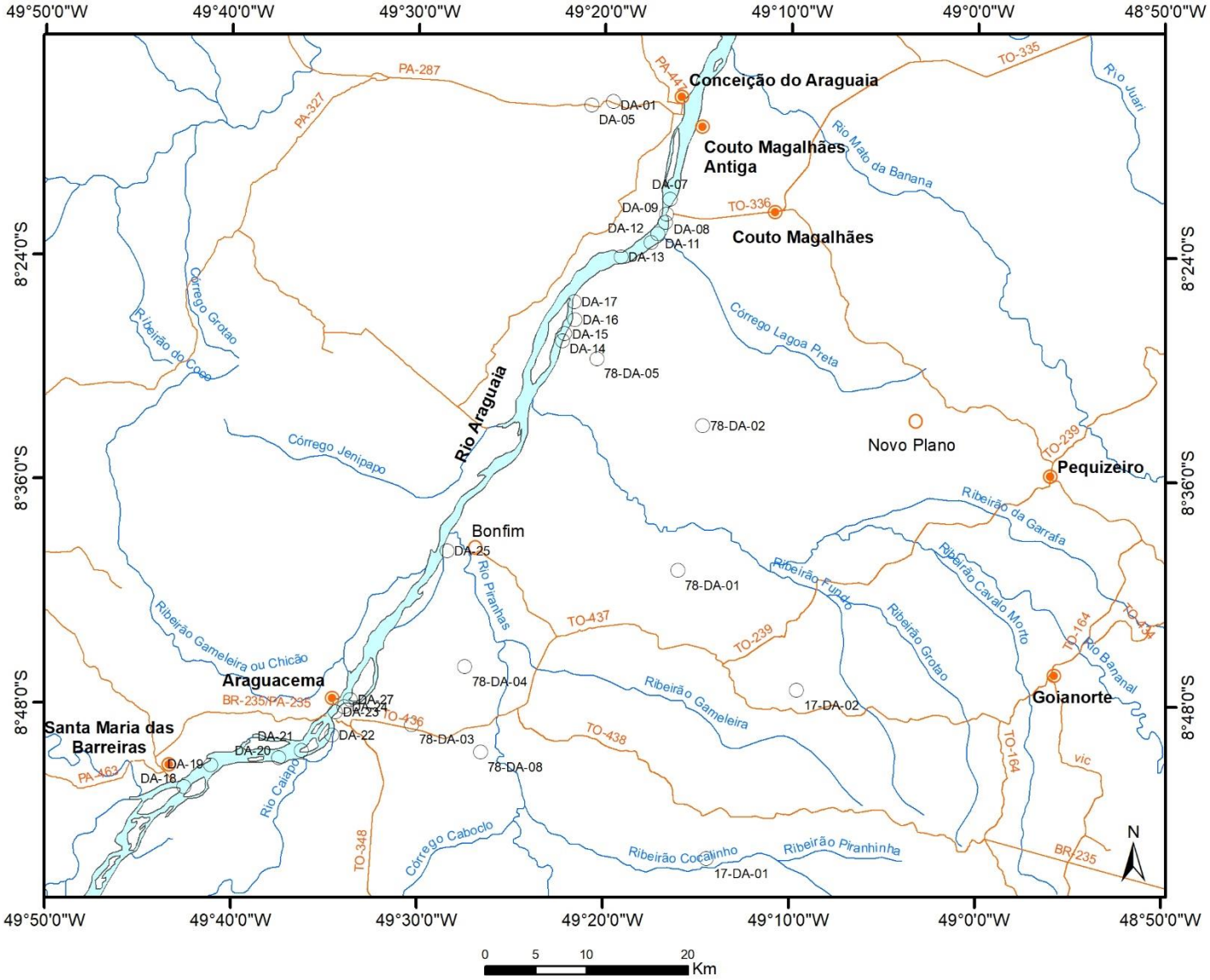

Legenda

- Sede municipal
- Localidade
- Ponto de amostragem
- Estrada
- Drenagem
- Massa D'Água